

International
Progress Report

IPR-00-24

Äspö Hard Rock Laboratory

Rock stress and rock stress measurements at Äspö HRL

Beatrice Lundholm

Luleå University of Technology

October 2000

Svensk Kärnbränslehantering AB

Swedish Nuclear Fuel
and Waste Management Co
Box 5864
SE-102 40 Stockholm Sweden
Tel 08-459 84 00
+46 8 459 84 00
Fax 08-661 57 19
+46 8 661 57 19



**Äspö Hard Rock
Laboratory**

Report no.	No.
IPR-00-24	
Author	Date
Beatrice Lundholm	2000-10-25
Checked by	Date
Rolf Christiansson	2000-11-16
Approved	Date
Olle Olsson	2000-11-20

Äspö Hard Rock Laboratory

Rock stress and rock stress measurements at Äspö HRL

Beatrice Lundholm
Luleå University of Technology

October 2000

Keywords: overcoring, hydraulic fracturing, rock stress measurement

This report concerns a study which was conducted for SKB. The conclusions and viewpoints presented in the report are those of the author(s) and do not necessarily coincide with those of the client.

Preface

The research work presented in this report was carried out during one year from June 1998.

The contents of the report are divided into three parts. Chapter 2 and Chapter 3 give a general overview of the state of the art of hydraulic fracturing and overcoring stress measurements. These two chapters also give a short description of the specific instrumentation used during the measurements at Äspö Hard Rock Laboratory (HRL). Chapter 4 gives a small glimpse into the theory behind the computer codes and Chapter 5 presents the information about the rock stress measurements conducted between 1988 and 1997. The results of these measurements are summarised in Chapter 6. Chapter 7 gives a general discussion and conclusion of the results achieved in the report.

The research work was made possible through financial support from the Swedish Nuclear Fuel and Waste Management Company (SKB). I am especially grateful to Christer Svemar and Olle Olsson who initiated the project.

I wish to express my sincere thanks to my supervisor Professor Erling Nordlund and everybody at the Division of Rock Mechanics for the worthwhile discussions. Special thanks to Professor Bengt Stillborg who was my supervisor in the beginning of this work.

Luleå Oktober 2000

Beatrice Lundholm

Abstract

The process of choosing a site for a nuclear waste repository means that many aspects have to be taken into consideration. One of these is that the repository has to be mechanically stable for a long time. The mechanical stability of the rock is very difficult to determine. One of several parameters, which determine the mechanical stability, is the virgin state of stress.

The project, of which the first part is presented in this report, consists of two parts. The first part is to define the state of stress at Äspö Hard Rock Laboratory. This is done based on earlier rock stress measurements conducted during the years 1988 to 1997. Two different measurement techniques have been used, hydraulic fracturing and overcoring. During the overcoring two types of cells have been used, CSIRO HI-cell and a cell developed by the Swedish State Power Board (SSPB). In the second part, investigation of the correlation between the stress and geological structures will be made.

The rock stress measurements using the hydraulic fracturing gave orientations of the horizontal stress that coincide with earlier hydraulic fracturing measurements conducted in Scandinavia. The magnitudes of rock stresses are slightly lower than the earlier reported stress magnitudes for the Scandinavian part of the earth crust. The rock stresses obtained from the overcoring resulted in higher stresses than what was predicted by the hydraulic fracturing measurements. However, the orientation of the maximum horizontal stresses coincides well between the two techniques. The orientation is also unvaried with respect to increasing depth.

The state of stress at Äspö is defined by using the results from the hydraulic fracturing and the measurements conducted by SSPB-cell. The measurements from the SSPB-cell are used since these have a Poisson's ratio that corresponds well with the uniaxial tests of rock samples and since the measurements have been done at a distance from the opening where no influence from the openings can be expected.

Since the magnitudes of the rock stresses differ between overcoring and hydraulic fracturing, some efforts have been made to find possible causes for this. The rock stresses when conducting overcoring gave higher values overall, which could be explained by high Poisson's ratios and a minor influence from the opening as the stress measurements might have been done in the disturbed zone.

The high Poisson's ratio may depend on the stress-induced microcracks, which might be initiated during the overcoring of the cell and also during the drilling of the minor borehole, in which the cell is installed. Statistical analysis showed that there is significant difference between the mean values of Poisson's ratio obtained from biaxial tests of cores containing the CSIRO HI-cell or the SSPB-cell. Poisson's ratio is about 0.34 for CSIRO HI-cell while the SSPB-cell gave a Poisson's ratio of 0.23. However, the analysis also showed that Young's modulus does not differ between the techniques.

Sammanfattning

Vid platsbestämning av ett djupförvar för utbränt kärnbränsle måste flera aspekter tas i beaktande, varav en av dessa är att förvaret måste vara mekaniskt stabilt för en lång tidsperiod. En av flera parametrar som styr den mekaniska stabiliteten är det naturliga spänningstillståndet som tillsammans med övriga parametrar gör det svårt att bestämma bergets mekaniska stabilitet.

Detta projekt, av vilken den första delen presenteras i denna rapport, består av två delar. I den första delen ska spänningstillståndet över Äspölaboratoriet definieras. Detta görs genom att studera bergspänningsmätningar som utförts under åren 1998 till 1997. Två skilda mättekniker har använts, hydraulisk spräckning samt friborring. I samband med friborring har två olika typer av mätceller använts, CSIRO HI-cell och en cell som utvecklats av Vattenfall (SSPB-cell). I den andra delen av detta projekt, ska de naturliga bergspänningarnas påverkan av geologiska strukturer studeras.

Bergspänningsmätningarna med hydraulisk spräckning resulterade i en orientering på den största horisontala spänningen som stämmer väl överens med tidigare mätningar som utförts i Skandinavien. Storleken på bergspräckningarna skiljer sig dock lite från dessa tidigare mätningar. Mätresultaten från hydrauliska spräckning ingår i dessa uppmätta tidigare runt om i Skandinavien. Resultaten från friborringen, gav bergspänningar som är högre än vad som förutspåddes utifrån hydraulisk spräckning. Det ska dock nämnas att orienteringen av den största horisontella spänningen stämmer bra överens mellan de två mätmetoderna, samt att orienteringen är konstant med ökat djup.

Spänningstillståndet i berggrunden under Äspö bestäms genom att använda resultaten från hydraulisk spräckning och mätningarna utförda med SSPB-cellen. Mätningarna utförda med den sistnämnda cellen används eftersom Poissons tal stämmer överens med resultaten från enaxiella trycktester samt därför att mätningarna har utförts på ett avstånd från tunneln, så att de antas vara opåverkad av tunneln.

Eftersom storleken på bergspänningarna skiljer sig mellan friborringen, speciellt när CSIRO HI-cellen har används och hydraulisk spräckning har detta lett till att söka möjliga orsaker till detta. Bergspänningsmätningar utförda med friborring gav generellt ett högre värde på bergspänningarna, vilken torde kunna förklaras med höga Poissons tal samt att spänningarna är påverkade av tunneln.

Höga Poissons tal kan bero på spänningsinducerade mikrosprickor, som kan initieras under friborringen och under borring av det mindre hålet, i vilket mätcellen installeras. Statistisk analys visar att det är en signifikant skillnad mellan medelvärdet för Poissons tal då CSIRO-cellen har används jämfört med då SSPB-cellen används. Poissons tal är ca. 0.34 för CSIRO HI-cell medan SSPB-cell har ett motsvarande värde på 0.23. Samma statistiska analys gav att skillnaderna i elasticitetsmodulen inte skiljer sig mellan de två mätcellerna.

Contents

Preface	i
Abstract	ii
Sammanfattning (in Swedish)	iii
Contents	iv
List of Figures	vi
List of Tables	vii
1 Introduction	1
1.1 Classification of rock stresses	1
1.2 Äspö Hard Rock Laboratory	2
1.3 Objectives	3
2 Hydraulic fracturing	4
2.1 Test procedure	4
2.2 Data evaluation and interpretation	6
2.2.1 Interpretation of the breakdown and reopening pressures	6
2.2.2 Interpretation of the instantaneous shut-in pressure	6
Interpretation of tensile strength	8
2.3 Stress determination	8
2.3.1 Fracture parallel to the borehole axis	8
2.3.2 Fractures parallel or perpendicular to the borehole axis	10
2.4 Remarks on the method	12
2.5 Equipment used at Äspö	13
2.5.1 Downhole packer assemblies	13
2.5.2 Pump and water system	14
2.5.3 Multihose drum and feeder	14
2.5.4 Data recording system	14
3 Overcoring	16
3.1 General	16
3.2 Swedish State Power Board Triaxial gauge	17
3.2.1 Instrumentation	17
3.2.2 Remarks on the method	19
3.3 CSIRO Hollow Inclusion	19
3.3.1 Instrumentation	19
3.3.2 Remarks on the method	22
3.4 Stress determination	22
3.5 Biaxial Testing	26
3.5.1 Remarks on the method	27

4	Computer codes for stress determination	29
4.1	CSIRO HI-cell	30
4.2	SSPB- cell	30
5	Rock Stress measurements at Äspö	31
5.1	Virgin rock stress measurements	32
5.2	Secondary stress measurements	33
6	Result of the rock stress measurements	34
6.1	Hydraulic fracturing	34
6.1.1	Orientation of the horizontal stresses	35
6.2	Overcoring	37
6.2.1	Uniaxial tests	37
6.2.2	Statistical analyses on the elastic properties	38
6.2.3	Rock stress measurements result	41
6.2.4	Monte Carlo simulation	46
6.3	Study of cores from overcoring	48
6.3.1	General	48
6.3.2	Core mapping	48
6.3.3	Conclusion	54
6.4	The State of Stress at Äspö	54
7	Discussion and conclusions	57
7.1	General	57
7.2	Hydraulic fracturing	57
7.3	Overcoring	58
7.4	Comparison between hydraulic fracturing and overcoring	58
7.5	Variation of the elastic properties	58
7.6	Core mapping	59
7.7	Conclusions	59
7.8	Further work	60
	References	61
	Appendix A	A
	Appendix B	B

List of figures

<i>Figure 1-1. Terminology of rock stresses (Amadei and Stephansson, 1997).</i>	1
<i>Figure 2-1. Fracturing (a) and fracture orientation (b) (Bjarnason, 1986).</i>	5
<i>Figure 2-2. Idealised pressure time curve during hydraulic fracturing Enever et al, 1992).</i>	5
<i>Figure 2-3. Inflection method to determine the shut-in pressure.</i>	7
<i>Figure 2-4. Tangent intersection method to determine the shut-in pressure.</i>	7
<i>Figure 2-5. Hoek and Brown's failure envelopes and stress paths for Equations (2-22) to (2-25) (Ljunggren and Amadei, 1989).</i>	12
<i>Figure 2-6. Pump and water system (Bjarnason, 1986).</i>	15
<i>Figure 3-1. General proceedings for installing when overcoring (Hallbjörn, 1989). The figure shows installation of a SSPB Cell.</i>	16
<i>Figure 3-2. Schematic illustration of the non-automatic probe (Hallbjörn, 1986).</i>	17
<i>Figure 3-3. Strain gauge configuration (Hiltscher et al., 1979).</i>	18
<i>Figure 3-4. Definition of the bearing of the local x-axis relative to the gravitational ball.</i>	18
<i>Figure 3-5. CSIRO HI Cell (Worotnicki, 1993).</i>	20
<i>Figure 3-6. Orientation of the nine strain gauges (Stillborg and Leijon, 1982).</i>	20
<i>Figure 3-7. Position of the twelve strain gauges (Worotnicki, 1993).</i>	21
<i>Figure 3-8. Location and orientation of the twelve strain gauges in a CSIRO HI Cell (Worotnicki, 1993).</i>	21
<i>Figure 3-9. The orientation of a borehole expressed by dip and dip-direction.</i>	26
<i>Figure 3-10. Axial tensile stress in a biaxial loaded core (Worotnicki, 1993).</i>	28
<i>Figure 5-1. The location and orientation of boreholes KA1045A and KA1054A and KA3086A related to the ramp in Äspö HRL. The arrow represents the local Äspö north.</i>	31
<i>Figure 5-2. The location of the boreholes drilled from the surface at Äspö, Leijon (1995).</i>	31
<i>Figure 6-1. Maximum and minimum horizontal stresses in KAS02 with the two zones of mylonite included.</i>	34
<i>Figure 6-2. Maximum and minimum horizontal stress in KAS03.</i>	36
<i>Figure 6-3 The orientation of the maximum horizontal stress in KAS02 and KAS03.</i>	37
<i>Figure 6-4. Box plot of Young's modulus (GPa), n =47 samples.</i>	38
<i>Figure 6-5. Box plot of Poisson's ratio, n=47 samples.</i>	38
<i>Figure 6-6. Density trace for Poisson's ratio.</i>	39
<i>Figure 6-7. Density trace for Young's modulus (GPa).</i>	39

<i>Figure 6-8. Horizontal stresses versus Poisson's ratio.</i>	40
<i>Figure 6-9. Principal stresses versus Poisson's ratio.</i>	40
<i>Figure 6-10. Orientation of the maximum horizontal stress versus Poisson's ratio.</i>	41
<i>Figure 6-11. Minimum horizontal stress, definition of the numbers see Table 6-3.</i>	42
<i>Figure 6-12. Maximum horizontal stress</i>	42
<i>Figure 6-13. Orientation of the maximum horizontal stress versus the depth.</i>	43
<i>Figure 6-14. The average maximum horizontal stress from Table 6-5.</i>	45
<i>Figure 6-15. The average orientation of the maximum horizontal stresses from Table 6-5.</i>	45
<i>Figure 6-16. Confidence interval on the maximum horizontal stress for each borehole obtained from the Monte Carlo simulation. The crosses represent the lower and upper values in the confidence interval.</i>	47
<i>Figure 6-17. Confidence interval for minimum horizontal stress in each borehole obtained from the Monte Carlo simulation. The crosses represent the lower and upper values in the confidence interval.</i>	47
<i>Figure 6-18 BIPS picture taken at the location of stress measurement point #8 in borehole KA3579.</i>	52
<i>Figure 6-19 BIPS picture taken at the location of stress measurement points #2 (left) and #3 (right) in borehole KA3579.</i>	52
<i>Figure 6-20 BIPS picture taken at the location of stress measurement points #4 (left) and #5 (right) in borehole KA3579.</i>	53
<i>Figure 6-21 BIPS picture taken at the location of stress measurement points #6 (left) and #7 (right) in borehole KA3579.</i>	53
<i>Figure 6-22. Maximum horizontal stress versus depth. The mylonite zones at Äspö are included.</i>	54
<i>Figure 6-23. Minimum horizontal stress versus depth.</i>	55
<i>Figure 6-24. The orientation of the maximum horizontal stress versus depth.</i>	56
<i>Figure 7-1. An arbitrary state of stress</i>	57

List of tables

Table 5-1. Information about the virgin stress measurements at Äspö.	32
Table 5-2. Information about the secondary stress measurements at Äspö.	33
Table 6-1. Results from uniaxial testing of rock samples (Delin et al, 1993a, Delin et al. 1993b).	37
Table 6-2. Mean values of Young's modulus and Poisson's ratio for the two overcoring cells.	39
Table 6-3. Definition of the numbers in Figures 6-11 and 6-12.	43
Table 6-4. The stress tensor for each borehole, represented by a mean value and a standard deviation (MPa).	44
Table 6-5. The average principal and horizontal stresses in each of the borehole.	44
Table 6-6. Principal stresses from the Monte Carlo simulation.	46
Table 6-7. The horizontal and vertical stresses obtained from the Monte Carlo simulation.	46
Table 6-8 Boreholes in which cores have been studied.	48
Table 6-9 Observations and comments on the measurement point in the cores (KA1054 – KA2510).	50
Table 6-10 Observations and comments on the measurement point in the cores (KA2870 – KA3579).	51

1 Introduction

1.1 Classification of rock stresses

Rock stresses can be divided into *in-situ* stresses and induced stresses. *In-situ* stresses are called natural, primitive or virgin stresses and exist in the rock prior to any disturbance. Induced stresses are related to artificial disturbance (excavation, drilling, pumping). These stresses can also be induced by changing of natural conditions (swelling, drying etc.).

The current *in-situ* stresses in a rock mass are the cumulative product of events in the geological history. Several authors have proposed different terminology for *in-situ* stress, which are summarised by Amadei and Stephansson (1997). The *in situ* stresses can be divided into four groups of origin, gravitational, tectonic, residual and terrestrial stresses (Figure 1-1).

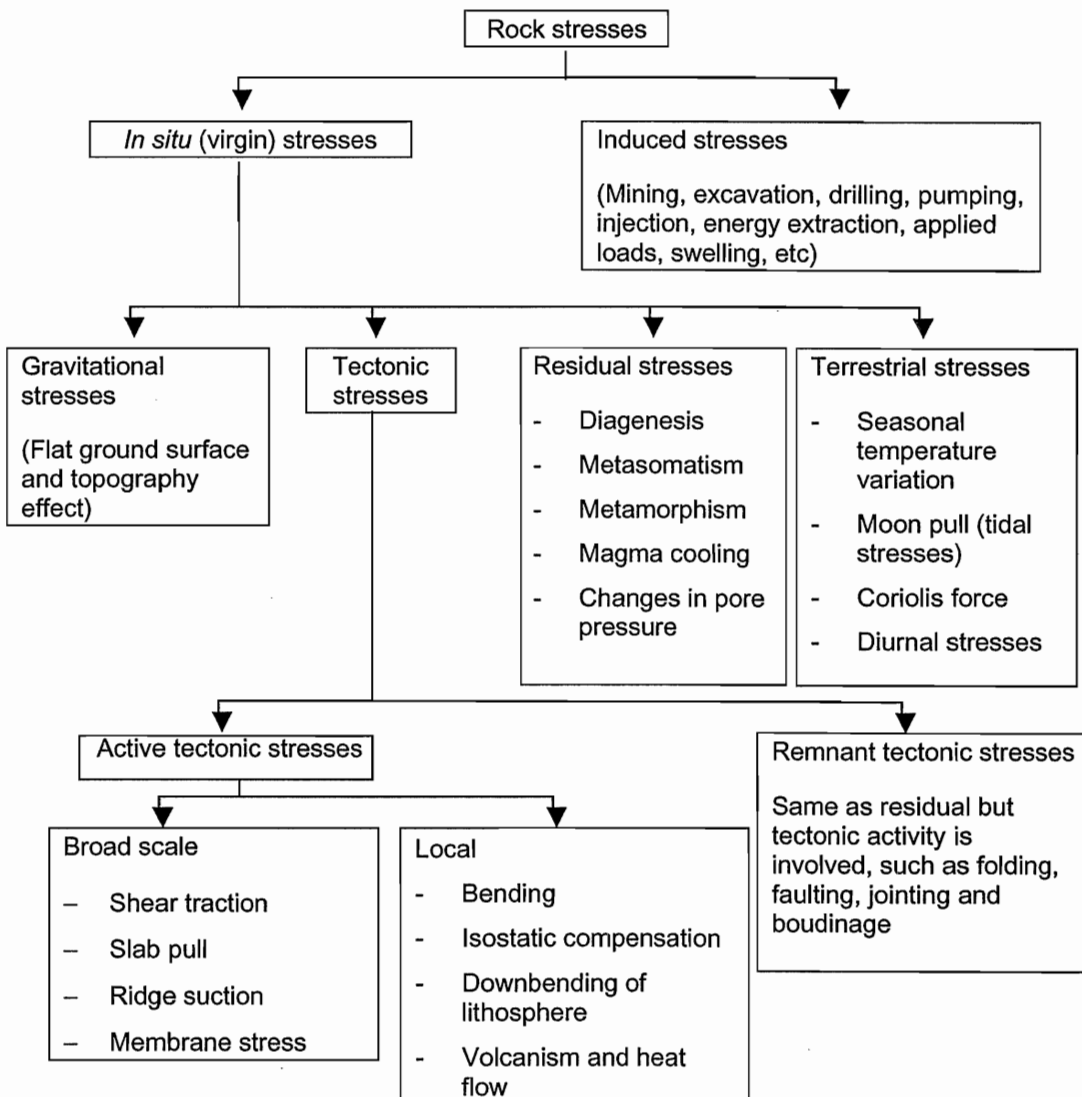


Figure 1-1. Terminology of rock stresses (Amadei and Stephansson, 1997).

The definition of induced stresses is that they are stress changes due to removal or addition of material. These induced stress changes are superimposed on the natural stresses that exist before the excavation. The result of this superposition will be named secondary rock stresses, whereas the *in-situ* stresses will be named virgin stresses in this report.

1.2 Äspö Hard Rock Laboratory

The Äspö Hard Rock Laboratory (HRL) constitutes an important part of the work of developing a deep repository and developing and testing methods for investigation and licensing a suitable site (SKB Technical Report 97-06). The laboratory is located in the area of Simpevarp in the municipality of Oskarshamn in the south of Sweden. In 1990 the excavation of the ramp started. The ramp, which is about 3600 metres, was continued down to 450 metres below ground surface. The first part was excavated by a conventional drill and blast method, while a Tunnel Boring Machine (TBM) excavated the last 400 metres.

The process of choosing a site for a nuclear waste repository means that many aspects have to be taken into consideration. One of these is that the repository has to be mechanically stable for a long time. The mechanical stability of the rock is very difficult to determine. One of several parameters, which determine the mechanical stability, is the virgin state of stress, and another is the strength of the rock mass.

While measuring the rock stresses a set of aspects and conditions influence the results e.g.;

- the accuracy in measurements
- heterogeneity or anisotropy of the rock mass
- level of measurement confidence (mean-values and variance)
- how representative the measurements are for the whole rock volume
- degree of subjectivity in the interpretation of the results

One of the research goals stated in RD&D Programme 92 is to enhance the level of confidence and understanding of how representative the stress measurements are for the whole rock mass. A database of the rock stress measurement results has been compiled (RD&D Programme 95). Another topic of concern is the different values obtained with different measurement techniques, a topic, which was raised in (RD&D Programme 95) and commented as follows.

“A comprehensive analysis of the rock stress condition at Äspö is needed to give a clear explanation of the significant difference between the rock stress magnitude measured from the surface and from the tunnel”.

Rock stress measurements were conducted in the pre-investigation phase. Three deep boreholes were drilled from the surface of Äspö. In two of these hydraulic fracturing tests were performed at varying depths. In the last borehole, overcoring measurements were done at two different depths by the method developed by The Swedish State Power Board (SSPB).

During the excavation of the ramp a number of overcoring measurements were made. The stress measurements in the ramp were mainly made to evaluate the prediction of the stress measurements made during the pre-investigation phase. The measurements in the

tunnel were made in short boreholes and the CSIRO Hollow Inclusion cell was mainly used except for a few boreholes where the SSPB-cell was used.

1.3 Objectives

This report is one of two, which are made in a licentiate work at Luleå University of technology and the Division of Rock Mechanics. The project aim at learning more about the accuracy of the stress measurements made in the Äspö Hard Rock Laboratory and at correlating the rock stresses to the geology. The main objectives of the project are

- to establish the state of stress at Äspö
- to correlate rock stresses with local as well as regional geology
- to investigate the reliability of the measuring data

The first part is to define the state of stress at Äspö Hard Rock Laboratory. This is done based on earlier rock stress measurements conducted during the years 1988 to 1997. Two different measurement techniques have been used, hydraulic fracturing and overcoring. During the overcoring two types of cells have been used, CSIRO HI-cell and a cell developed by the Swedish State Power Board (SSPB).

Since this is a part of a licentiate work, a major part of the report is a theoretical study of the measurement techniques.

2 Hydraulic fracturing

In the 50s, hydraulic fracturing was introduced as a method to stimulate the flow of oil and gas towards the production-holes inside an oil or gas-field. The use of the method increased rapidly, and about 100.000 individual treatments were performed before 1955. Today, the method is still widely used for well production stimulation. During this period the fracture process was poorly understood. Even if the use of hydraulic fracturing for stress determination differs from the well treatment, the basic concept of creating fractures in the borehole wall and propagating them into the rock mass is identical.

In 1957 the classic paper of Hubert and Willis "Mechanics of Hydraulic Fracturing" was published. The paper was based on the theoretical studies of the state of stress underground and the stress field around a vertical borehole in elastic rock. In their paper, they presented the relationship between the breakdown pressure, the stresses acting in the plane perpendicular to the borehole and the tensile strength of the rock. The paper also concluded that the fracture should be formed perpendicular to the least principal stress. In tectonically relaxed areas characterised by normal faulting, the least principal stress should be horizontal.

In the early sixties, Kehle (1964) among others discussed the implications of hydraulic fracturing with regards to the stresses and the orientation of the induced fractures. Since then, the use of the method for rock stress measurements increased gradually and is now used worldwide.

The first hydraulic fracturing measurements in Sweden were conducted in 1981 in the Stripa Mine (Doe et al., 1983)

2.1 Test procedure

To avoid macroscopic fractures in the test section, the cores from the borehole are examined and a test section is chosen.

The straddle packers are lowered to the chosen test section, see Figure 2-1a. To avoid high stress concentrations at the ends of the test section the straddle packer and the test section are pressurised simultaneously. The straddle packers have slightly higher pressure than the pressure applied in the test section through the test cycle.

The water pressure, which is generated by a pump, is then increased until there is a sudden drop in the recorded pressure. This indicates that a fracture has been induced in the borehole wall. Directly after the borehole breakdown, the test line is shut down and the hydraulic circuit is closed. The pressure in the borehole decreases to a stable level called the shut-in pressure. This shut-in pressure is usually recorded during 3 to 4 minutes to assure that the pressure is stable. After this, the test section is then drained.

In all, two or three cycles are conducted at the same constant flow rate. At every cycle, the fracture is reopened and extended and the pumping time is increased. The reason for performing several pressurisation cycles is to extend the fracture far enough from the borehole to avoid the stress field being influenced by the borehole. An idealised pressure-time curve of the testing can be seen in Figure 2-2.

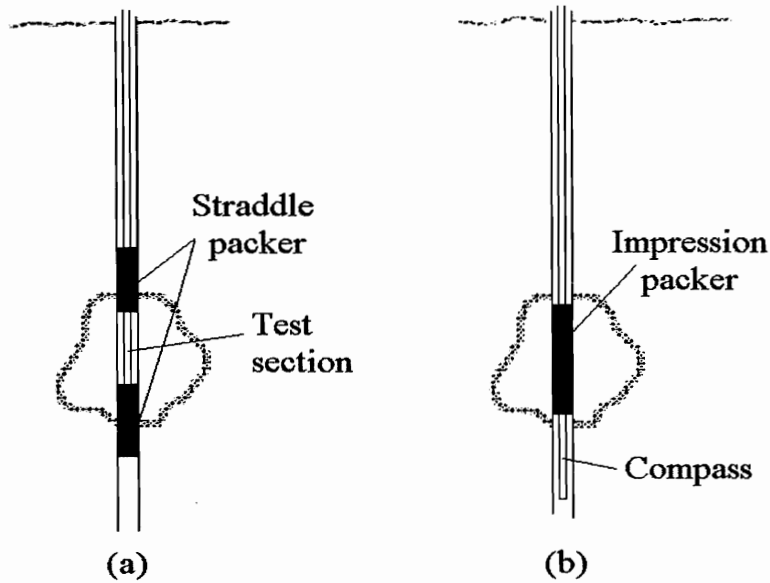


Figure 2-1. Fracturing (a) and fracture orientation (b) (Bjarnason, 1986).

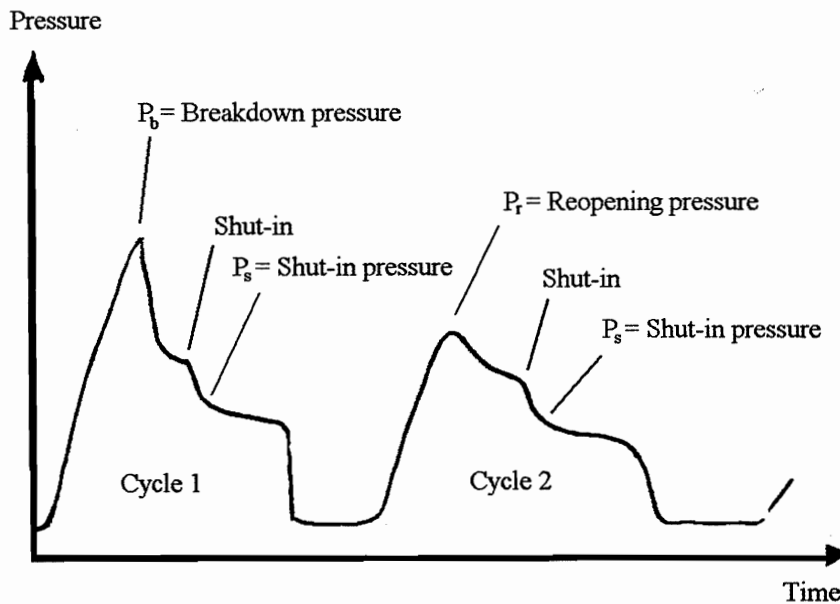


Figure 2-2. Idealised pressure time curve during hydraulic fracturing (Enever et al, 1992).

Fracture impressions are conducted at the test points with satisfying results, Figure 2-1b. The impression packer is lowered to the test point and pressurised for 30 – 40 minutes. During this time the impression packer measures the orientation of the hydraulic fracture in the borehole wall by squeezing a soft rubber into the fracture. Beneath the impression packer, a single-shot magnetic compass and a borehole camera are fixed. This compass measures the orientation of the impression packer during the impression period. Other borehole and surface geophysics devices can also be used to determine the orientation and inclination of the hydraulic fracture (Haimson, 1978). A borehole TV camera containing a magnetic compass has been evaluated to detect and locate

hydraulic fractures (Bjarnason et al., 1989). There is also some ongoing research to apply BIPS-images to determine the orientation of fractures in boreholes (Johansson, 1999).

During the hydraulic fracturing the downhole pressure in the test section and the packers are continuously recorded. Since it can be a loss of friction in the cable due to the flow rate, the test section pressure is also measured at the surface. In addition, the flow rate to the test section is also measured.

2.2 Data evaluation and interpretation

During the pressurisation cycles the pressure versus time is recorded Figure 2-2. From the pressure curve, the breakdown pressure, shut-in pressure and reopening pressure are evaluated. In reality the pressure record is not as idealised as in Figure 2-2. This means that it is very difficult to determine the shut-in pressure as well as the breakdown and reopening pressures. Different interpretation methods are available and will be explained in following sections.

2.2.1 Interpretation of the breakdown and reopening pressures

By examining the first cycle at the part of the curve where the pressure is increasing, interpretation of the breakdown pressure is made. The point at which the curve is deviating from linearity is defined as the breakdown pressure.

The procedure to interpret the reopening pressure is the same as for breakdown pressure, except that the second, third and eventually a fourth cycle are examined. The value of the breakdown pressure is defined as the point at which the curve is deviating from linearity.

2.2.2 Interpretation of the instantaneous shut-in pressure

The shut-in pressure is the lowest pressure capable of maintaining the fracture open against the far-field least horizontal stress. Determination of the shut-in pressure is done when a distinct break is observed after the fast pressure-decline that follows the pump shut-off, see Figure 2-3. However, the pressure is often decreased gradually and therefore the shut-in pressure is indistinct.

There exist several interpretation methods to determine the shut-in pressure from the pressure-time curve. Most of these are graphical and the best known ones are the inflection point method (Gronseth, 1982) and the tangent intersection method (Enever and Chopra, 1986). Both these interpretation methods can be based on pressure-time curve as well as modified pressure-time curves. These modified pressure-time curves can be

- pressure vs. $\log(t)$ (Doe et al., 1983),
- $\log(\text{pressure})$ vs. $\log(t)$ (Zoback and Haimson, 1982),
- pressure versus $\log(T/(T-T_0))$ (McLennan and Roegiers, 1983),
- the Muskat method (Aamodt and Kuriyagawa, 1983).

Hayashi and Sakurai (1989) compared different modified pressure-time curves and found that the interpretation based on pressure vs. $\log(t)$, $\log(\text{pressure})$ vs. $\log(\text{time})$ and pressure vs. $\log(\text{time}/\text{time after shut in})$ plots gave approximately the same shut-in pressure and that the Muskat method gave less reliable results.

Inflection point method

In this method the tangent to the pressure vs. time curve is drawn for a time immediately after the shut-in Figure 2-3. The instantaneous shut-in pressure is then the pressure where the tangent line diverges from the curve. If the divergence is not well defined, a second tangent line is drawn at a slightly greater time. The shut-in pressure is then defined at the intersection between the two tangent lines.

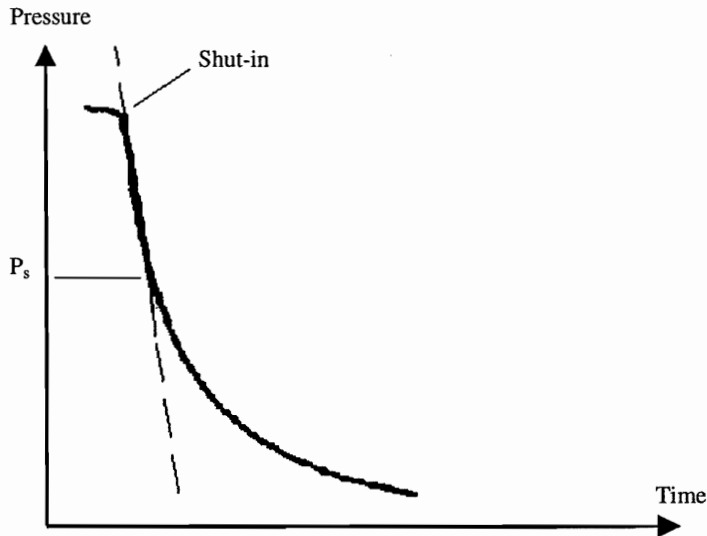


Figure 2-3. Inflection method to determine the shut-in pressure.

Tangent intersection method

The shut-in pressure is defined as the intersection of the tangent to the pressure curve immediately after shut off and the tangent of the stable section of the curve (Figure 2-4).

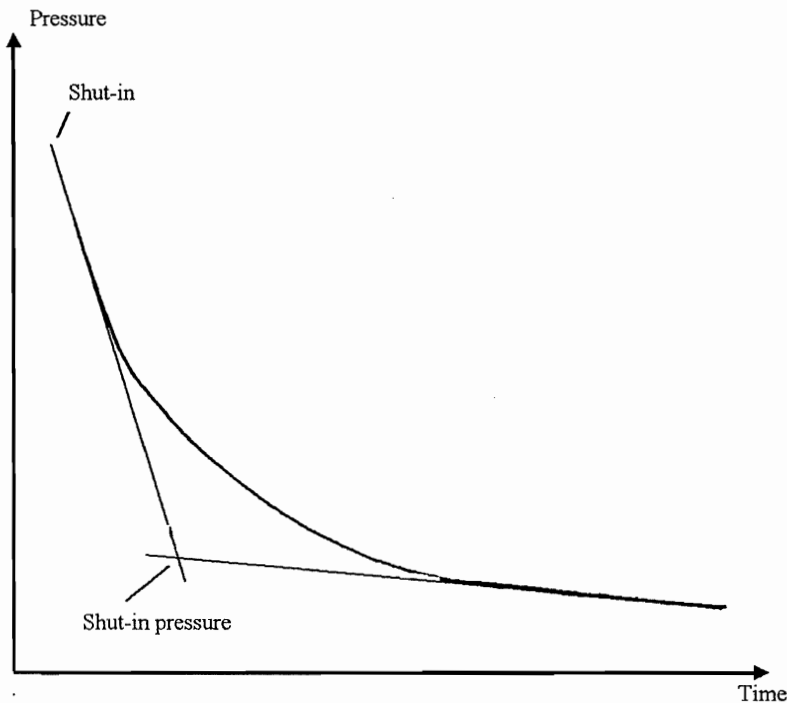


Figure 2-4. Tangent intersection method to determine the shut-in pressure.

Interpretation of tensile strength

There are several approaches to determine the tensile strength. One of these approaches is to determine the tensile strength, T_{app} , by realistic laboratory tests on cores from the test section of the actual borehole. Another approach is to determine the field tensile strength, T_f , by carrying out several cycles to reopen the fracture (Bjarnason et al. 1989). In the last method, the tensile strength is determined by subtracting the reopening pressure, P_r , from the breakdown pressure, P_c . This method assumes that when a fracture is initiated, the tensile strength of the rock has vanished at that point. In other words, when reopening the fracture a lower pressure is required than when the fracture was initiated.

2.3 Stress determination

When the test section is pressurised by a fluid, usually water, a tensile fracture will be induced in the borehole wall. The initiated fracture is in most cases oriented parallel to the borehole axis. Fractures, which are perpendicular to the borehole axis, can occur at certain stress conditions. In the last case the usual formulas can not be used. Section 2.3.1 will deal with the case of fracture parallel to the borehole axis and Section 2.3.2 can be applied to both types of fractures.

2.3.1 Fracture parallel to the borehole axis

In most cases when the method is used to determine the virgin stresses before excavation, the borehole is drilled vertically. The assumption for a vertical borehole is that one of the principal stresses is parallel to the borehole axis, and equal to the weight of the overburden.

$$\sigma_v = \gamma z \quad 2-1$$

where z is the depth from the surface to the test section.

The stresses around the pressurised borehole can be determined by Kirsch solution (Jaeger and Cook, 1979) and since most of the rock formation in Sweden is impermeable the effect of the pore pressure can be neglected.

$$\sigma_\theta = \frac{\sigma_H + \sigma_h}{2} \left(1 + \frac{R^2}{r^2} \right) - \frac{\sigma_H - \sigma_h}{2} \left(1 + \frac{3R^4}{r^4} \right) \cos 2\theta - P_i \quad 2-2$$

$$\sigma_r = \frac{\sigma_H + \sigma_h}{2} \left(1 - \frac{R^2}{r^2} \right) + \frac{\sigma_H - \sigma_h}{2} \left(1 - \frac{4R^2}{r^2} + \frac{3R^4}{r^4} \right) \cos 2\theta - P_i \quad 2-3$$

$$\sigma_{r\theta} = -\frac{\sigma_H - \sigma_h}{2} \left(1 + \frac{2R^2}{r^2} - \frac{3R^4}{r^4} \right) \sin 2\theta - P_i \quad 2-4$$

where

σ_θ = tangential stress

σ_r = radial stress

$\sigma_{r\theta}$ = shear stress

σ_h = minimum horizontal stress

- σ_H = maximum horizontal stress
- R = borehole radius
- r = distance from the centre of the borehole
- θ = angle measured counter-clockwise from the orientation of the maximum horizontal stress
- P_i = internal pressure in the borehole

When the borehole is pressurised, a fracture will be induced at the borehole wall ($r = R$). The fracture will propagate perpendicular to the minor horizontal stress orientation ($\theta = 0^\circ, 180^\circ$), resulting in a vertical fracture (Hubbert and Willis, 1957). The tangential and radial stresses at that point on the borehole will be,

$$\sigma_\theta = 3\sigma_h - \sigma_H - P_i \quad 2-5$$

$$\sigma_r = P_i \quad 2-6$$

The initiation of the fracture occurs when the tangential stress exceeds the tensile strength, T , of the rock.

$$\sigma_\theta = -T \quad 2-7$$

At this moment the internal pressure, P_i , is called the breakdown pressure, P_c . By combining the Equations (2-5) and (2-7), the breakdown pressure can be expressed as

$$P_c = 3\sigma_h - \sigma_H + T \quad 2-8$$

However, this requires that the tensile strength of the rock is known. The tensile strength is determined by a realistic laboratory test on a core from the specific test section and is designated T_{app} . The test method should resemble the hydraulic fracturing field test as much as possible. The least horizontal stress, σ_h , is assumed to be equal the shut-in pressure, P_s and therefore the maximum horizontal stress can be determined using the relation

$$\sigma_{HI} = 3\sigma_h - P_c + T \quad 2-9$$

The above-described procedure to determine the stresses is called the first breakdown method.

If the circumstances are such that it is not possible to determine the tensile strength of the rock, the second breakdown method can be used instead. This method relies on the assumption that there is no tensile strength in the rock mass when the fracture is reopened. Therefore, the field tensile strength, T_f , is said to be the difference between the breakdown and reopening pressures, P_r .

$$T_f = P_c - P_r \quad 2-10$$

By substituting P_i with P_r in Equation 2-5 and using the relation $T = 0$ in Equation 2-7 the maximum horizontal stress can then be expressed as

$$\sigma_{HII} = 3\sigma_h - P_r \quad 2-11$$

2.3.2 Fractures parallel or perpendicular to the borehole axis

Sometimes a horizontal fracture is initiated at the wall of a vertical borehole. If this occur another approach has to be used to determine the rock stresses. Ljunggren and Amadei (1989) presented a theory to determine the *in situ* stresses when the hydrofractures are either vertical or horizontal. The theory is also based on Kirsch solution in (Jaeger and Cook, 1979). The tangential, the radial and the vertical stresses at the wall of a vertical borehole is therefore,

$$\sigma_{\theta} = 3\sigma_h - \sigma_H - P_i \quad 2-12$$

$$\sigma_r = P_i \quad 2-13$$

$$\sigma_z = \sigma_{z0} - 2\nu(\sigma_H - \sigma_h) \quad 2-14$$

where σ_{z0} is the vertical virgin stress, assumed to be equal to the weight of the overlying rock and ν is Poisson's ratio. The maximum and minimum principal stresses, σ_1 and σ_3 , at failure are according to Hoek and Brown, (1981),

$$\sigma_1 = \sigma_3 + \sqrt{m\sigma_c\sigma_3 + \sigma_c^2} \quad 2-15$$

where σ_c is the uniaxial compression strength and m is an empirical material constant.

By substituting $\sigma_1 = 0$ and $\sigma_3 = -T$ in the Equation 2-15, the uniaxial strength, T , of the intact rock can be expressed as

$$T = \frac{\sigma_c}{2} \left[\sqrt{m^2 + 4} - m \right]. \quad 2-16$$

If the empirical constant m is not known, Equation 2-16 can be rewritten so that m is expressed in terms of the tensile strength and the uniaxial compression strength

$$m = \frac{\sigma_c}{T} - \frac{T}{\sigma_c}. \quad 2-17$$

The tensile strength is either determined through laboratory tests, T_{app} or directly evaluated from the hydraulic fracturing test in the field, T_f .

Tensile fracturing can occur as a vertical or a horizontal fracture when either σ_θ or σ_z in Equations 2-12 and 2-14 is tensile. Depending on the ordering of σ_z , σ_θ and σ_r , six possible combinations exist. Since fracturing occurs when σ_z or σ_θ is the minor principal stress, only four combinations are interesting,

1. $\sigma_z > \sigma_r > \sigma_\theta$;

$$\sigma_z = \sigma_\theta + \sqrt{m\sigma_c\sigma_\theta + \sigma_c^2} \quad 2-18$$

2. $\sigma_r > \sigma_z > \sigma_\theta$;

$$\sigma_r = \sigma_\theta + \sqrt{m\sigma_c\sigma_\theta + \sigma_c^2} \quad 2-19$$

3. $\sigma_r > \sigma_\theta > \sigma_z$;

$$\sigma_r = \sigma_z + \sqrt{m\sigma_c\sigma_z + \sigma_c^2} \quad 2-20$$

4. $\sigma_\theta > \sigma_r > \sigma_z$;

$$\sigma_\theta = \sigma_z + \sqrt{m\sigma_c\sigma_z + \sigma_c^2} \quad 2-21$$

Substituting Equations 2-12- 2-14) into Equations 2-18-2-21 the maximum horizontal stress can be determined. The minimum horizontal stress is equal to the shut-in pressure as earlier and P_i represents the breakdown pressure when fracturing occurs.

1. $\sigma_{zo} - 2\nu(\sigma_H - \sigma_h) > P_i > 0 > 3\sigma_h - \sigma_H - P_i$;

$$\sigma_{zo} - 2\nu(\sigma_H - \sigma_h) = 3\sigma_h - \sigma_H - P_i + \sqrt{m\sigma_c(3\sigma_h - \sigma_H - P_i) + \sigma_c^2} \quad 2-22$$

2. $P_i > \sigma_{zo} - 2\nu(\sigma_H - \sigma_h) > 3\sigma_h - \sigma_H - P_i$;

$$P_i = 3\sigma_h - \sigma_H - P_i + \sqrt{m\sigma_c(3\sigma_h - \sigma_H - P_i) + \sigma_c^2} \quad 2-23$$

3. $P_i > 3\sigma_h - \sigma_H - P_i > \sigma_{zo} - 2\nu(\sigma_H - \sigma_h)$;

$$P_i = \sigma_{zo} - 2\nu(\sigma_H - \sigma_h) + \sqrt{m\sigma_c(\sigma_{zo} - 2\nu(\sigma_H - \sigma_h)) + \sigma_c^2} \quad 2-24$$

4. $3\sigma_h - \sigma_H - P_i > P_i > 0 > \sigma_{zo} - 2\nu(\sigma_H - \sigma_h)$;

$$3\sigma_h - \sigma_H - P_i = \sigma_{zo} - 2\nu(\sigma_H - \sigma_h) + \sqrt{m\sigma_c(\sigma_{zo} - 2\nu(\sigma_H - \sigma_h)) + \sigma_c^2} \quad 2-25$$

The failure envelope of the Hoek-Brown failure criterion and the stress path when P_i increases is illustrated in Figure 2-5. Stress relations in Equation 2-22 and 2-23 result in a vertical fracture as P_i increases while Equation 2-24 results in a horizontal fracture. Since the stress path does not reach the failure envelope in the last case in Equation 2-25 no fracturing occurs.

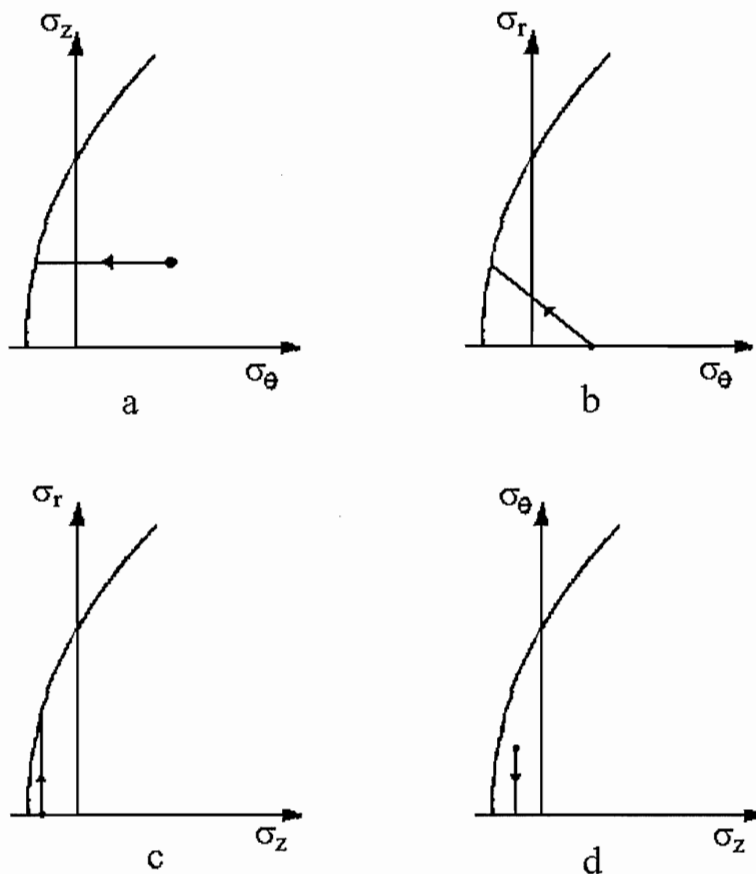


Figure 2-5. Hoek and Brown's failure envelopes and stress paths for Equations (2-22) to (2-25) (Ljunggren and Amadei, 1989).

2.4 Remarks on the method

The assumptions that are made in hydraulic fracturing might in one way or the other contribute to error in the stress determination. The assumption that the rock is an isotropic, homogeneous elastic medium might lead to an incorrect determination of σ_H . At some measurements a wide scatter in the fracture orientation has been observed, particularly when low injection rates were used. The fracture initiation might be influenced by weakness planes in the rock mass (bedding planes, healed fractures) (Baumgärtner and Rummel, 1989). The pre-existing weakness planes can even obliterate the interpretation method (Cornet, 1983). The interpretation of the horizontal stresses can also be influenced by the assumptions that the borehole is parallel to one of the principal stress directions and the fracture remains planar as it propagates away from the borehole. Ignorance of the mechanics of fracture initiation and fracture extension in the conventional method of calculating can contribute to error of the maximum compressive in-situ stress (Abou-Sayed et al., 1978).

McLennan and Roegiers (1981) have summarised factors that can complicate interpretation of instantaneous shut-in pressures. These factors can be leak-off,

equipment, packer bypass, fracture inclination and change in fracture orientation. Leak-off might occur in permeable formations, where fluid can migrate into secondary fractures, which intersect the primary hydraulic fracture. The next two, equipment and packer bypass, occur due to leakage in the mechanical pressurisation system or imperfect seating of the packers. Pressurisation of an inclined fracture results in a secondary principal stress that may not be an indication of the true principal stress. The last factor reflects the idea that the propagation of the fracture will tend to adjust to an optimum orientation. There are two cases where this is critical,

1. Where significant geological control is developed (extreme foliation, well-developed bedding, weak inter-beds and discontinuities).
2. Where the vertical stress is less than the minimum horizontal stress, there are strong indications that the initial created fracture would be along the borehole axis and then reorient itself to a more favourable orientation. Consequently, shut-in pressure is going to be anomalous.

The first point can indicate that the geological control may be more dominant than the stress control.

Klasson (1989) carried out a comparative study of different graphical interpretation techniques for the shut-in pressure. He showed that there could be a considerable mismatch between shut-in pressure calculated by different intersection methods. Though the tangent intersection method produces the lowest shut-in pressures no graphical method is superior.

The difference between the initial breakdown and fracture reopening pressure is taken to be the hydraulic fracture strength. Development of this method requires the assumption that the state of stress around a borehole during pressurisation is the same with and without the fracture (Ratigan, 1992). In this paper, Ratigan concluded that the fracture reopening pressure is a function of fracture geometry, pumping rates and fracturing fluid and the *in situ* stresses. However, the second breakdown method can be appropriate in certain situations, like

- Slow pumping, low viscous fluid, initial crack length is greater than four or five borehole radii and horizontal stress ratio, K_o is equal to two.
- Fast pumping, high viscous fluid, initial crack length is less than one-borehole radius.

For other situations the reopening pressure is a complex function of the above stated factors.

2.5 Equipment used at Äspö

Special equipment was used for the measurements at Äspö. The instrumentation consists of several units and is fully described in (Bjarnason, 1986) and (Bjarnason and Torikka, 1989). All units are fixed on a truck and powered by the truck engine.

2.5.1 Downhole packer assemblies

The pair of straddle packers is about 90 cm each and isolates a 65-cm long test section. To avoid the packers to elongate during pressurisation the packers are equipped with an internal piston.

The impression packer has a length of 1 to 3 metres. The impression packer measures the orientation of the hydraulic fracture in the borehole wall by squeezing a soft rubber into the fracture. Beneath the impression packer, a single-shot magnetic compass and a borehole camera are fixed. This compass measures the orientation of the impression packer during the impression period.

2.5.2 Pump and water system

The water system includes a 100 MPa water pump that generates the pressure that is required to fracture the rock. The maximum peak pressure of the system is 80-90 MPa, which is considered adequate for the maximum stress magnitudes expected at 1000 metres depth. The maximum flow rate in the hose is restricted to 7-8 l/min, but fracturing is usually done at a constant flow rate of 3.5 l/min. Two bypass valves are used to adjust the pressure in the system.

The packer pressure and the test section pressure are controlled separately by the manifold, which consists of one inlet and four outlets. Two outlets, where the first controls the test line and the second controls the packer line. One outlet also controls the water back to the water tank during venting of the fracture or from packer depressurisation. The fourth outlet is used to control the atmospheric pressure for zero adjustment for pressure transducers, see Figure 2-6.

The water tank contains 900 litres of water. All water is led back to the tank to minimise water consumption.

2.5.3 Multihose drum and feeder

The multihose is 1000 metres long and consists of three high-pressure hoses with the internal diameter of 8, 8 and 10 mm, one 16 mm wire signal cable and one wire that carries the load from the downhole assemblies. The hose is run up and down in the hole by a hydraulically driven drum. During fracturing, the packers are pressurised through one of the 8-mm hoses and the test section is pressurised by the 10-mm hose.

The advantage of this multihose is that there is less risk of getting stuck, since all components are kept together. Simplicity and efficiency are two other important advantages. One of the disadvantages is that there is high initial cost. The manufacturing of the multihose is specialised work, and once finished no changes can be made to the design or performance. Since the multihose is expensive, it is connected to the downhole assemblies by a weak tension link, which can be torn off in case of it getting stuck. Two other disadvantages are flow-dependent pressure drops in the test lines and the low stiffness of the system (Bjarnason and Torikka, 1989).

2.5.4 Data recording system

The system that is recording the pressure and the fluid rates consists of several parts. First, there is an interface box that collects all data. Connected to this box are the downhole pressure gauges, both for the test section and the packers. The surface pressure gauge, the flow meter and the time based strip-chart recorder (4 pens) are also connected to the interface box.

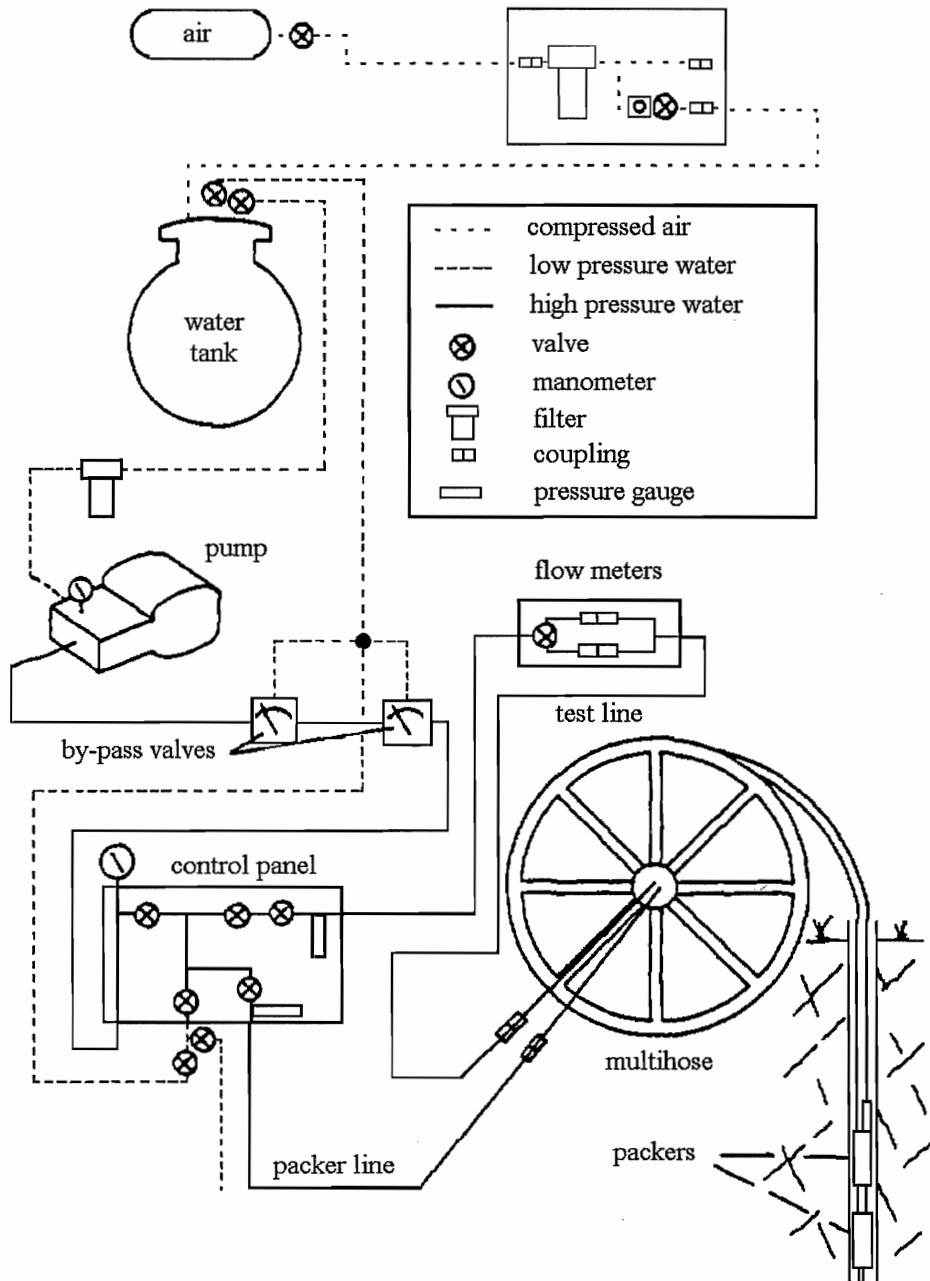


Figure 2-6. Pump and water system (Bjarnason, 1986).

3 Overcoring

3.1 General

A borehole with a diameter of about 76-86 mm is drilled to the desired depth (Figure 3-1). The core detaches perpendicular to the borehole axis if the last bit of the core is pulled and not twisted.

A smaller drill is then centred with high precision at the bottom of the larger borehole. A long borehole with a diameter of about 36 mm is drilled. This core is then examined to see if the test section is suitable for measurements. The test section should be free from joints and an intact core of 200 mm indicates a suitable test section (Worotnicki, 1993). When a single joint exists in the core, great care has to be taken when placing the gauge. The core could break behind the cell during overcoring and then the broken part would start to rotate.

The borehole must then be washed properly to avoid particles on the borehole wall that can disturb the gluing. After overcoring, by a diamond drill, the bottom of the core and the glue pot can be investigated to see if the installation was successful.

When the gauge is in the right position the glue is released either by the piston which squeezes out the glue or by the glue pot is being pushed away. The piston and the glue pot are triggered off by the wooden rod or by releasing pins. During the hardening time, orientation of the strain gauge is measured. When the overcoring is finished the hollow core is hoisted to the surface.

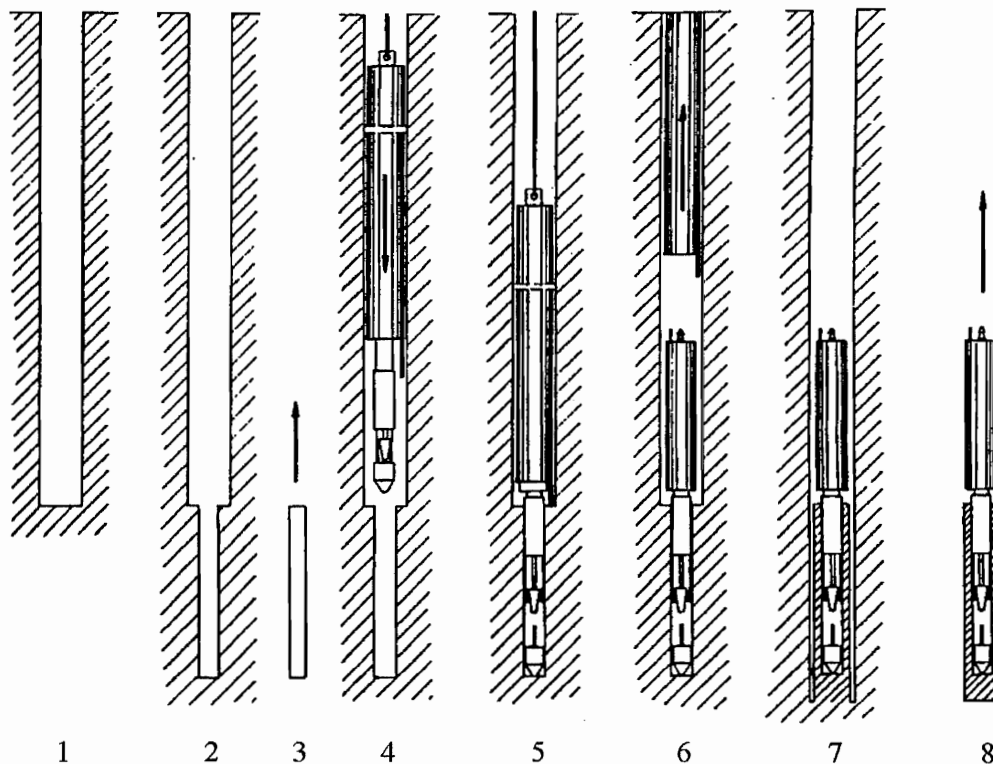


Figure 3-1. General proceedings for installing when overcoring (Hallbjörn, 1989). The figure shows installation of a SSPB Cell.

3.2 Swedish State Power Board Triaxial gauge

The method is based on the method of Leeman and Hayes (1966). This automatic probe, Borre, is a development of the Hiltcher SSPB-gauge (Hiltcher et al., 1979). The Hiltcher SSPB-gauge is described in Hallbjörn (1986) and the method of the automatic probe is described in Hallbjörn et al. (1989).

3.2.1 Instrumentation

The method is based on a computerised probe, a carrying cable and a drilling unit. A winch and a motor driven drum operate the cable. After the measurements, the probe is connected to a personal computer.

Probe

The Swedish State Power Board developed the computerised probe in 1989. The advantage of this probe is that the strain and the temperature can be measured automatically and continuously before, during and after the overcoring. No connections are needed to the surface.

Connected to the computerised probe is an adapter that consists of a compass and a weight. The magnetic compass contains a fluid, which freezes at temperatures below $+15^{\circ}$ Celsius. This will fix the position of the compass needle when the strain gauges are cemented and the relation between the needle and the gauges can be read off later.

The probe itself consists of a pot of glue, a strain gauge set, a cone and a logger unit (Figure 3-2). The cone is pressed down in the pot of glue.

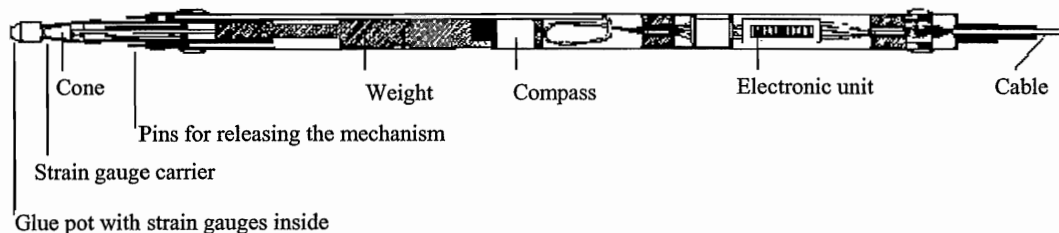


Figure 3-2. Schematic illustration of the non-automatic probe (Hallbjörn, 1986).

Glue

Depending on the rock temperature the pot contains either a two-component acrylic resin or a two-component epoxy resin. The second resin is used when the rock temperature is above $+10^{\circ}$ C. It is also used if the cementing is done overnight. The epoxy resin has a very slow hardening, while the acryl resin has a pot life of about 20 minutes. Regulating the amount of the catalyst easily controls the hardening of the acryl resin.

Strain gauge

The strain gauge set consists of nine strain gauges distributed among three rosettes. Each of the rosettes, which are separated by 120 degrees, is placed on a plastic tongue (Figure 3-3). The nine gauges are orientated in three directions, longitudinal, transverse and at 45 degrees to the borehole axis. The plastic tongues are pushed to the borehole wall by the cone and the gauges are cemented to the rock. The borehole axis, z, is in the paper.

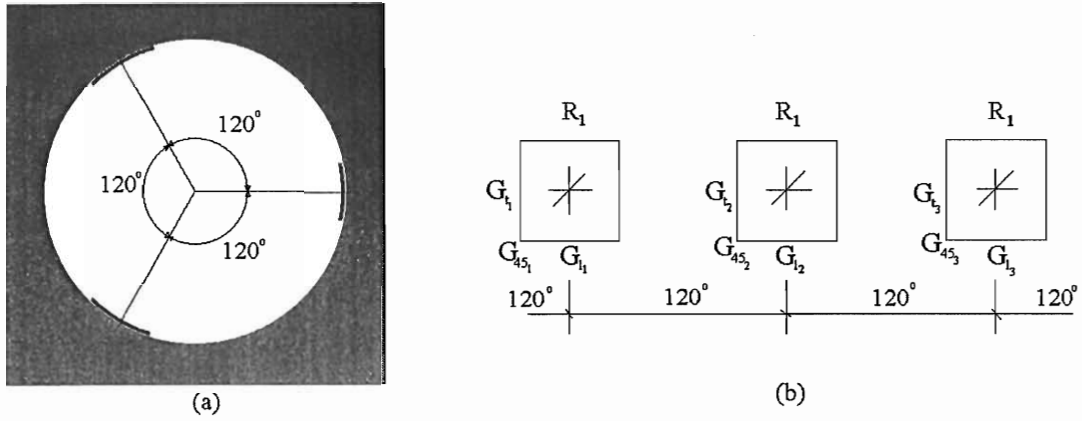


Figure 3-3. Strain gauge configuration (Hiltscher et al., 1979).

The orientation of the local x -axis is determined by a compass (vertical borehole) or by a gravitational ball (inclined borehole), see Figure 3-4.

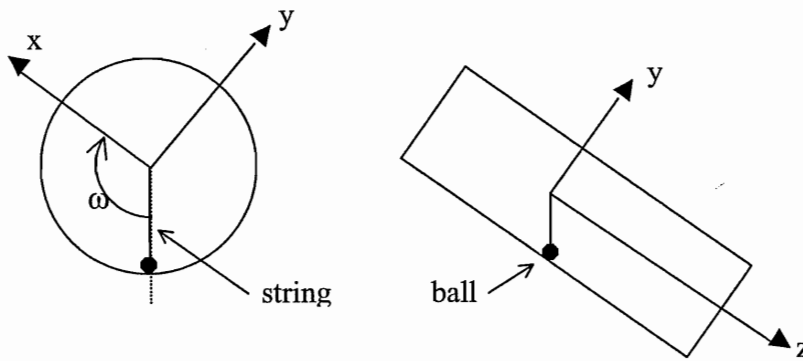


Figure 3-4. Definition of the bearing of the local x -axis relative to the gravitational ball.

The transformation from the cell stress system to the regional system is made in two steps. The first step is to transform the stress around the cell to the local system by using the bearing from the gravitational ball. The x -axis of the local system is horizontal and y -axis is vertical and positive upward.

$$[\sigma]_{cell} = [b][\sigma]_{x0}[b]^t \quad 3-1$$

where

$$[b] = \begin{bmatrix} \cos(\omega - 90) & \sin(\omega - 90) & 0 \\ -\sin(\omega - 90) & \cos(\omega - 90) & 0 \\ 0 & 0 & 1 \end{bmatrix} \quad 3-2$$

3.2.2 Remarks on the method

Hiltscher et al. (1979) has mentioned a number of problems when measuring in water filled boreholes. However, not all of them are due to the water but are only strictly geometrical. For example one geometrical problem is the difficulty to correlate the cylindrical surface of the borehole and the strain gauge and its carrier exactly. With a rubber intermediate layer, the pressure on the glue will not be uniform and result in a bad quality of the glue layer. If an intermediate layer of a plastically deformable substance is used this will result in a uniform distribution of the pressure. The intermediate layer is thicker in the middle than at the ends and the pressing out of glue and water will therefore start in the middle of the rosette.

To obtain reliable results in the gluing, the borehole must be a perfect circular cylinder. The borehole wall must also be absolutely smooth and free from undulations. This can be achieved if the small diamond drill is centred exactly (± 0.5 mm) with a special device and by using a reaming shell.

3.3 CSIRO Hollow Inclusion

CSIRO in Australia developed the Hollow Inclusion (HI) in 1972 –1973. The method is described in Stillborg and Leijon (1982) and Worotnicki (1993). The first stress measurements performed in 1992 at Äspö where the nine-strain gauges cell was used, refer to the former reference. The later reference is a more general description of the method.

3.3.1 Instrumentation

The instrumentation consists of a HI stress cell including epoxy resin and drilling equipment.

HI stress cell

The hollow inclusion stress cell itself consists of a number of components, see Figure 3-5. The main components are an epoxy resin pipe, an acrylic resin plunger, a wood piston rod and a core cable.

Inside the pipe, there is a trip wire across the gauge. The plunger breaks the wire, which is checked by an ohmmeter or a warning light, when it hits the bottom of the pipe. This indicates that all the glue has been extruded.

A thermistor is monitoring the rock and drill-water temperature during overcoring. The temperature changes cause a bias in gauge readings. It is therefore preferable that conditions contributing to temperature changes are avoided. If temperature changes are unavoidable and large, the temperature records can help in correlating for the errors involved.

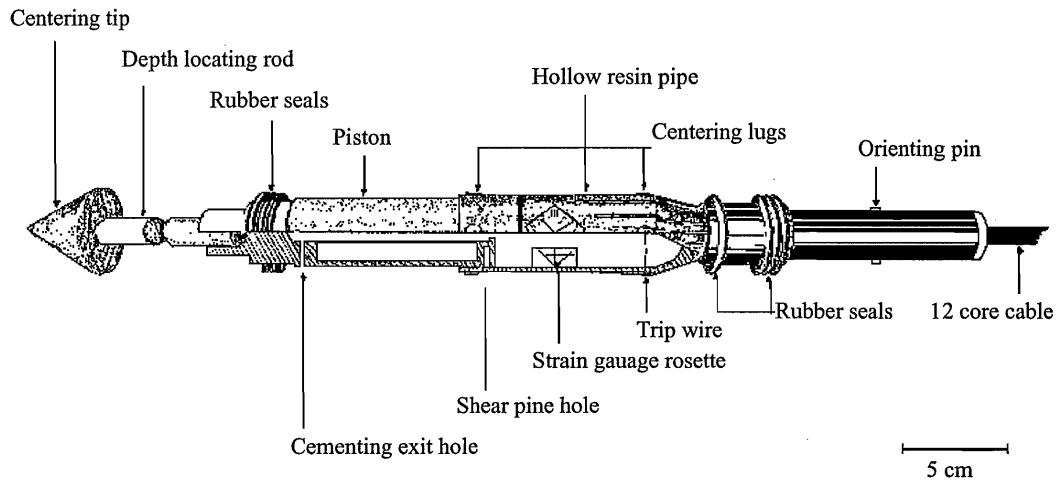


Figure 3-5. CSIRO HI Cell (Worotnicki, 1993).

In a borehole with a diameter of 38 mm, the epoxy resin pipe is 36 mm in diameter. The strain gauges are mounted 0.5 mm below the outer surface of the pipe. During the measurements at Äspö, both nine and twelve strain gauges have been used. Regarding the HI-gauge with nine strain gauges, three of these are circumferential, four are oriented at $\pm 45^\circ$ to the borehole axis and two are parallel to the borehole (Figure 3-6). The HI-cell with twelve strain gauges, five of these are circumferential, five are oriented at $\pm 45^\circ$ to the borehole axis and two are parallel to the borehole axis (Figures 3-7 and 3-8).

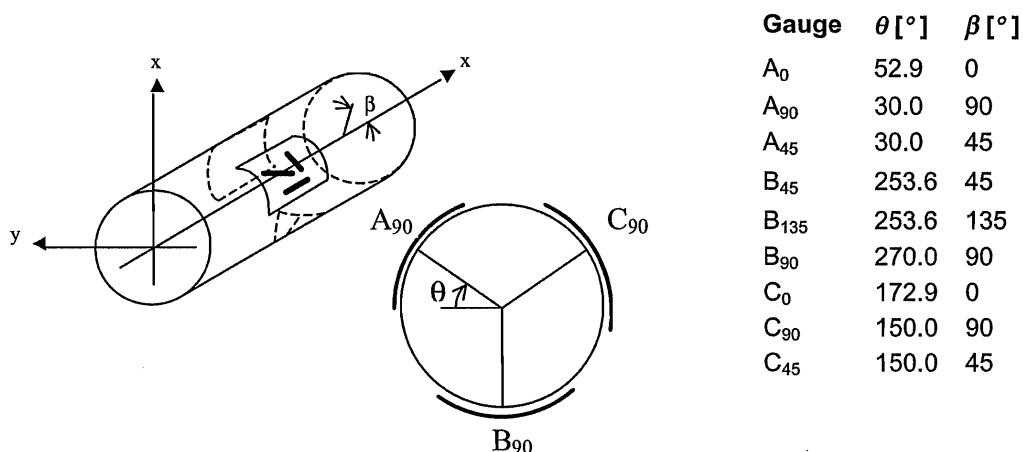


Figure 3-6. Orientation of the nine strain gauges (Stillborg and Leijon, 1982).

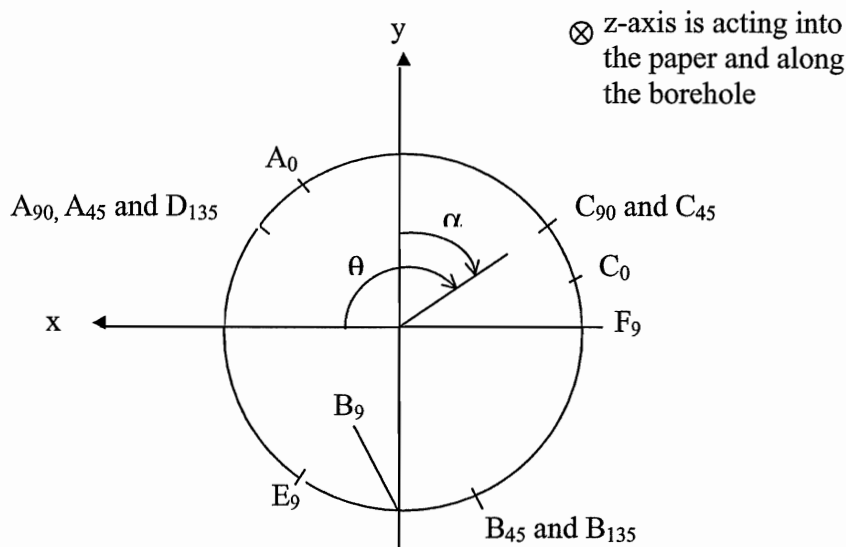


Figure 3-7. Position of the twelve strain gauges (Worotnicki, 1993).

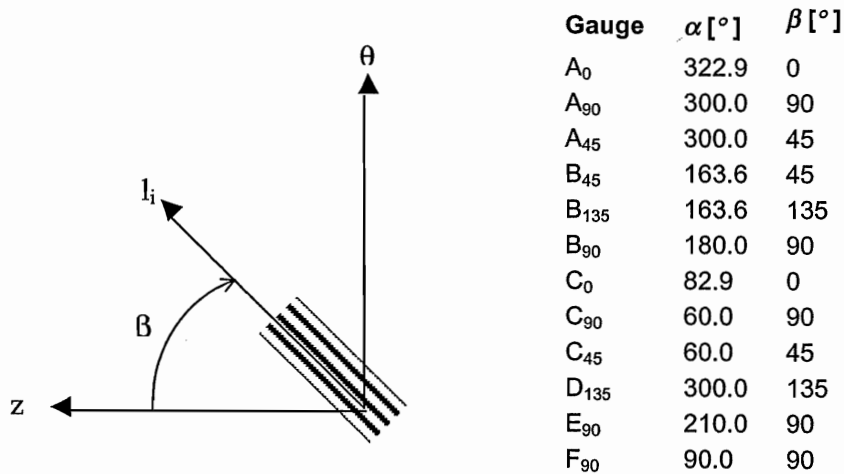


Figure 3-8. Location and orientation of the twelve strain gauges in a CSIRO HI Cell (Worotnicki, 1993).

Epoxy resin

Great attention has to be paid to the glue. The glue is very sensitive to the rock temperature and must therefore be mixed specifically for every test site. When the resin components are mixed the glue must immediately be poured into the gauge. If the glue is poured in a thin stream down the inner wall of the gauge, the air bubbles that are formed while mixing the glue are released. The pot life is limited to about 25 minutes

then the glue starts to harden. Therefore, the installation has to be done as soon as possible.

3.3.2 Remarks on the method

Several possible causes of errors are mentioned in the paper of Worotnicki (1993). Firstly, the fact that the rock is treated as a homogeneous, linear, elastic and isotropic material. If a gauge is cemented on a larger granule, this could contribute to bad readings of the strains. As mentioned earlier the changes in temperature can cause a drift in gauge readings.

If the rock has high porosity or if intensive water flow from the joints occurs, it can be impossible to achieve a good bond between the HI cell and the rock. Even if the rock has low porosity, bad bonding still occurs. It appears that there might be some differences between the same resin supplied in different countries. In addition, the composition and properties of a resin with the same trade name may change. For this reason it is wise to test the suitability of the cement mix in the laboratory under the simulated *in-situ* condition, or if possible carry out field experiments. Drying and cleaning the pilot hole is also of great importance since unsatisfying bonding can occur.

Causes of errors can also be related to bad installation of the cell. The gauge position in the pilot hole should be based on the examination of the cores, to avoid fractures and weakness planes. The preparation of the cell, the installation of the cell and the orientation of the same within the pilot hole are events not to be neglected either. Errors can also occur when the strain gauges are not in contact with the rock. The strain gauges are 1.5 mm from the rock and in-between there is glue. This may influence the calculation of the stresses if it is not taken into account. During the installation and overcoring the temperature should be held at a constant level, since changes in temperature can cause drifts in gauge readings.

The vicinity to the excavation opening will disturb the stress field. Consequently, the measurements have to be done at a distance of at least three times the diameter of the opening. Since most of the measurements are made in near-horizontal boreholes, and the maximum practical depth of overcoring is limited to about 18 metres, it is important to establish the minimum distance from the opening at which far-field stress measurements can be taken (Martin and Christiansson, 1991).

3.4 Stress determination

Leeman and Hayes, (1966) suggested an isotropic analytic solution for determination of the state of stress around a single borehole. The stress at the borehole wall at some angle θ is

$$p_{rr} = 0 \quad 3-3$$

$$p_{\theta\theta} = \sigma_x(1 - 2 \cos 2\theta) + \sigma_y(1 + 2 \cos 2\theta) - 4\tau_{xy} \sin 2\theta \quad 3-4$$

$$p_{zz} = -\nu [2(\sigma_x - \sigma_y) \cos 2\theta + 4\tau_{xy} \sin 2\theta] \quad 3-5$$

$$p_{\theta z} = -2\tau_{xz} \sin \theta + 2\tau_{yz} \cos \theta \quad 3-6$$

$$p_{r\theta} = 0 \quad 3-7$$

$$p_{rz} = 0 \quad 3-8$$

Duncan-Fama and Pender, (1980) suggested a linear elastic, isotropic analytic relation between the local strain components in the cell and the six stress components,

$$E_2 \varepsilon_z = \sigma_z - \nu_2 (\sigma_x + \sigma_y) \quad 3-9$$

$$E_2 \cdot \varepsilon_\theta = \bar{K}_1 (\sigma_x + \sigma_y) - \bar{K}_2 [(\sigma_x - \sigma_y) \cos 2\theta + 2\tau_{xy} \sin 2\theta] - \bar{K}_4 \sigma_z \quad 3-10$$

$$E_2 \gamma_{\theta z} = \bar{K}_3 [\tau_{yz} \cos \theta - \tau_{xz} \sin \theta] \quad 3-11$$

where

$$\bar{K}_1 = K_1 \quad 3-12$$

$$\bar{K}_2 = 2(1 - \nu_2^2) K_2 \quad 3-13$$

$$\bar{K}_3 = 4(1 + \nu_2) K_3 \quad 3-14$$

$$\bar{K}_4 = \nu_2 K_4 \quad 3-15$$

For the SSPB-cell the K-factors, K_1 to K_4 are equal to unity. However, when using the CSIRO HI- cell the K-factors are as follows (Duncan Fama & Pender, 1980),

$$K_1 = d_1 (1 - \nu_1 \nu_2) \left[1 - 2\nu_1 + \frac{R_1^2}{\rho^2} \right] + \nu_1 \nu_2 \quad 3-16$$

$$K_2 = (1 - \nu_1) d_2 \rho^2 + d_3 + \frac{\nu_1 d_4}{\rho^2} + \frac{d_5}{\rho^4} \quad 3-17$$

$$K_3 = d_6 \left[1 + \frac{R_1^2}{\rho^2} \right] \quad 3-18$$

$$K_4 = -\frac{(\nu_1 - \nu_2) d_1}{\nu_2} \left[1 - 2\nu_1 + \frac{R_1^2}{\rho^2} \right] + \frac{\nu_1}{\nu_2} \quad 3-19$$

where

E_1 = Young's modulus of epoxy (GPa)

E_2 = Young's modulus of rock (GPa)

ν_1 = Poisson's ratio of epoxy

ν_2 = Poisson's ratio of rock

R_1 = Inner radius of the probe (mm)

R_2 = Radius of the pilot hole (mm)

ρ = Radial co-ordinate at position of strain gauge (mm)

The constants d_1 to d_6 are defined as,

$$d_1 = \frac{1}{1 - 2\nu_1 + m^2 + \epsilon(1 - m^2)} \quad 3-20$$

$$d_2 = \frac{12(1 - \epsilon)m^2(1 - m^2)}{R_2^2 D} \quad 3-21$$

$$d_3 = \frac{1}{D} [m^4(4m^2 - 3)(1 - \epsilon) + \chi_1 + \epsilon] \quad 3-22$$

$$d_4 = -\frac{4R_1^2}{D} [m^6(1 - \epsilon) + \chi_1 + \epsilon] \quad 3-23$$

$$d_5 = \frac{3R_1^4}{D} [m^4(1 - \epsilon) + \chi_1 + \epsilon] \quad 3-24$$

$$d_6 = \frac{1}{1 + m^2 + \epsilon(1 - m^2)} \quad 3-25$$

where

$$m = R_1/R_2 \quad 3-26$$

$$\chi_1 = 3 - 4\nu_1 \quad 3-27$$

$$\chi_2 = 3 - 4\nu_2 \quad 3-28$$

$$\epsilon = \frac{E_1(1 + \nu_2)}{E_2(1 + \nu_1)} \quad 3-29$$

$$D = (1 + \chi_2 \epsilon) [\chi_1 + \epsilon + (1 - \epsilon)(3m^2 - 6m^4 + 4m^6)] + (\chi_1 - \chi_2 \epsilon) m^2 [(1 - \epsilon)m^6 + (\chi_1 + \epsilon)] \quad 3-30$$

The longitudinal strains, ϵ_{li} , measured by the gauges in the cell are related to the local strain components as,

$$\epsilon_{li} = \begin{bmatrix} 0 & \sin^2 \beta_i & \cos^2 \beta_i & \sin \beta_i \cos \beta_i & 0 & 0 \end{bmatrix} \cdot \begin{bmatrix} \epsilon_r \\ \epsilon_\theta \\ \epsilon_z \\ \gamma_{\theta z} \\ \gamma_{rz} \\ \gamma_{r\theta} \end{bmatrix}, \quad 3-31$$

where β is the inclination of the strain gauge with respect to z -axis, see Figure 3-9.

Since the borehole is drilled in an arbitrary direction, the stress state around the borehole has to be transformed to the regional stress state.

The local stresses around the borehole are transformed to the regional stress state as,

$$[\sigma]_{xyz} = [A][\sigma]_{XYZ}[A]^T \quad 3-32$$

where $[\sigma]_{xyz}^T = [\sigma_x \ \sigma_y \ \sigma_z \ \tau_{xy} \ \tau_{yz} \ \tau_{zx}]$ is the local stress tensor around the borehole and $[\sigma]_{XYZ}^T = [\sigma_X \ \sigma_Y \ \sigma_Z \ \tau_{XY} \ \tau_{YZ} \ \tau_{ZX}]$ is the regional stress tensor. The transformation matrix A is equal to

$$A = \begin{bmatrix} a_{xx} & a_{xy} & a_{xz} \\ a_{yx} & a_{yy} & a_{yz} \\ a_{zx} & a_{zy} & a_{zz} \end{bmatrix} \quad 3-33$$

where a_{ij} is the direction cosines, $\cos\alpha_{ij}$, ($i,j=x,y,z$) and α_{ij} is equal to the angle between axis i in the new co-ordinate system and axis j in the old co-ordinates system. The old co-ordinate system is the regional system XYZ and the new co-ordinate system is the local system xyz around the borehole. The borehole axis and the z -axis coincide.

By performing the matrix operation in Equation 3-32 the relation between the local and regional stress tensor can be simplified.

$$[\sigma]_{xyz} = [A][\sigma]_{XYZ}[A]^T = [B][\sigma]_{XYZ} \quad 3-34$$

The new matrix B is equal to

$$[B] = \begin{bmatrix} a_{xx}^2 & a_{xy}^2 & a_{xz}^2 & 2a_{xx}a_{xy} & 2a_{xy}a_{xz} & 2a_{xz}a_{xx} \\ a_{yx}^2 & a_{yy}^2 & a_{yz}^2 & 2a_{yx}a_{yy} & 2a_{yy}a_{yz} & 2a_{yz}a_{yx} \\ a_{zx}^2 & a_{zy}^2 & a_{zz}^2 & 2a_{zx}a_{zy} & 2a_{zy}a_{zz} & 2a_{zz}a_{zx} \\ a_{xx}a_{xy} & a_{xy}a_{yy} & a_{xz}a_{yz} & a_{xx}a_{yy} + a_{xy}a_{yx} & a_{xy}a_{yz} + a_{xz}a_{yy} & a_{xz}a_{yx} + a_{xx}a_{yz} \\ a_{yx}a_{zx} & a_{yy}a_{zy} & a_{yz}a_{zz} & a_{yx}a_{zy} + a_{yy}a_{zx} & a_{yy}a_{zz} + a_{yz}a_{zy} & a_{yz}a_{zx} + a_{yx}a_{zz} \\ a_{zx}a_{xx} & a_{zy}a_{xy} & a_{zz}a_{xz} & a_{zx}a_{xy} + a_{zy}a_{xx} & a_{zy}a_{xz} + a_{zz}a_{xy} & a_{zz}a_{xx} + a_{zx}a_{xz} \end{bmatrix} \quad 3-35$$

Since the local stress tensor is known, the relation in Equation 3-34 is rearranged to

$$[\sigma]_{XYZ} = [B]^{-1}[\sigma]_{xyz} \quad 3-36$$

and the regional stress tensor can be solved.

The transformation matrix A is equal to,

$$A = \begin{bmatrix} \cos(DD - 90) & \sin(DD - 90) & 0 \\ \cos(|d| - 90)\sin(DD + 90) & \cos(|d| - 90)\cos(DD + 90) & -\sin(|d| - 90) \\ \cos d \cos DD & \cos d \sin DD & \sin d \end{bmatrix} \quad 3-37$$

where DD is the dip direction of the borehole measured clockwise from the north and d is the dip measured positive downward from the horizontal plane (Figure 3-9).

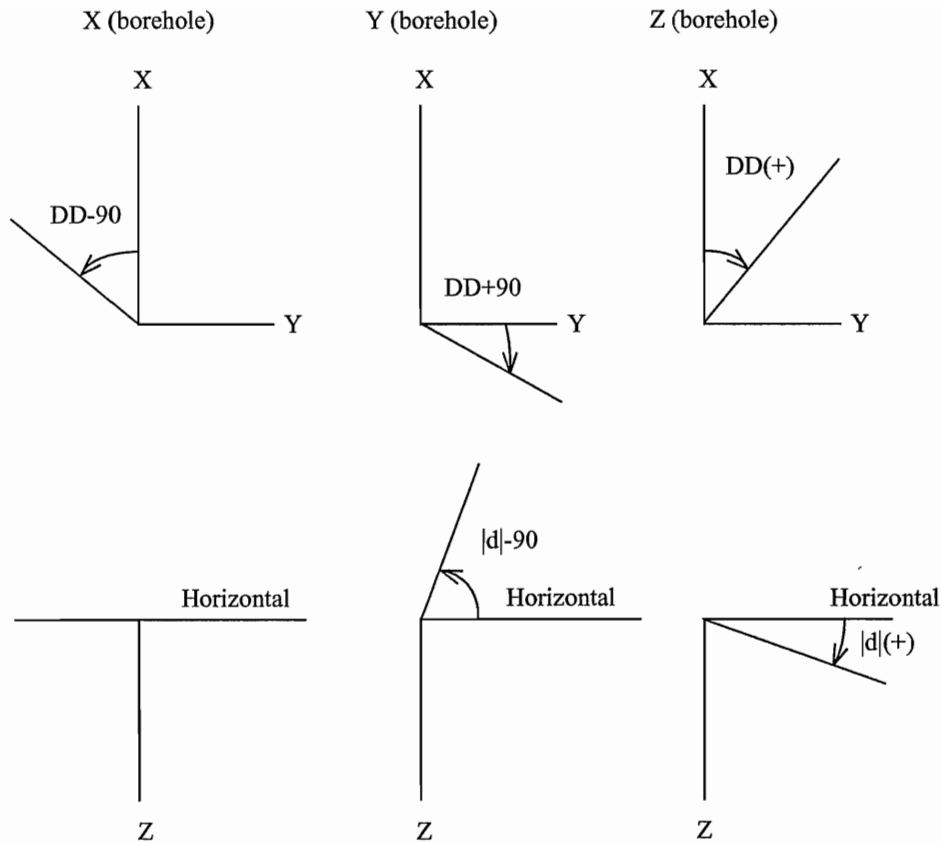


Figure 3-9. The orientation of a borehole expressed by dip and dip-direction.

3.5 Biaxial Testing

The rock cores, recovered after an overcoring test are tested under biaxial loading to establish the stress-strain relationship in the rock. The biaxial loading test is also made in order to evaluate if the gauges were bonded well to the rock and behaved normally. The final purpose of performing biaxial testing is to determine Young's modulus and Poisson's ratio, in order to calculate the stresses from the strain readings.

The rock core is placed in the biaxial chamber with the strain gauges located near the midpoint of the chamber. A radial hydraulic pressure is then applied to the outer surface of the hollow core. The cell monitors the deformation of the inner hole of the core. The testing should be performed as soon as possible after the overcoring test, so the *in situ* moisture content and temperature can be preserved. Changes in rock moisture content can affect the properties of some rocks, while a reduction of temperature can cause failure of the bond between the cell and the rock (Worotnicki, 1993).

For the SSPB Cell the load is increased stepwise in load increments of 1 MPa up to about 10 MPa, to reduce the risk of cracking the hollow cylinder (Ljunggren and Bergsten, 1998) and then unloaded stepwise by 1 MPa. According to measurement records for CSIRO HI Cell, (Litterbach et al, 1994), the loading are made by increments of 5 MPa up to 15 MPa and then the hollow core is unloaded stepwise by 5 MPa.

Based on the assumption that the load is applied along the length and that the rock is much stiffer than the epoxy, the rock core can be treated as a plane stress condition. In

the case of using a hollow inclusion during the stress measurements, the stress conditions in the cell are more complicated. If Poisson's ratio of the rock is similar to that of the plastic inclusion then the condition of the inclusion is close to plane stress. But if the Poisson's ratio of the rock is low and its axial strain is close to zero, the conditions in the inclusion should be closer to plane strain (Worotnicki, 1993).

According to Worotnicki (1993), Young's modulus for hard rock can be calculated using the following relation,

$$E_2 = K_1 \frac{2P_0 M}{\varepsilon_{\theta sg} (M - 1)} \quad 3-38$$

where

K_1 is the factor used in the overcoring analysis, see equation 3-16, M is the square of the ratio of the outer and inner radii of the rock core and $\varepsilon_{\theta sg}$ is the circumferential strain at the location of the strain gauge. Equation 3-38 is valid for both for CSIRo HI and SSPB Cell. However, for the SSPB-cell, the factor K_1 is set to unity. In soft rock a modified K_1 -factor should be used to obtain more accurate results. Interested readers can find more information in the paper by Worotnicki (1993).

Poisson's ratio can be determined with an accuracy of about 10 % using the equation (Worotnicki, 1993),

$$\nu_r = -K_1 \frac{\varepsilon_{zsg}}{\varepsilon_{\theta sg}} \quad 3-39$$

where $\varepsilon_{\theta sg}$ and ε_{zsg} is the measured axial and circumferential strain. This equation is valid for cores with a diameter of 86 mm or smaller and if the cell is located in the middle third of the loading area. The motivation for this can be seen in Figure 3-10 where the tensile stresses in the middle third are small (distance from midpoint, 0-20 mm).

3.5.1 Remarks on the method

Several possible sources of error are presented in Worotnicki (1993). There can be errors associated with the cells themselves i.e. the strain gauges being located at a distance from the rock surface and errors due to the resistance of the cell to deform under a biaxial loading. There can also be errors due to the loading conditions, i.e. that only a part of the core is loaded and that the end remains free of load.

If the core is too short to be loaded in the chamber, Young's modulus and Poisson's ratio are usually taken from another core in the vicinity (Hallbjörn, 1986). This procedure might lead to incorrect values of the stresses. Even if the gauges are performing properly, the biaxial loading can contribute to deformations in the core, which can initiate more microcracks in the sample.

When conducting biaxial testing the assumption is made that the outer pressure, P_0 , is applied at the rock surface along its total length is made. However, in reality the cores are of different lengths and are recovered with irregularly shaped ends, and the cores are only partially loaded. Since only a part of the core is loaded, tensile stresses are developed on the outer surface near the ends of the loaded area (Figure 3-10). Tensile stresses also occurred on the opposite inner surface (Worotnicki, 1993).

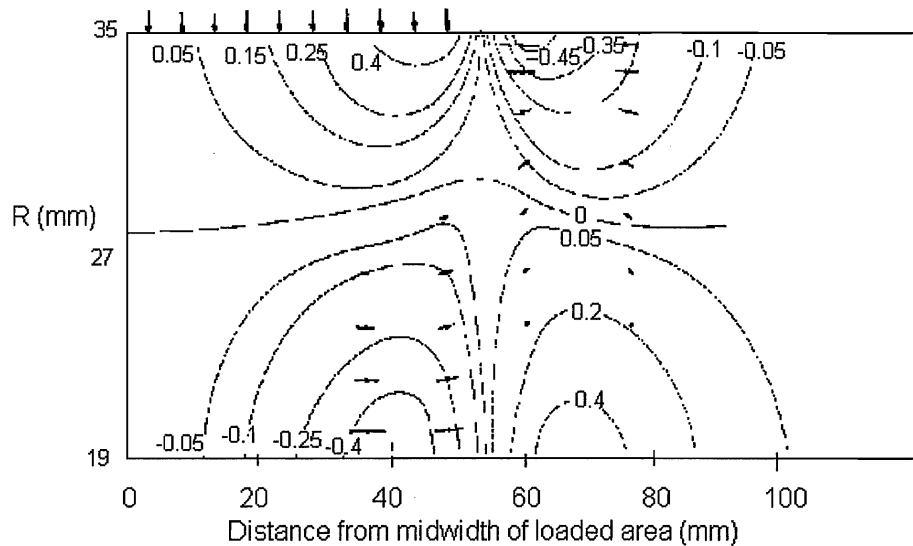


Figure 3-10. Axial tensile stress in a biaxial loaded core (Worotnicki, 1993).

Martin and Christiansson (1991) reported about microcracks in stressed granite. They found that the amount of stress-induced micro-cracks were greatest when the overcored samples was taken from boreholes drilled perpendicular to the major principal stress. This phenomenon may be valid in a biaxial chamber, where the major principal stress is acting perpendicular to the sample ($\sigma_3=0$).

Stacey (1981) presented a failure criterion that states that fracture of brittle rock will initiate when the total extension strain in the rock exceeds a critical value which is characteristic of that rock type, i.e. when $\epsilon_c \leq \epsilon$. This indicates that the rock is exposed to critical extension strain and fractures may be initiated and propagated, which invalidate the assumption of linear elastic behaviour of the material. The Poisson's ratio evaluated under elastic assumptions from biaxial tests may therefore be affected, since Poisson's ratio is direct proportional to axial strain during biaxial testing.

4 Computer codes for stress determination

The codes are based on the theory mentioned in Section 3.4. However, since both CSIRO HI and SSPB-cells have more strain gauges than what is needed to determine the state of stress around a borehole, the system of equations is solved by least square analysis. A short summary of the least square procedure presented by Amadei and Stephansson (1997) will be presented here.

Consider N strains or displacements measured during overcoring. Since the theory of linear elasticity is used, these N observations are linearly related to the six *in situ* stress components by following equation,

$$[Y] = [X] \cdot [b] + [\varepsilon] \quad 4-1$$

where

[Y] = The observations, ($N \times 1$) matrix

[X] = An ($N \times 6$) matrix of known form based on Equations 3-9 - 3-11

[b] = Contains the six *in situ* stress components, (6×1) matrix

[\varepsilon] = The residual errors associated with the measurement, ($N \times 1$) matrix.

In least square analysis it is assumed that the components of the matrix [\varepsilon] are independent variables with zero means and common variance. This assumption is often made, but seldom checked when applied to the analysis of overcoring measurements (Worotnicki, 1993). The solution of the following system,

$$[X]^t [X] [b] = [X]^t [Y] \quad 4-2$$

will be the least square estimation of the stress matrix [X]. The solution of the system gives the most likely values of the normal and shear stresses around the borehole. Out of this, the expected strains, [Y'] can be calculated,

$$[Y'] = [X] [b] \quad 4-3$$

The residual matrix, [\varepsilon], is defined as the difference between [Y] and [Y']. By calculating the coefficient of the multiple correlation, R ,

$$R = \sqrt{\frac{[b]^t [X]^t [Y] - N\bar{Y}^2}{[Y]^t [Y] - N\bar{Y}^2}} \quad 4-4$$

a measure of how good the linear regression analysis is can be obtained.

4.1 CSIRO HI-cell

Recommendations for the rejection procedure when using CSIRO HI-cell is given by the Australian Mining Consultants Pty Ltd (AMC) in their General Appendix about *In situ* Virgin Stress Measurement (Nilsson et al., 1997). Strains that have the largest difference, with respect to the mean or average calculated strains are rejected successively if

1. Chavenet's empirical criterion for outliers is exceeded. Chavenet's empirical criterion is based on a multiple of the standard deviation of the differences between the measured and mean or "average" calculated strains. The value of this multiple depends on the amount of redundant strains used to calculate a result (i.e. the degree of freedom). A wider spread of strain data is more likely and tolerated when there is more redundant data.
2. The variability of the strain data is such that the F-test of the Student-T distribution is not satisfied at a 95% level of confidence.

Iteration by rejecting strains proceeds until the first acceptable solution is found, which is then called the best-fit result.

4.2 SSPB- cell

Even when using the SSPB-cell redundant strain data are obtained since nine strain gauges are used. The evaluation program for SSPB uses a least square regression procedure to find the solution best fitting the strain data (Ljunggren and Bergsten, 1998).

5 Rock Stress measurements at Äspö

Since 1988 several rock stress measurements have been performed at the Äspö area. In this chapter, information about every measurement is given, with respect to location, date, number of measurements at a single test site, method etc. The stress measurements are divided into two groups, virgin stresses and secondary stresses. In this report, the definition of secondary stresses is the sum of induced and virgin stresses. For example, measurements in borehole KA1045 will result in secondary rock stresses since the borehole is located close to the ramp (Figure 5-1). Borehole KA3086 on the other hand is drilled perpendicular to the ramp and the influences of the ramp are minimal and will therefore be grouped as a virgin stress measurement. In Figure 5-2, the locations of the surfaced drilled boreholes at Äspö are marked.

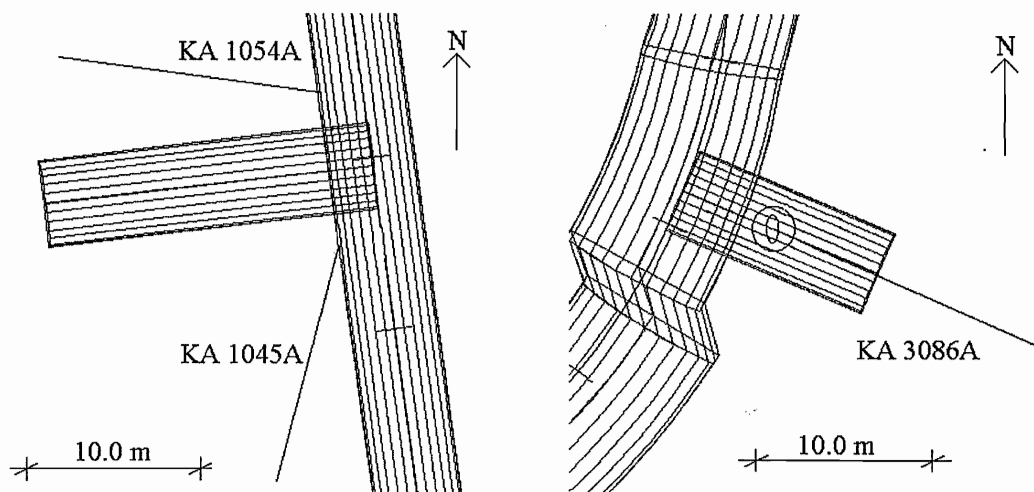


Figure 5-1. The location and orientation of boreholes KA1045A and KA1054A and KA3086A related to the ramp in Äspö HRL. The arrow represents the local Äspö north.

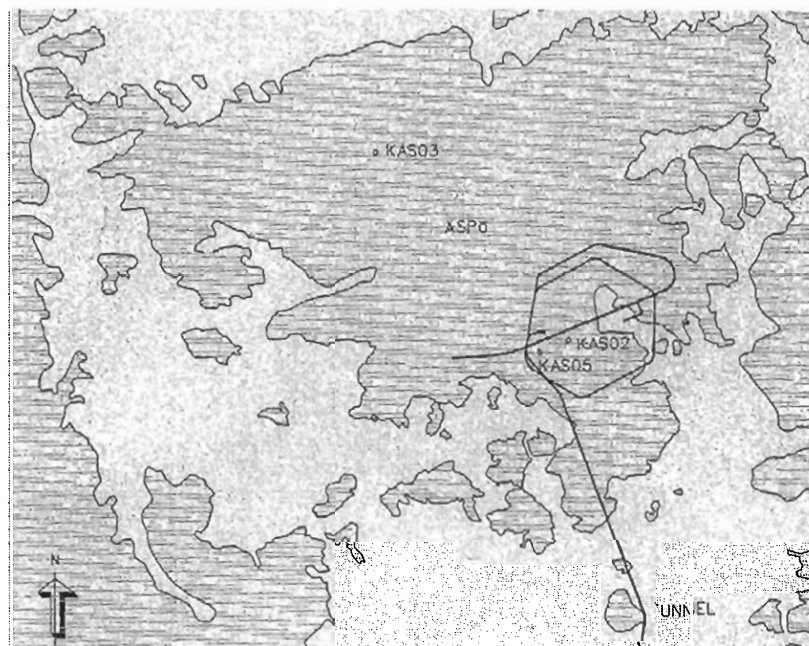


Figure 5-2. The location of the boreholes drilled from the surface at Äspö, Leijon (1995).

5.1 Virgin rock stress measurements

In Table 5-1 the virgin rock stress measurements are listed. Information about date, depth under surface, number of measurements as well as the method and reference are also given. Elastic parameters and stresses from the measurements are given in Appendix A.

Table 5-1. Information about the virgin stress measurements at Äspö.

ID	Date	Depth [m]	Number	Reference	Method
KAS03	July 1988	131-963	17	B. Bjarnason, H. Klasson B. Leijon 25-89-17	HF
KAS02	April 1989	113 – 740	21	H. Klasson, B. Leijon 25-89-17	HF
KAS05	Jan-Feb 1989	196 and 356	7	L. Strindell, T. Öhman 25-89-17	OC - SSPB
KA1054A	June 1992	143	3	M. Lee, M. Bridges B. Stillborg 25-93-02	OC - CSIRO HI
KA1623A	Dec. 1992	223	3	M. Lee, M. Bridges B. Stillborg 25-93-02	OC - CSIRO HI
KA1625A	Dec. 1992	223	3	M. Lee, M. Bridges B. Stillborg 25-93-02	OC - CSIRO HI
KA1626A	Dec. 1992	223	3	M. Lee, M. Bridges B. Stillborg 25-93-02	OC - CSIRO HI
KA1899A	Nov. 1993	257	5	M. Lee, T. Hewitt B. Stillborg 25-94-02	OC - CSIRO HI
KA2198A	Nov. 1993	294,5	4	M. Lee, T. Hewitt B. Stillborg 25-94-02	OC - CSIRO HI
KA2510A	Nov. 1993	335	6	M. Lee, T. Hewitt B. Stillborg 25-94-02	OC - CSIRO HI
KA2870A	April 1994	380	5	N. Litterbach, M. Lee, M. Struthers, B. Stillborg 25-94-32	OC - CSIRO HI
KA3068A	May-June 1994	408,5	4	N. Litterbach, M. Lee, M. Struthers, B. Stillborg 25-94-32	OC - CSIRO HI
KA3597G	Sept-Oct 1997	448	4	Vattenfall hydropower HRL-98-09	OC - SSPB

5.2 Secondary stress measurements

The secondary stress measurements are listed in the same way as the virgin stress measurements in Table 5-2. Elastic parameters and stresses from the measurements are given in Appendix B except for boreholes KXZSD8HR and KXZSD8HL. The secondary stresses are not used in the analysis of the virgin stresses at Äspö. However, they will probably be used for back-calculation in numerical analyses.

Table 5-2. Information about the secondary stress measurements at Äspö.

ID	Date	Depth [m]	Number	Reference	Method
KA1045A	June 1992	143	3	M. Lee, M. Bridges B. Stillborg 25-93-02	OC - CSIRO HI
KA1192A	Nov. 1992	164	3	M. Lee, M. Bridges, B. Stillborg 25-93-02	OC - CSIRO HI
KXZSD8HR	Feb-March 1996	416	7	Vattenfall hydropower TN-96-08	OC - SSPB
KXZSD8HL	Feb-March 1996	415,5	4	Vattenfall hydropower TN-96-08 G. Nilsson, N. Litterbach, M. Lee	OC - SSPB
KZ0059B	June 1997	416	6	B. Stillborg TN-97-25g	OC - CSIRO HI
KA3597G	Sept - Oct 1997	450 - 456	6	Vattenfall hydropower HRL 98-09	OC - SSPB

6 Result of the rock stress measurements

6.1 Hydraulic fracturing

Hydraulic fracturing has been done in two deep boreholes, KAS02 and KAS03 and the results have been presented earlier (Bjarnason et al, 1989). KAS02 is located above the hard rock laboratory itself, while the other, KAS03 is about 500 metres northwest of the laboratory. The stress measurement results are therefore separated, since local geological structures may have an influence on the result.

The maximum and minimum horizontal stresses versus depth show a jump at about 500 metres below surface as shown in Figure 6-1. The maximum horizontal stress is obtained by using the second breakdown method (Equation 2-11). This is valid for both the minimum and maximum horizontal stresses. However, this is expected since the maximum and the minimum horizontal stresses are dependent.

Wikman et al. (1988) found two major mylonite zones at 455-485 m and 550-570 m in borehole KAS02. By including these two zones in the Figure 6-1, one might see an effect from the zones.

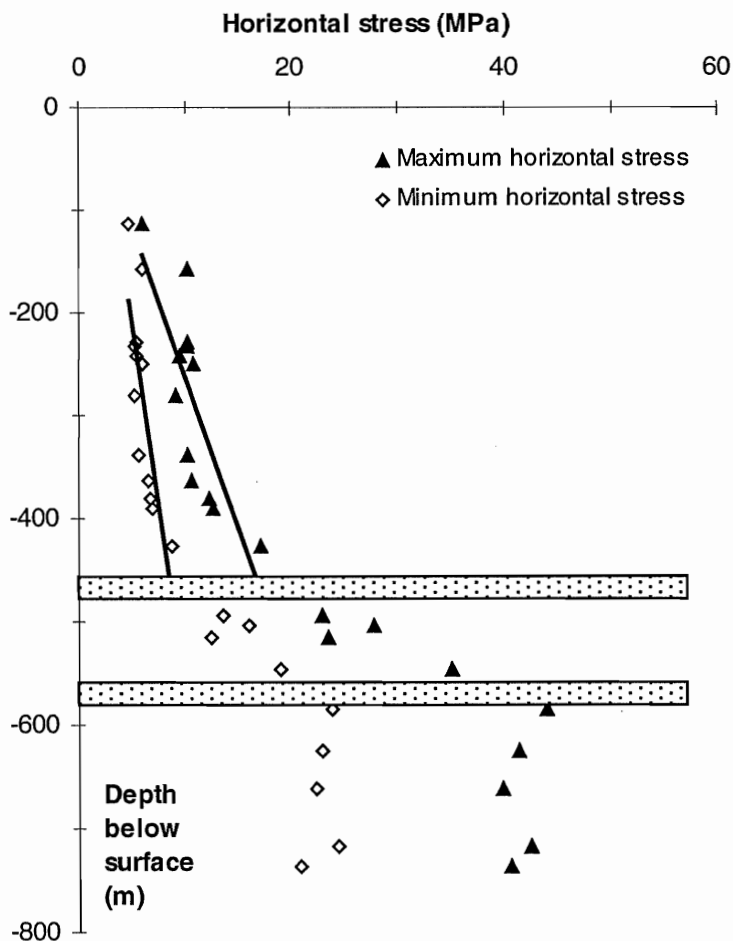


Figure 6-1. Maximum and minimum horizontal stresses in KAS02 with the two zones of mylonite included.

Since the mylonite zones may influence the state of stress, only the stress measurement results above 450 m are considered in a linear regression analysis. The two solid lines represent the linear regression analysis of the input data. The equations for these two lines are,

$$\sigma_H = 1.12 + 0.034z \quad (\text{MPa}) \quad 6-1$$

$$\sigma_h = 1.23 + 0.02z \quad (\text{MPa}) \quad 6-2$$

These relations agree quite well with the relations presented by Stephansson et al. (1991)

$$\sigma_H = 2.8 + 0.04z \quad (\text{MPa}) \quad 6-3$$

$$\sigma_h = 2.2 + 0.024z \quad (\text{MPa}) \quad 6-4$$

which are based on hydraulic stress measurements in Scandinavia.

The stresses measured in KAS03 also show a significant increase in the magnitude at a depth of about 800 metres (Figure 6-2). No distinct major mylonite zones or other geological zones, which may influence the state of stress zones, can be identified (Wikman et al, 1988).

The ratios between maximum and minimum horizontal stress are ranging between 1.23 and 2.13, with an average value of 1.8 and a standard deviation of 0.02. The ratios are listed in Appendix A.

6.1.1 Orientation of the horizontal stresses

The orientation of the maximum horizontal stresses evaluated during the measurements in KAS02 and KAS03 are shown in Figure 6-3. The orientations show no abrupt change with respect to depth. This may indicate that the mylonite zones do not affect the orientation.

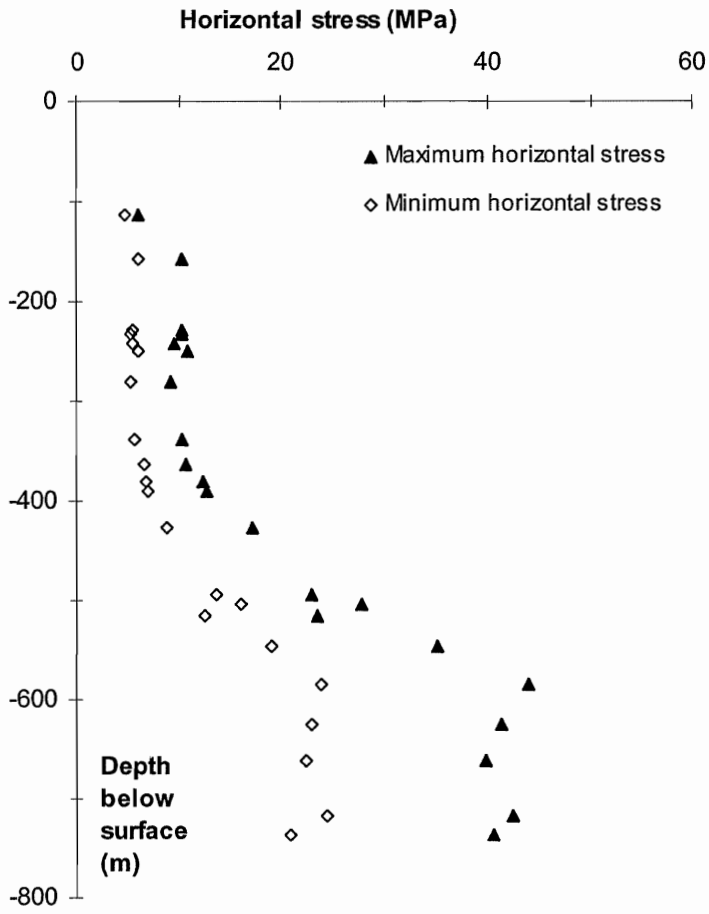


Figure 6-2. Maximum and minimum horizontal stress in KAS03.

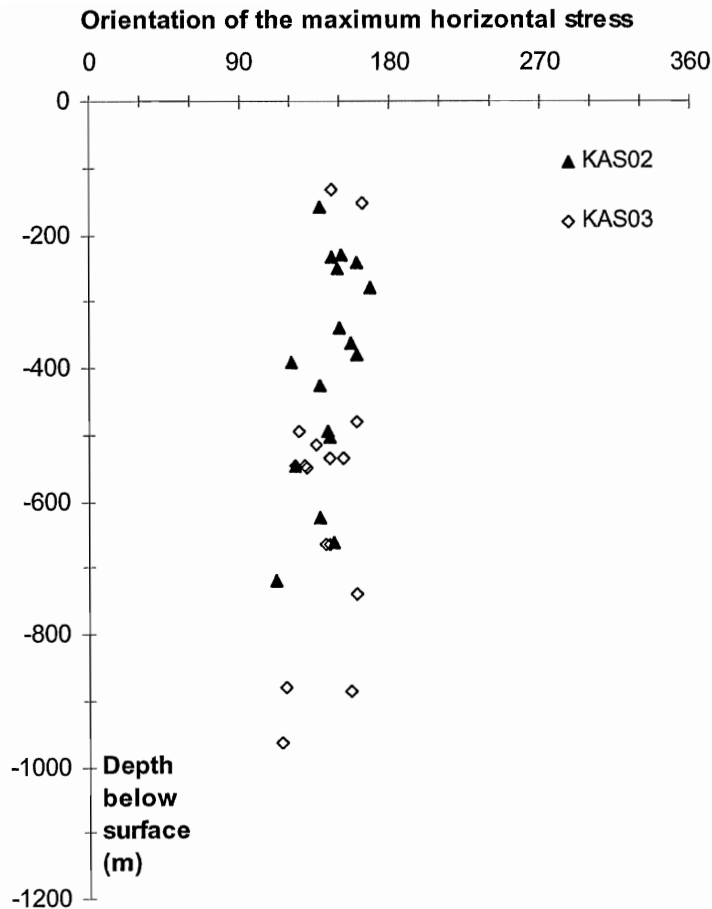


Figure 6-3 The orientation of the maximum horizontal stress in KAS02 and KAS03.

6.2 Overcoring

In overcoring, the elastic properties are of major importance. If the elastic parameters vary among different measurements one might expect a corresponding scatter in magnitude and orientation of the stresses.

6.2.1 Uniaxial tests

Uniaxial testing has earlier been performed on rock samples from the section 0/900-1/475 and 1/623-1/673 (Delin et al., 1993a, Delin et al., 1993b). The rock types that were tested were fine-grained granite, Småland granite, diorite and greenstone. The results from the test can be seen in Table 6-1

Table 6-1. Results from uniaxial testing of rock samples (Delin et al, 1993a, Delin et al. 1993b).

	Fine-grained granite	Småland granite	Diorite	Greenstone
Poisson's ratio	0.24	0.21	0.24	0.24
Young's modulus (GPa)	77	74	73	78

6.2.2 Statistical analyses on the elastic properties

Using the statistics program, *Stat Graphic Plus 3.0*, the variation of the elastic parameters is analysed. In Figures 6-4 and 6-5 box plots of Young's modulus and Poisson's ratio are shown. The box plots are based on the results from the 47 biaxial tests of the CSIRO HI-cell and SSPB-cell from the virgin stress measurements.

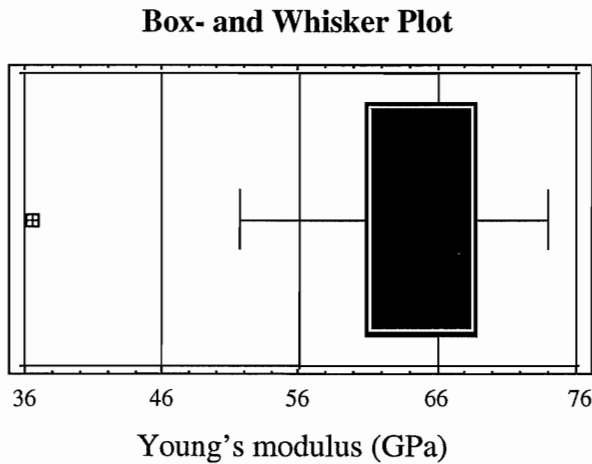


Figure 6-4. Box plot of Young's modulus (GPa), n =47 samples.

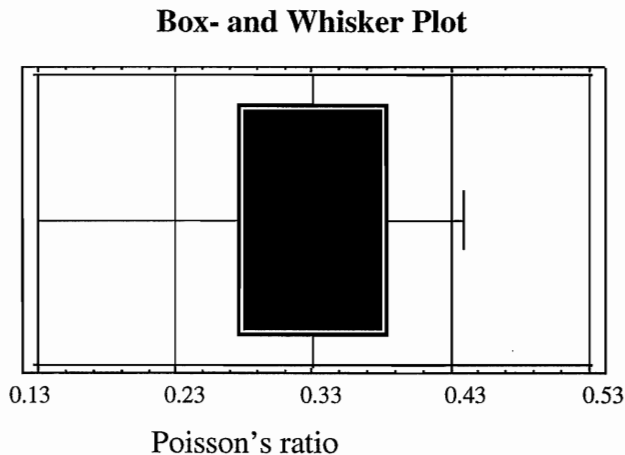


Figure 6-5. Box plot of Poisson's ratio, n=47 samples.

With 95% confidence, the interval of Young's modulus, 64.2 ± 2.2 GPa, and the interval of Poisson's ratio, 0.32 ± 0.02 , were determined by the statistics program.

If the results from the two methods are treated separately, statistical analyses show that the values of especially Poisson's ratio depend on what method has been used. In Figure 6-6 the density trace for Poisson's ratio is shown and in Figure 6-7 that for Young's modulus is shown.

The statistical analysis of Poisson's ratio indicated that there is significant difference between the two mean values, while this is not the case for Young's modulus. Table 6-2 shows the mean values for the elastic parameters, when the methods were treated separately.

Table 6-2. Mean values of Young's modulus and Poisson's ratio for the two overcoring cells.

Method	Young's modulus (GPa)	Poisson's ratio
SSPB	67.4	0.23
CSIRO HI	63.9	0.34

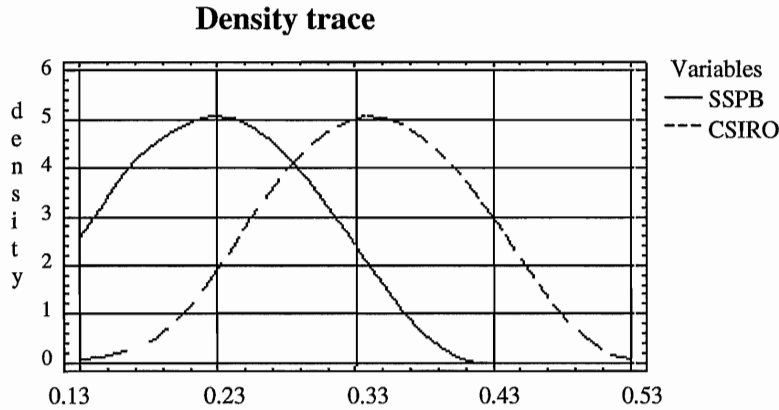


Figure 6-6. Density trace for Poisson's ratio.

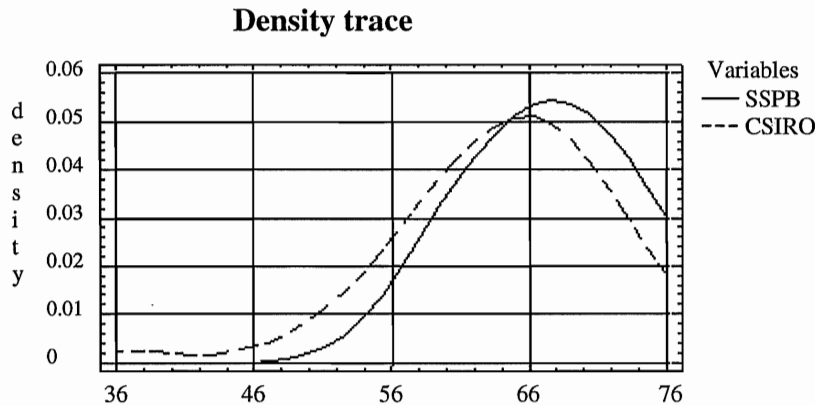


Figure 6-7. Density trace for Young's modulus (GPa).

Comparing these results with the results from uniaxial testing (Table 6-1) the values of Young's modulus are lower and the values of the Poisson's ratio are higher especially when using CSIRO HI-cells. This might be explained by the stress-induced microcracks. These microcracks may be induced when the pilot hole is drilled and then propagated when the overcoring is conducted.

Sensitivity analysis

Sensitivity analyses have been made on Poisson's ratio to investigate how they influences the magnitude of both principal and horizontal stresses as well as the orientation of the stresses. In Figure 6-9 to 6-10 the effects of Poisson's ratio on the magnitude of the principal and horizontal stresses and the orientation of the maximum horizontal stress are illustrated. The strain data from borehole KA1899A and

measurement number 3 have been used in the analysis. The values of Young's modulus and Poisson's ratio for the measurement are 62 GPa and 0.42, respectively.

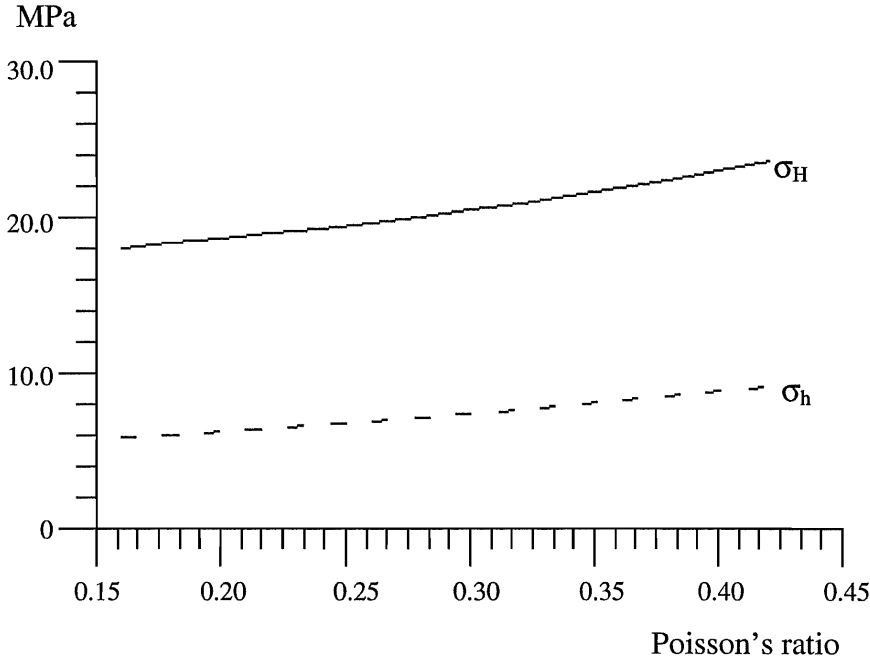


Figure 6-8. Horizontal stresses versus Poisson's ratio.

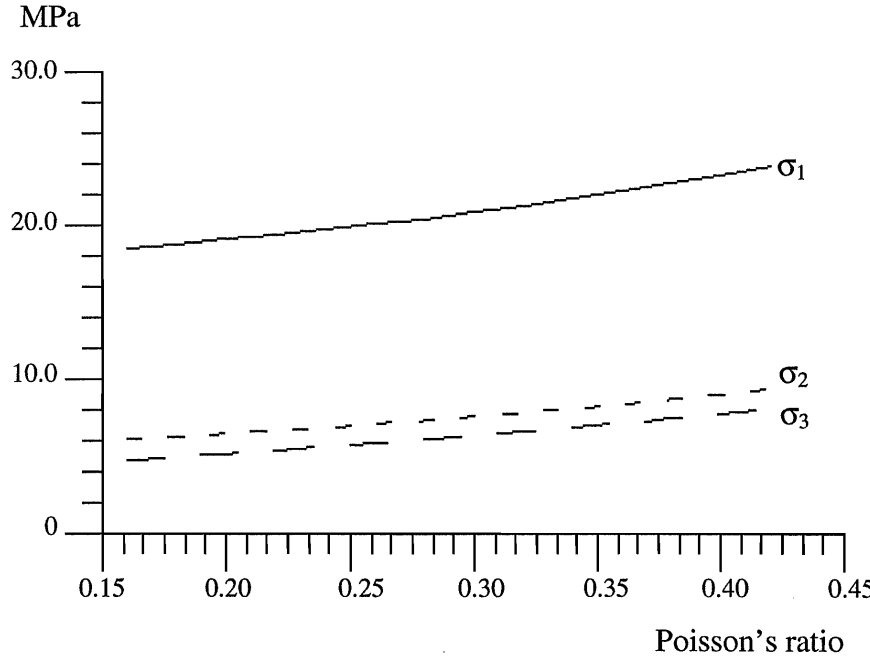


Figure 6-9. Principal stresses versus Poisson's ratio.

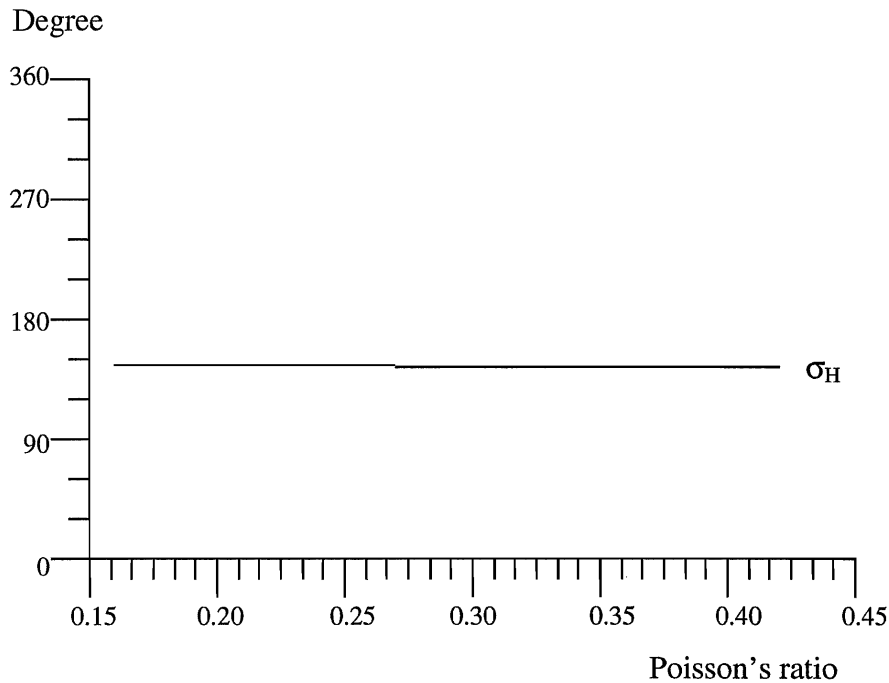


Figure 6-10. Orientation of the maximum horizontal stress versus Poisson's ratio.

The maximum horizontal stress is increased by 13 % if a Poisson's ratio of 0.34 instead of 0.23 is used and even more for minimum horizontal stress (23%). The results from the sensitivity analyses show that the magnitude of the stresses is influenced by the value of Poisson's ratio, while the orientation of the maximum horizontal stress is barely effected. This results coincide with the results from a similar analysis made at the ZEDEX test area at Äspö by Myrvang (1997) where is found that the stresses are highly influenced by the Poisson's ratio and that the orientation of the stresses is influence very little.

6.2.3 Rock stress measurements result

The results of the measurements with overcoring have been reported earlier by Bjarnason et al. (1989), Lee et al. (1993) Lee et al. (1994), Litterbach et al. (1994) and Ljunggren and Bergsten (1998). In Figures 6-11 and 6-12, the minimum and maximum horizontal stresses from the overcoring measurements can be seen. See Appendix A for the data from the rock stress measurements. The explanations to the numbers in the figures are presented in Table 6-3. The orientation of the maximum horizontal stress is shown in Figure 6-13.

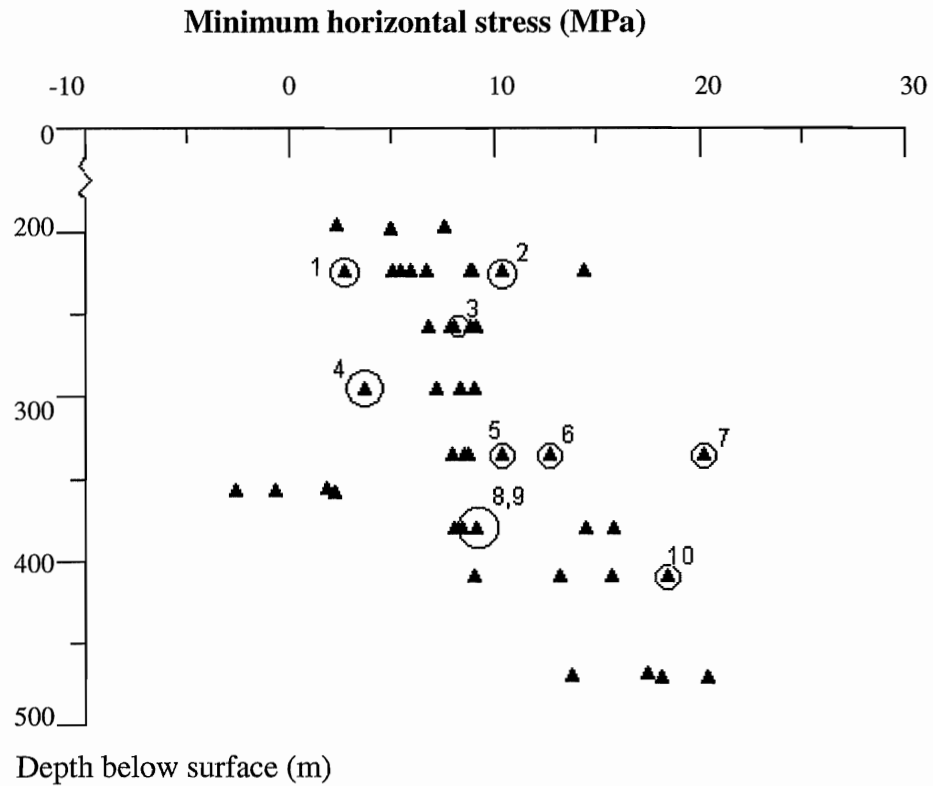


Figure 6-11. Minimum horizontal stress, definitions of the numbers see Table 6-3.

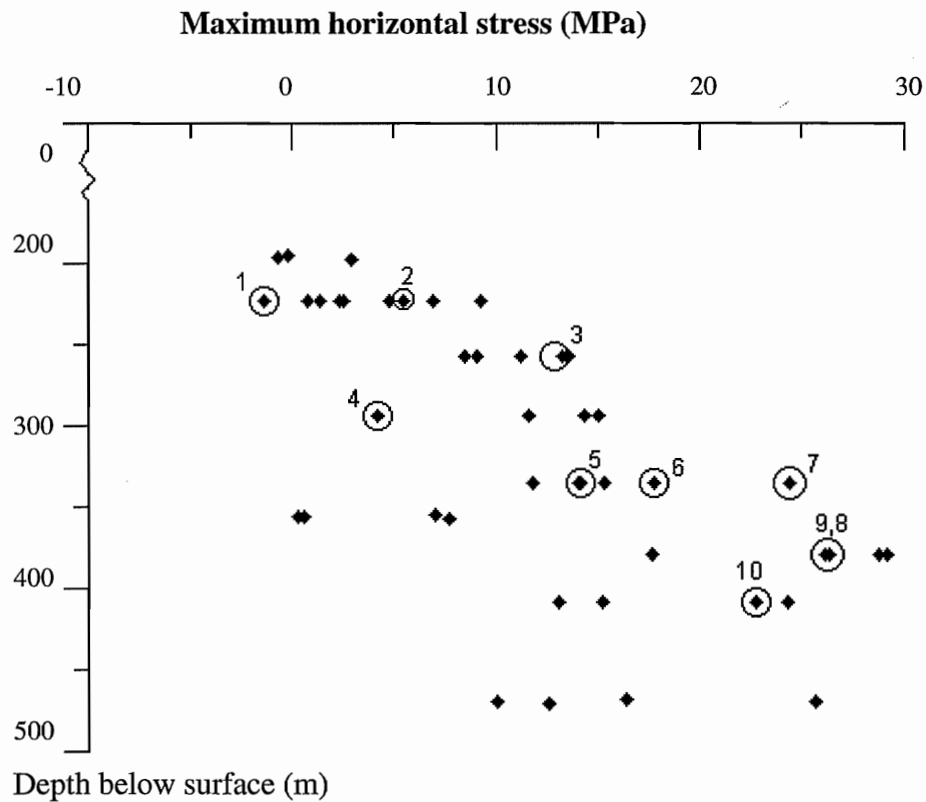


Figure 6-12. Maximum horizontal stress

Table 6-3. Definition of the numbers in Figures 6-11 and 6-12.

Number	Definition
1	Measurement is fair, $E = 63.8 \text{ GPa}$, $\nu = 0.4$
2	Measurement is fair, $E = 53.3 \text{ GPa}$, $\nu = 0.4$
3	Measurement is fair, $E = 59.7 \text{ GPa}$, $\nu = 0.4$
4	Extremely low Young's modulus, $E = 36.5 \text{ GPa}$, $\nu = 0.29$
5	Measurement is fair, $E = 68.8 \text{ GPa}$, $\nu = 0.3$
6	Measurement is poor, $E = 66.7 \text{ GPa}$, $\nu = 0.4$
7	Measurement is fair, $E = 71.8 \text{ GPa}$, $\nu = 0.39$
8	Measurement is poor, $E = 62.5 \text{ GPa}$, $\nu = 0.21$
9	Measurement is poor, $E = 64.8 \text{ GPa}$, $\nu = 0.28$
10	Measurement is fair, $E = 72.1 \text{ GPa}$, $\nu = 0.34$

The ratios between the maximum and minimum horizontal stress are ranging between 1.22 to 8.95, with an average value of 2.70 and a standard deviation of 1.5. The ratios are listed in Appendix A.

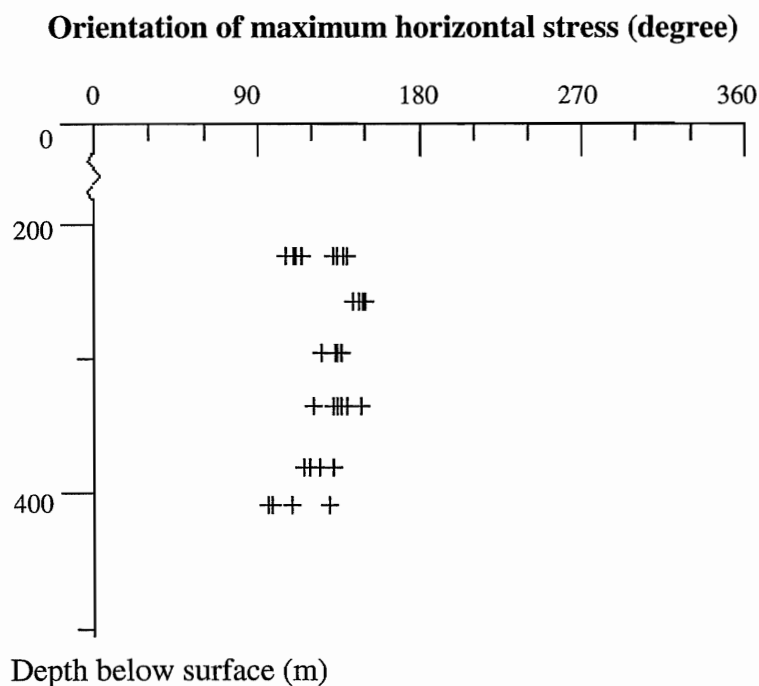


Figure 6-13. Orientation of the maximum horizontal stress versus the depth.

The marked measurements are not included when an average value of the rock stresses is calculated for each specific borehole. The mean stress tensor for each borehole can be seen in Table 6-4 and the average principal and horizontal stresses for each borehole can be seen in Table 6-5.

Table 6-4. The stress tensor for each borehole, represented by a mean value and a standard deviation (MPa).

Borehole	Depth	σ_x	\pm	σ_y	\pm	σ_z	\pm	τ_{xy}	\pm	τ_{zy}	\pm	τ_{xz}	\pm
KA1623	223	12.2	3.1	16.5	6.9	9.7	1.2	-1.6	0	-0.2	1.2	-2.8	0.2
KA1625	223	10.1	3.6	9.3	2.0	8.4	0.5	-3.9	0.9	-1.1	0.6	1.9	0.5
KA1626	223	8.8	1.0	10.3	1.8	6.6	1.9	-1.8	1.0	0.2	0.9	0.2	0.1
KA1899	257	16.5	2.4	12.2	1.1	7.2	0.1	-5.9	0.6	0.9	0.3	-1.0	0.5
KA2198	295	14.8	2.1	17.1	0.6	8.6	2.3	-7.6	0.7	2.5	0.4	-1.9	0.8
KA2510	335	17.5	1.7	14.7	2.3	10.6	0.9	-7.4	1.4	1.8	0.9	2.0	0.8
KA2870	380	18.5	7.7	29.6	5.8	18.9	2.6	-9.6	3.0	-1.0	0.9	-7.5	0.2
KA3086	409	15.0	6.9	25.2	2.7	9.3	0.3	-3.7	5.0	-4.8	0.3	-1.2	1.2
KA3579	≈470	- ¹	-	-	-	-	-	-	-	-	-	-	-

Table 6-5. The average principal and horizontal stresses in each of the borehole.

ID	Depth	Magnitude (MPa)			Orientation (dip direction/dip)			Magnitude (MPa)		Strike
		σ_1	σ_2	σ_3	σ_1	σ_2	σ_3	σ_H	σ_h	
KA1623	223	17.1	13.5	7.80	111/06	205/34	013/55	17.1	11.7	108
KA1625	223	14.4	7.80	5.70	319/20	102/66	224/14	13.6	5.8	318
KA1626	223	11.5	7.70	6.60	124/00	034/15	214/75	11.5	7.6	124
KA1899	257	20.7	8.10	7.00	145/05	054/10	263/79	20.6	8.0	325
KA2198	295	24.2	8.40	7.90	131/11	035/26	242/62	23.6	8.3	131
KA2510	335	23.6	12.4	6.70	321/02	054/55	229/62	23.6	8.6	138
KA2870	380	35.7	23.0	8.20	123/11	229/54	026/34	35.1	12.9	120
KA3086	409	27.4	14.8	7.30	286/13	191/20	047/65	26.4	13.8	108
KA3579	≈470	34.2	17.7	13.1	188/39	094/06	356/51	26.0	11.0	18

The two solid lines in Figure 6-14 represent the linear regression of the points. These two lines have the equations,

$$\sigma_H = -9.64 + 0.10z \quad (\text{MPa}) \quad 6-5$$

$$\sigma_h = -4.94 + 0.05z \quad (\text{MPa}) \quad 6-6$$

In Figure 6-15 the average orientation is shown. Even if it looks like there are two different orientations, they are the same since they are 180 degrees apart. The average orientation is 127°.

¹ The stress tensor from each measurement is not available from the report.

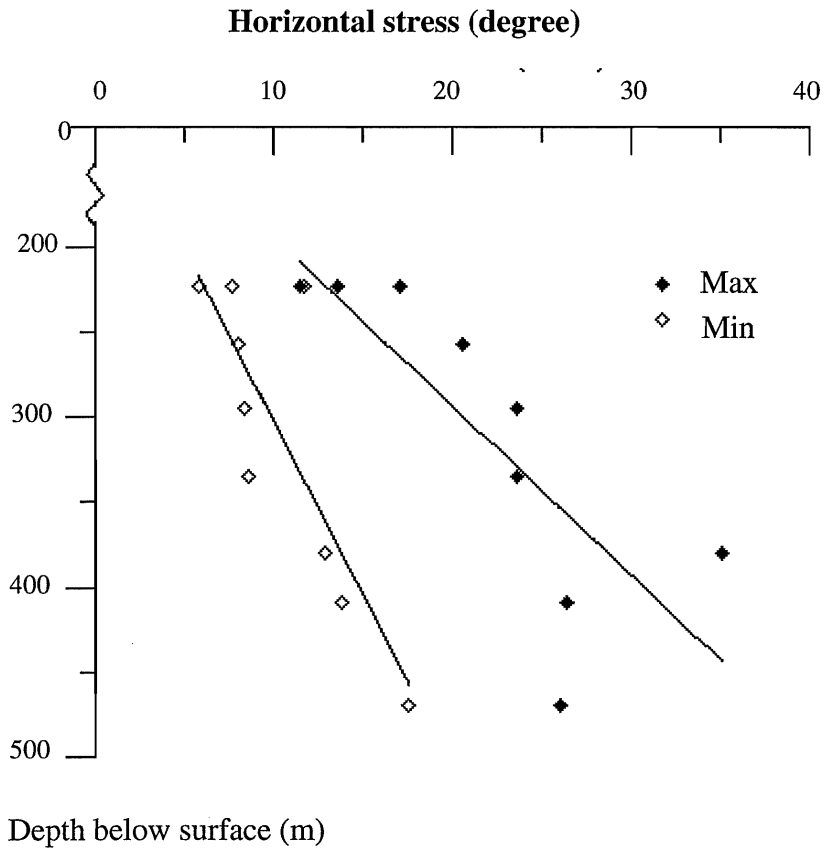


Figure 6-14. The average maximum horizontal stress from Table 6-5.

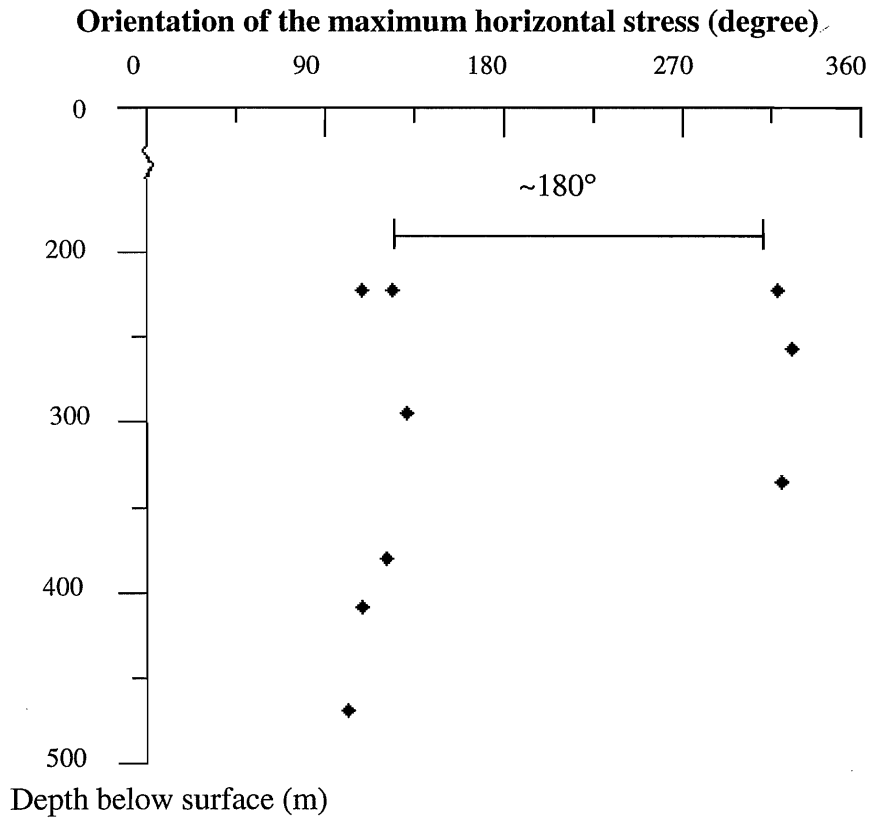


Figure 6-15. The average orientation of the maximum horizontal stresses from Table 6-5.

6.2.4 Monte Carlo simulation

Confidence interval of the in-situ stress measurements can be determined using the Monte Carlo simulation method. The simulation technique is based on repeated cycles. In every cycle, random sampling of values from each of the normal distributions that represent the six independent components of $\bar{\sigma}$ as defined by Table 6-4 is carried out. By generating many cycles, a great number of possible stress tensors are obtained, from which possible principal stresses can be determined.

Monte Carlo simulations were made on all boreholes except on KA3579, since no mean stress tensor was available. The results from the Monte Carlo simulation, which are based on 20 000 cycles, are summarised in Tables 6-6 and 6-7.

Table 6-6. Principal stresses from the Monte Carlo simulation.

ID	σ_1 (MPa)			σ_2 (MPa)			σ_3 (MPa)		
	lower	mean	upper	lower	mean	upper	Lower	mean	upper
KA1623	12.95	18.95	27.97	8.05	12.55	16.64	3.51	6.87	9.34
KA1625	11.61	14.90	18.71	6.75	8.00	9.39	1.37	4.90	7.59
KA1626	9.59	11.92	14.40	6.13	8.01	9.88	3.20	5.73	7.95
KA1899	18.16	20.89	23.81	6.81	8.34	10.02	5.24	6.64	7.97
KA2198	22.53	24.36	26.32	7.03	9.34	11.88	4.02	6.76	9.11
KA2510	20.75	23.84	27.03	10.60	12.52	14.59	3.68	6.42	8.96
KA2870	28.42	36.81	45.36	18.55	23.02	27.73	-1.26	7.11	13.94
KA3086	23.95	29.08	35.49	8.39	14.40	22.79	0.28	5.95	8.20

Table 6-7. The horizontal and vertical stresses obtained from the Monte Carlo simulation.

ID	σ_H (MPa)			σ_h (MPa)			σ_v (MPa)		
	lower	mean	upper	lower	mean	upper	lower	mean	upper
KA1623	11.09	18.35	28.13	4.38	10.31	15.50	7.74	9.69	11.68
KA1625	10.44	14.12	18.21	1.51	5.32	8.83	7.58	8.40	9.23
KA1626	9.42	11.78	14.34	5.20	7.31	9.29	3.49	6.60	9.71
KA1899	18.07	20.78	23.73	5.91	7.96	9.94	5.71	7.21	8.72
KA2198	21.79	23.71	25.70	5.82	8.20	10.45	4.78	8.61	12.38
KA2510	20.55	23.77	26.98	5.05	8.44	11.79	9.09	10.59	12.07
KA2870	27.18	35.94	44.94	1.23	11.98	22.33	14.60	18.88	23.15
KA3086	22.48	28.12	35.03	1.32	12.12	22.03	8.81	9.30	9.80

To illustrate the wide variation in rock stresses in a single borehole the results from the Monte Carlo simulation are plotted. In Figures 6-16 and 6-17 the mean values, the upper and the lower values for the maximum and minimum horizontal stresses are shown. These intervals will correspond to a 95% confidence interval.

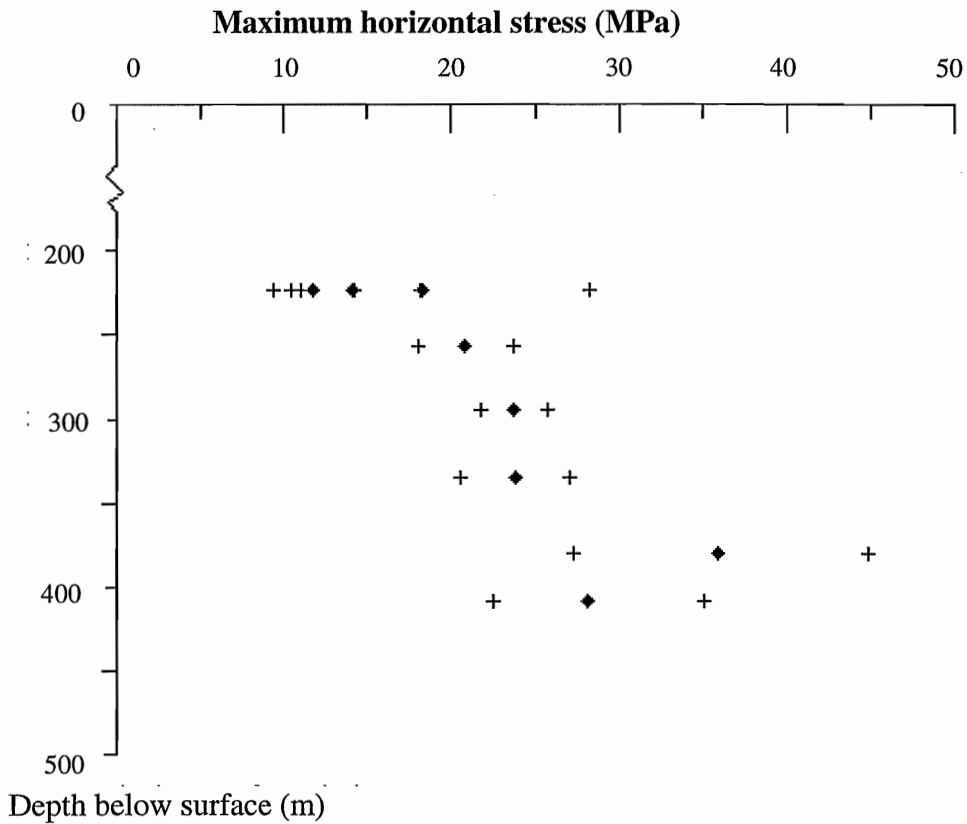


Figure 6-16. Confidence interval on the maximum horizontal stress for each borehole obtained from the Monte Carlo simulation. The crosses represent the lower and upper values in the confidence interval.

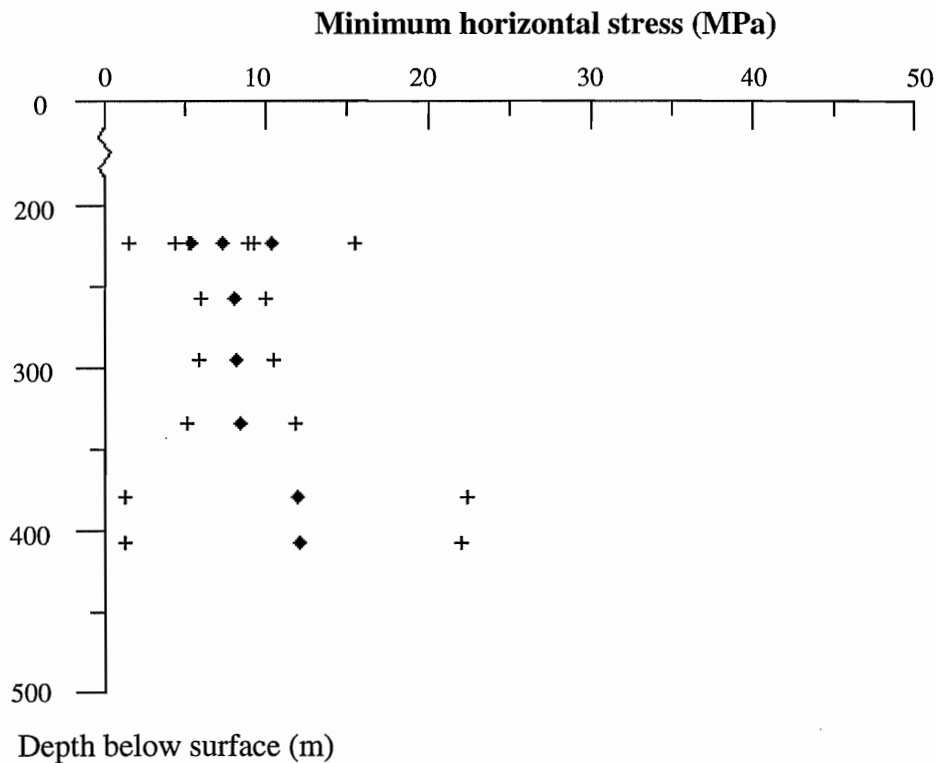


Figure 6-17. Confidence interval for minimum horizontal stress in each borehole obtained from the Monte Carlo simulation. The crosses represent the lower and upper values in the confidence interval.

6.3 Study of cores from overcoring

6.3.1 General

Rock cores from the boreholes listed in Table 6-8 have been mapped in order to detect zones, fractures or abnormal mineral grains that could influence the results of the rock stress measurements. The whole borehole was mapped but only the measurement points and their vicinity were mapped in more detail. Vicinity here means the immediate surroundings of the location of the gauges in the hollow core and the core from the pilot drilling (if it was stored).

Table 6-8 Boreholes in which cores have been studied.

Borehole	Remarks
KA1054	Core exists
KA1623	No core from the actual measurements site
KA1625	No core from the actual measurements site
KA1626	No core from the actual measurements site
KA1899	Core exists
KA2198	Was not found in the store at Äspö
KA2510	Core exists
KA2870	Core exists
KA3086	Core exists
KA3579	Core exists

The observations of the measurement points in the cores as well as comments on the actual measurement results are summarised in Tables 6-9 and 6-10. The comments (Poor to Excellent) on the measurement results have been obtained from the stress measurement reports (Lee et al, 1993, Litterbach et al, 1994, Lee et al, 1994 and Ljunggren and Bergsten, 1998). The orientation in which the boreholes were drilled is also included in the table to compare it with the orientation of the major principal stress direction at Äspö ($\sim 130^\circ$).

6.3.2 Core mapping

The main rock type in borehole KA1054 is diorite, except at measurement point #6 where the rock type is greenstone with a quartz vein. Chlorite and calcite-filled cracks are present in the vicinity of the measurement point #8. The core from point #10 is intact with small visible closed cracks.

No cores were available at the location of stress measurement points in boreholes KA1623, KA1625 and KA1626. The rock type is medium grained diorite for the existing cores of all the three boreholes (Litterbach et al, 1994).

In KA1899, no fracture is observed in the vicinity of the measurement points, however at point #5 a pink material, probably quartz or feldspar has intruded the light medium grained diorite.

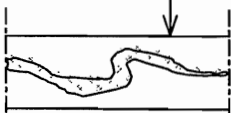
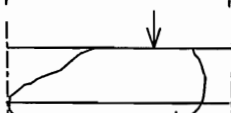

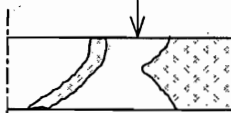
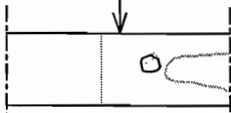

The cores from KA2510 are of grey granite (medium grained). The core at point #1 is coarse grained and contains a healed fracture. No fractures are visible in the vicinity of the points #2, #3, #5 and #6. At point #4 the core is broken at an existing fracture. Some large mineral grains can also be seen in this core.

Both the pilot core and the hollow core remain at the measurement points in KA2870. Nothing special could be seen in the pilot core. The rock type is medium grained diorite varying in colour. A remark should, however, be made on the grain size. Grains of size larger than 10 mm are visible in the core, which may affect the measurement results if the strain gauges are glued over such a large grain. On the hollow core, visible fractures can only be seen on the core at point #5. At this measurement point the major principal stress is almost parallel to the borehole axis and has a magnitude of about 36 MPa, which is two times the magnitude of the intermediate principal stress.

The core at point #2 in borehole KA3086 is broken at a fracture about 7 cm from the location of the measurement point. Healed fractures though exist near measurement points #3, #4 and #5. The rock type in the borehole, is diorite (medium grained).

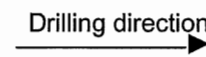
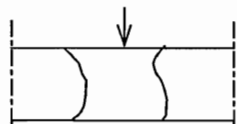

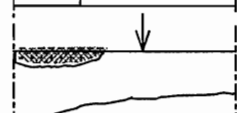
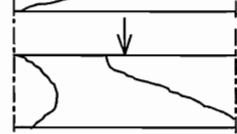
In the borehole, KA3579, the Borehole Image Processing System (BIPS) was used. BIPS pictures were taken between depth 0.700 m and 21.604 m in the borehole, but from 21.070 m and downwards the camera did not film the borehole. The cores from measurement points #8, #9, #10 and #11 were selected for the study since they are thought to be the virgin measurement results. Unfortunately, the borehole walls at points #9, #10 and #11 were not successfully filmed by BIPS. Therefore, only the core taken from point #8 can be compared with the BIPS pictures. The core at point #8 contains no fracture and the BIPS picture at the same location does not show any fracture either (Figure 6-18). The BIPS pictures taken at points #2 - #7 which are not involved in this stage of study are shown in Figures 6-19 to 6-21.

Table 6-9 Observations and comments on the measurement point in the cores (KA1054 –KA2510).

Bore-hole	Point	Rock type	Measurement results	Observation in the vicinity of the point	Sketch (arrow at measurement point)	Orientation of borehole
KA1054	#6	Greenstone	Fair	Quartz vein in the core		294/05
	#8	Diorite	Poor	Chlorite and calcite filled cracks		294/05
	#10	Diorite	Good	Small closed cracks		294/05
KA1899	#1	Light m. g. ² Diorite	Good	No observation		317/02
	#2	Light m. g. Diorite	Good	No observation		317/02
	#3	Light m. g. Diorite	Good	No observation		317/02
	#4	Light m. g. Diorite	Good	No observation		317/02
	#5	Light m. g. Diorite	Fair	Quartz intruded the main rock type		317/02
KA2510	#1	Grey m. g. Granite	Fair	Larger grains and a healed fracture exist		191/03
	#2	Grey m. g. Granite	Poor	No observation		191/03
	#3	Grey m. g. Granite	Excellent	No observation		191/03
	#4	Grey m. g. Granite	Good	The core has been broken at a fracture and some larger grains can be seen.		191/03
	#5	Grey m. g. Granite	Fair	No observation		191/03
	#6	Grey m. g. Granite	Excellent	No observation		191/03

² m. g. = Medium grained

Table 6-10 Observations and comments on the measurement point in the cores (KA2870 – KA3579).

Bore-hole	Point	Rock type	Measurement results	Observation in the vicinity of the point	Sketch (arrow at measurement point)	Orientation of borehole
KA2870	#1	M. g. Diorite	Good	Visual grains of cm size.		339/02
	#2	M. g. Diorite	Fair to good	Visual grains of cm size.		339/02
	#3	M. g. Diorite	Good	Visual grains of cm size.		339/02
	#4	M. g. Diorite	Poor	Visual grains of cm size.		339/02
	#5	M. g. Diorite	Poor	Fractures		339/02
KA3086	#2	M. g. Diorite	Good	The core broken about 7 cm from the measurement point along a fracture.		102/03
	#3	M. g. Diorite	Fair	Healed fractures.		102/03
	#4	M. g. Diorite	Good	Healed fractures.		102/03
	#5	M. g. Diorite	Good	Healed fractures.		102/03
	KA3579	#8	Granite		No observation	
#9		Granite		No observation		298/89
#10		Granite		No observation		298/89
#11		Granite		No observation		298/89

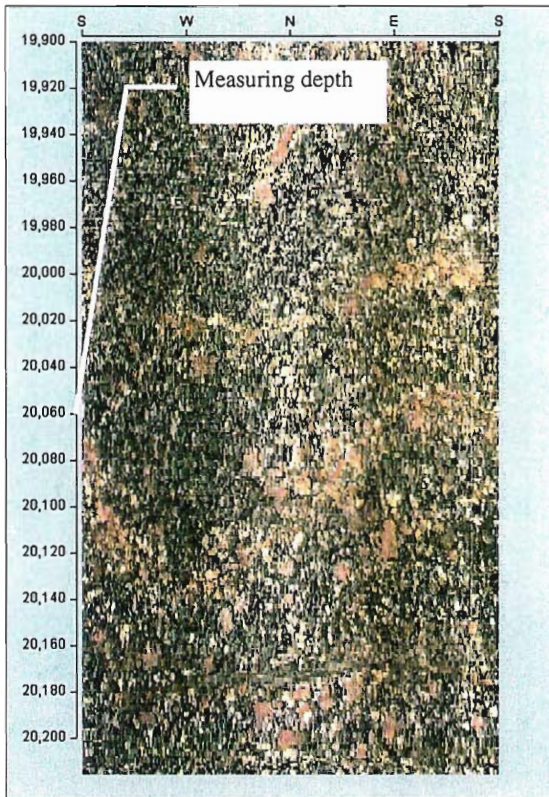


Figure 6-18 BIPS picture taken at the location of stress measurement point #8 in borehole KA3579.

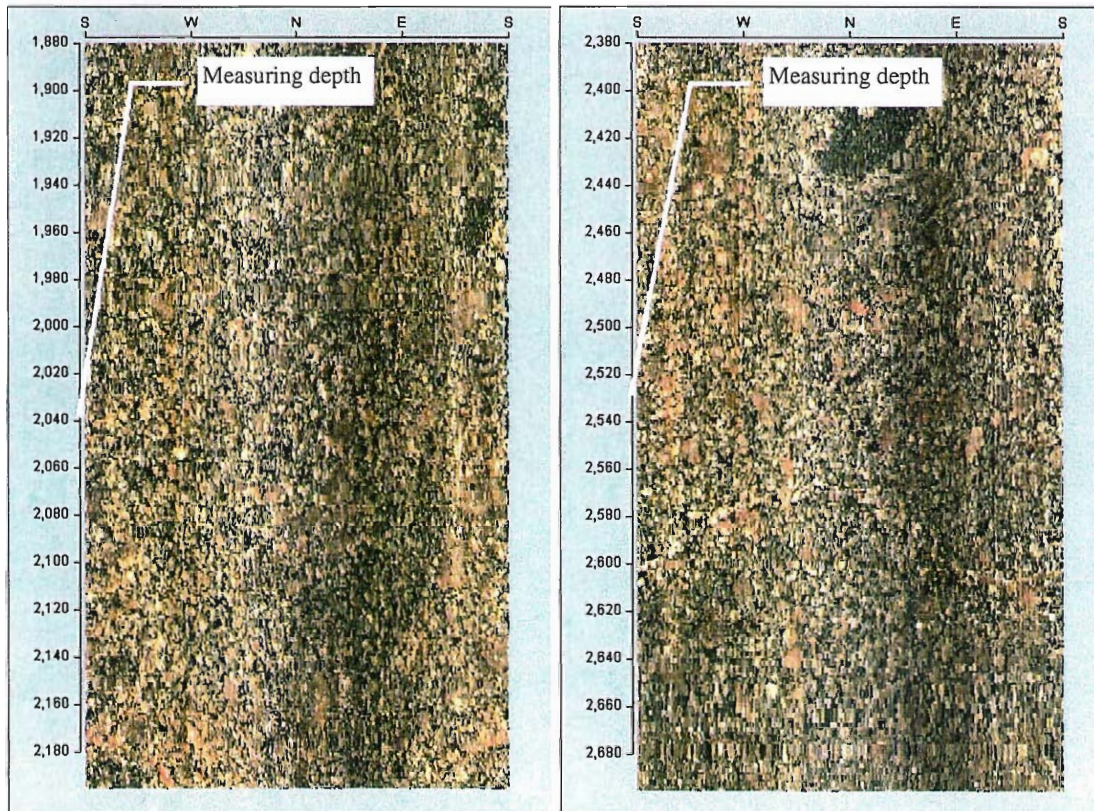


Figure 6-19 BIPS picture taken at the location of stress measurement points #2 (left) and #3 (right) in borehole KA3579.

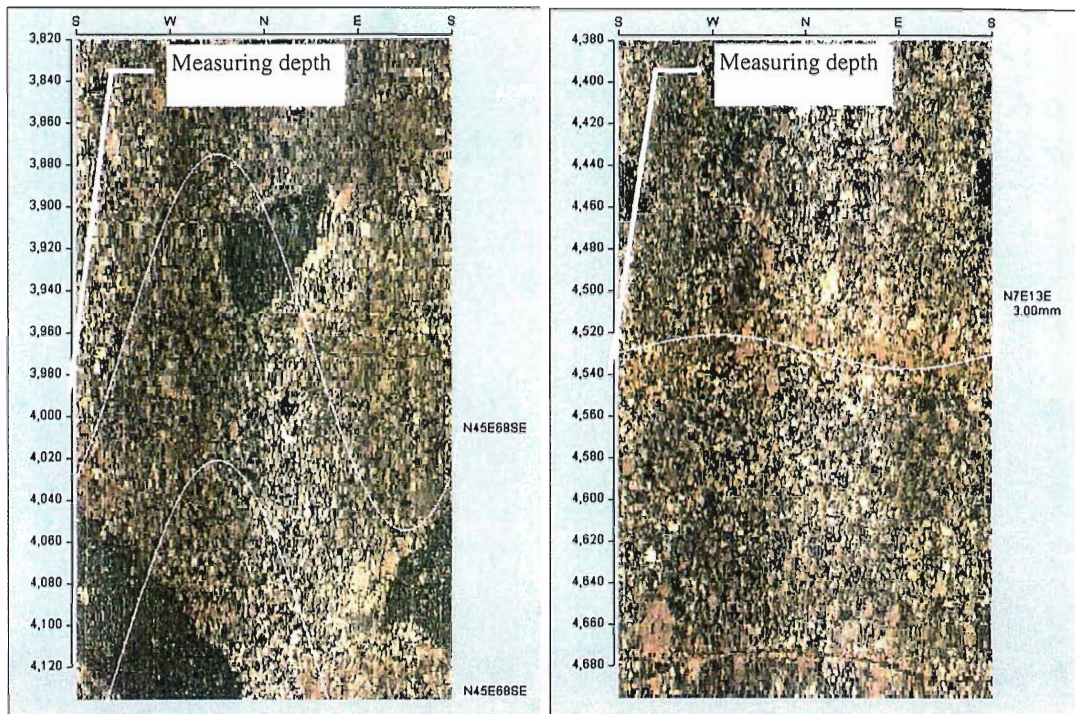


Figure 6-20 BIPS picture taken at the location of stress measurement points #4 (left) and #5 (right) in borehole KA3579.

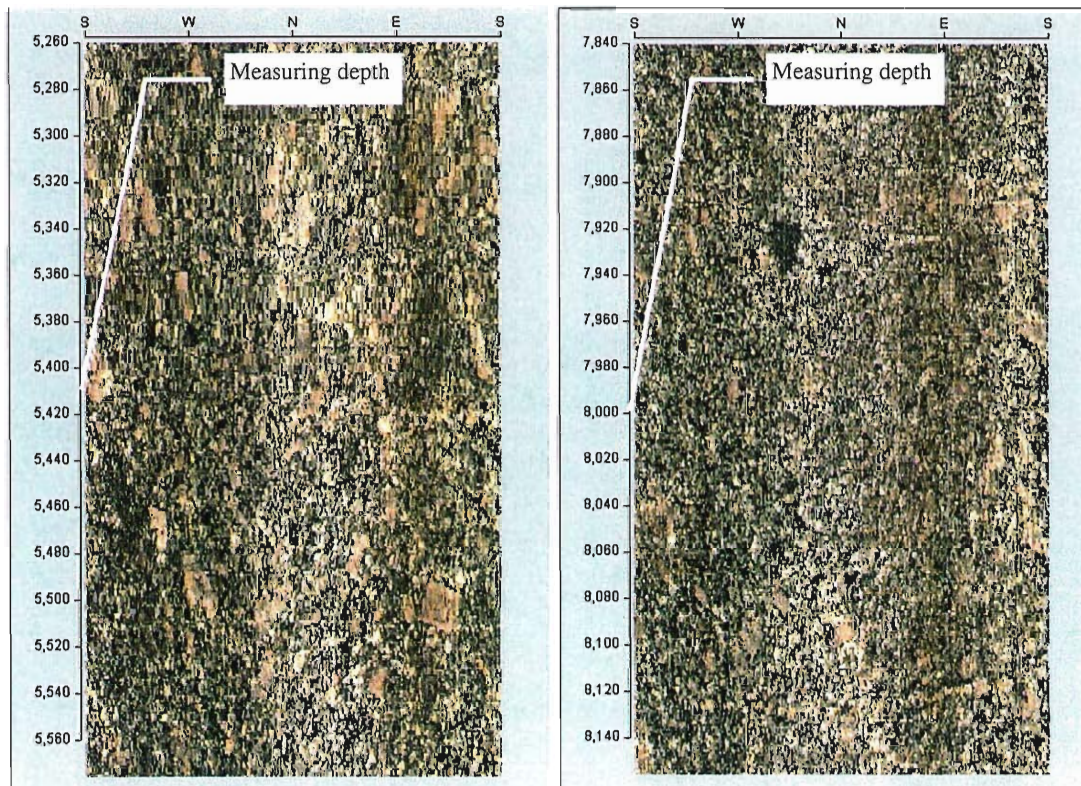


Figure 6-21 BIPS picture taken at the location of stress measurement points #6 (left) and #7 (right) in borehole KA3579.

6.3.3 Conclusion

It appears that some of the visible fractures could be the cause of strange stress magnitudes and orientation. One should remember that core mapping is very objective but core mapping is, however, a contribution to the interpretation of the rock stress measurement results.

6.4 The State of Stress at Äspö

The state of stress at Äspö is defined by using the results from the hydraulic fracturing in borehole KAS02 and the measurements conducted by the SSPB-cell. The measurements from the SSPB-cell are used since these have a Poisson's ratio that corresponds well with the uniaxial tests of rock samples and since the measurements have been done at a distance from the opening so the opening does not influence them. A few measurements conducted by SSPB-cell are excluded due to reliability in the results. These measurements are, the one from borehole KAS05 at depth 357 metres, since the minimum horizontal stress shows an extremely low value (≈ 0 MPa) and all measurements from KA3579G since the credibility of these results is low (Christiansson, 2000).

The linear regression analysis of the maximum and minimum horizontal stresses is shown in Figures 6-22 and 6-23.

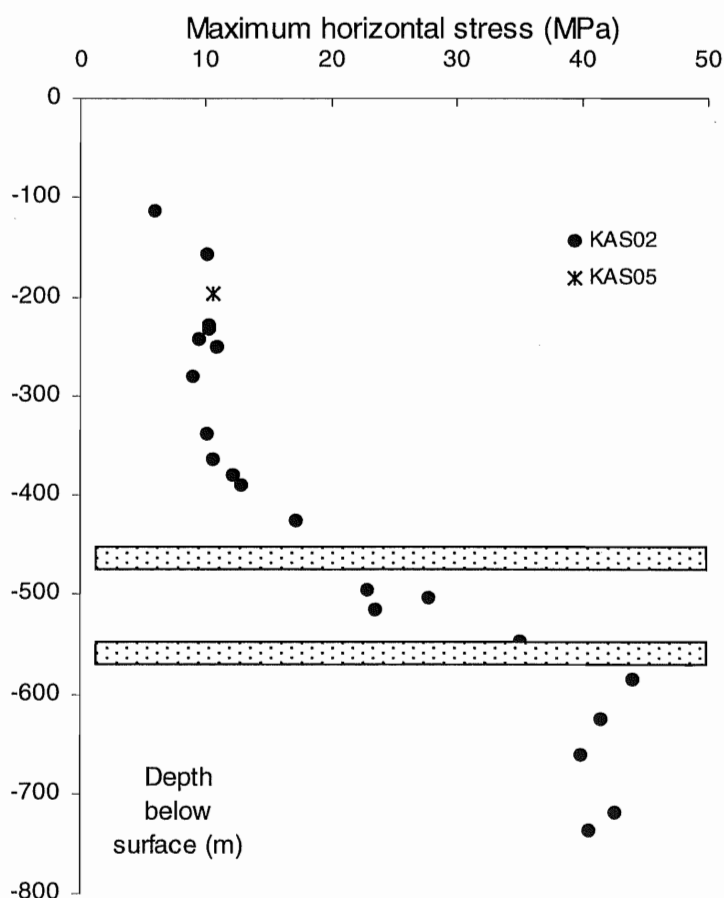


Figure 6-22. Maximum horizontal stress versus depth. The mylonite zones at Äspö are included.

The regression analysis is made on the stresses above and beneath the mylonite zones, and the equations for these two lines are

$$\sigma_H = 1.4 + 0.034z \quad [\text{MPa}] \quad 0 < z < 450 \quad [\text{m}] \quad 6-7$$

$$\sigma_H = -33.2 + 0.11z \quad [\text{MPa}] \quad 450 < z < 550[\text{m}] \quad 6-8$$

where the first one is valid down to a depth, z , of 450 metres.

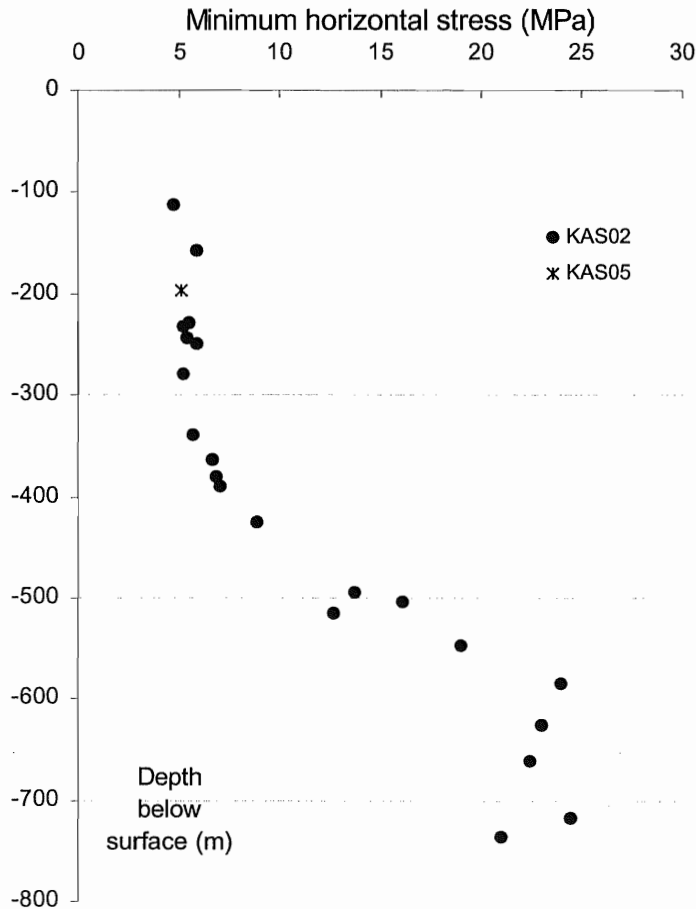


Figure 6-23. Minimum horizontal stress versus depth.

The corresponding linear regression on the minimum horizontal stresses resulted in the following equations

$$\sigma_h = 2.1 + 0.014z \quad [\text{MPa}] \quad 0 < z < 450[\text{m}] \quad 6-9$$

$$\sigma_h = -18.1 + 0.063z \quad [\text{MPa}] \quad 450 < z < 550[\text{m}] \quad 6-10$$

In Figure 6-24 the orientation of the maximum horizontal stress is shown. The trend interval of the steeply fractures found at Äspö (ZEDEX, 1996) is also shown in the figure.

Orientation of the maximum horizontal stress

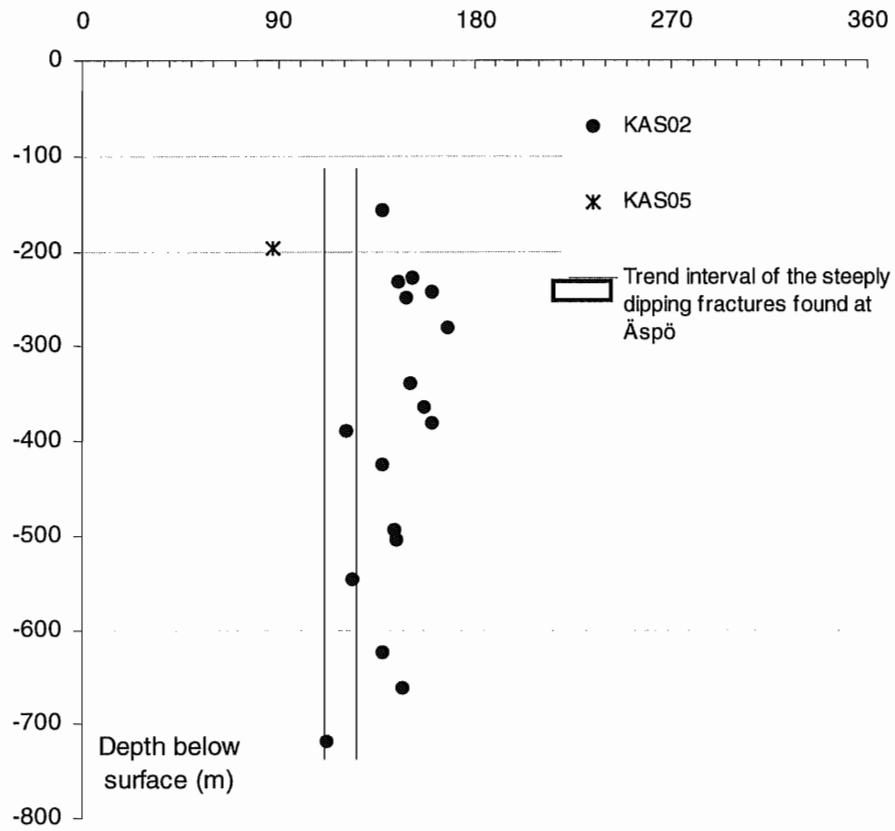


Figure 6-24. The orientation of the maximum horizontal stress versus depth.

7 Discussion and conclusions

7.1 General

When comparing two completely different measuring techniques like overcoring and hydraulic fracturing, one must be aware of certain facts. Hydraulic fracturing assumes that the vertical stress is one of the principal stresses, and therefore the horizontal stresses that are measured will also be principal stresses. Using overcoring, the true principal stresses are achieved. However, these stresses are often transformed to horizontal secondary principal stresses to correlate the measurements against hydraulic fracturing. When this is done, information is lost since one or more of the principal stresses can be oriented in-between the horizontal and vertical axes (Figure 7-1).

Information is lost since the shear stresses that exist in this secondary principal stress state are not taken into consideration.

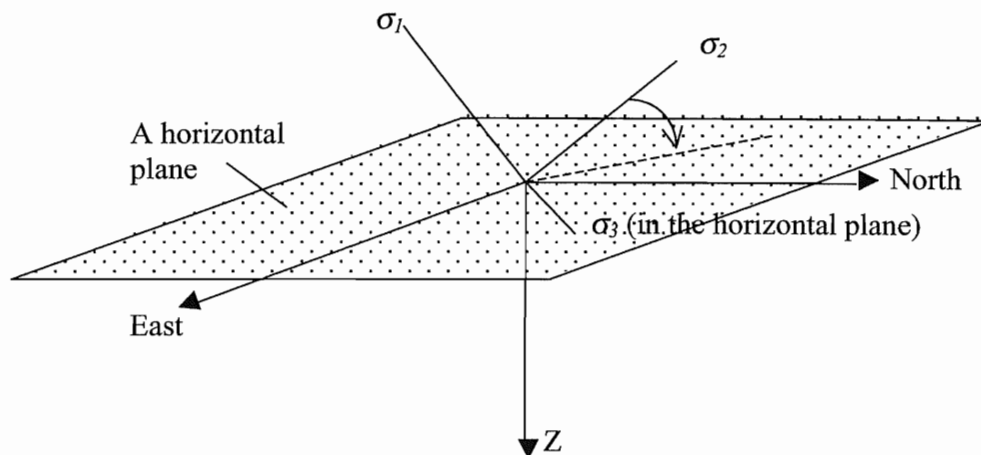


Figure 7-1. An arbitrary state of stress

7.2 Hydraulic fracturing

The magnitudes of the horizontal stresses versus the depth in KAS02 show an increase in the magnitude at a depth around 500 and 560 metres. The major mylonite zones that exist at these locations might be an explanation for this behaviour. However, the same tendency cannot be seen for the orientation of the maximum horizontal stress. Since the mylonite zone is assumed to be sub-horizontal, the horizontal stresses are acting parallel to the zone, and no re-orientation of the stresses will be expected.

The results agree quite well with the stress state in Fennoscandia according to Stephansson et al (1991). The results show a lower minimum horizontal stress than the stress magnitude presented by Stephansson et al 1991. This will also affect the maximum horizontal stress, which also may be slightly low compared to the stress state in Fennoscandia. The orientation of the maximum horizontal stress however, correspond well with the orientation measured in Fennoscandia and is about 143 degrees from north.

7.3 Overcoring

The results from the overcoring measurements show a large scatter in the magnitude of the stresses. The scatter is larger for measurements performed using the CSIRO HI- cell than for the measurements done by using the SSPB Cell. This scatter can also be seen in the Monte Carlo simulation where the confidence interval is quite large for boreholes KA1623A, KA625, KA1626A, KA2870 and KA3086A. However, the orientation of the maximum horizontal stresses is constant with the depth and a very small scatter is shown. The average orientation of the maximum horizontal stress is about 127°.

There is no information if the mylonite zones that intersect borehole KAS02 also intersect the Hard Rock Laboratory at some depth. The increase in horizontal stress at the depth of 380 metres might be related to some geological structures or zones.

7.4 Comparison between hydraulic fracturing and overcoring

The overcoring results show higher stresses than predicted from the pre-investigation, where hydraulic fracturing was made. There can be several reasons to this. One may be that the measurements are performed in the outer section of the influenced zone from the opening. The role of thumb gives that the disturbed zone extent to about 3 times the diameter from the wall of the opening. The measurements done at Äspö have been conducted at a distance of 14 to 17 metres from the opening. The diameter of the opening is 5 metres, which may generate a 15-metre large disturbed zone.

The second cause of higher stresses than expected can be the high values of Poisson's ratio, especially the stresses calculated from the strains measured by the CSIRO HI-cell. The stresses determined from the strain measurements by the SSPB-cell coincide better with the results from the hydraulic fracturing.

The measurements from hydraulic fracturing are much lower than the results from overcoring. The reason to this could be that the interpretation method that has been used (tangent intersection method), can result in lower stresses than other methods (Klasson, 1989).

The ratio between the maximum horizontal stress and minimum horizontal stresses obtained from hydraulic fracturing is quite constant about 1.8, while the ratio obtained from overcoring is much more varying. The ratio is ranging between 1.22 to 8.95. Attention to the constant ratio obtained from hydraulic fracturing should be taken, since a variation should be expected. Rutqvist et al (1999) has listed a number of possible uncertainties due to the induced fracture. In the extreme case, where a more conductive fracture is induced, the reopening pressure would be equal to the minimum horizontal stress. This leads to a ratio of 2 between the maximum and minimum horizontal stresses if the second breakdown method is used to determine the maximum horizontal stress. If this is the case, there is not possible to determine the maximum horizontal stress because the pressure response would not show any effect of the tangential borehole stress (Rutqvist et al., 1999).

However, the orientation of the maximum horizontal stress, coincides rather well between overcoring and hydraulic fracturing, which is positive since the orientation of a deep repository will be chosen such that favourable stability conditions can be achieved.

7.5 Variation of the elastic properties

The elastic parameters, Young's modulus and Poisson's ratio will affect the results from the overcoring, especially Poisson's ratio. Poisson's ratios are ranging from 0.16 to 0.43 in the area of interest. Using these two extreme values in the calculation of the stresses

out from the strain the magnitude increases with about 33% for the maximum horizontal stress and 58 % for the minimum horizontal stress when the upper extreme value is used.

Poisson's ratios are differing depending on the overcoring method used. In the samples from the overcoring with an SSPB-cell, Poisson's ratio is about 0.23 and when CSIRO HI-cell is used, Poisson's ratio is about 0.34. A statistical analysis, comparing these two groups shows a significant difference between the means. The reason for this may be the different handling of the core at the biaxial testing. The CSIRO HI Cell is pressurised up to 15 MPa with loading increments of 5 MPa (Litterbach et al, 1994) while the SSPB Cell is pressurised up to 10 MPa with loading increments of 1 MPa (Ljunggren and Bergsten, 1998).

No significant difference can, however, be observed in the values of Young's modulus when comparing the two overcoring methods.

In a paper by Martin and Christiansson (1991), the influence of microcracking on overcoring has been investigated and presented. Overcoring samples from boreholes drilled at an angle perpendicular to the major principal stress direction showed the greatest amount of stress-induced microcracking. Laboratory tests presented in the paper showed that the difference in the properties of pink and grey granite was associated with the presence of stress-induced microcracks of the grey granite. Poisson's ratio was higher and Young's modulus was lower in the samples of grey granite.

In the case of the measurements conducted at Äspö HRL, the samples from the overcoring of CSIRO HI-cell might have more stress-induced microcracks and therefore show higher value of Poisson's ratio and lower value of Young's modulus. The uniaxial tests show Poisson's ratios, which do not differ between rock types, more similar to the results of the SSPB-cells.

7.6 Core mapping

The study of the cores from overcoring was made in order to detect any correlation between the quality of the measurements with the presence of larger visible fractures in the vicinity of the gauges. In some cores, the poor or fair result could partly be assumed to depend on the presence of small filled cracks or of grains of cm-size. On the contrary, in some cores good measurement results were achieved even with the presence of grains of cm-size or healed fractures.

BIPS pictures taken in a borehole where stress measurements have been performed were also studied to detect causes to poor quality of the measurements. This study did not reveal any useful information.

7.7 Conclusions

Following conclusion can be drawn from the results and the discussion

- The results from the overcoring with CSIRO HI show higher magnitudes than expected by the hydraulic fracturing but coincide in the orientation
- The results from overcoring with the SSPB Cell agree better with the results from the hydraulic fracturing measurements, which coincide well with the stress of state at Fennoscandia, both in magnitude and orientation.
- There is significant difference in Poisson's ratio between the samples of SSPB Cell and CSIRO HI Cell.

- The main reason for deviation in the stress magnitudes between overcoring by CSIRO HI Cell and SSPB Cell might be the high Poisson's ratio that are obtained from the measurements from CSIRO HI Cell. An explanation to this can be the handling of the biaxial tests, which can cause microcracks in the sample if the applied pressure is too high.
- The state of stress is based on that the results from the hydraulic fracturing and overcoring made by SSPB Cell, since overcoring made by using CSIRO HI Cell shown high values of the Poisson's ratio and the test results may not be reliable.

7.8 Further work

There are some indications that stresses and geological structures correlate in some way. Further work should be done in this area, by using numerical analysis to see how the stresses change in the vicinity of a geological structure.

The results showed that using a Poisson's ratio of 0.34 instead of 0.23 could affect the magnitude of the minimum horizontal stress up to 23 %. More work should then be done to increase the knowledge of the behaviour of the core when the overcoring is made, and also how this will effect the elastic parameters. Therefore, some effort should also be made to understand and study the biaxial tests. Investigate if there exist better methods to determine the elastic parameter, for example a triaxial chamber.

References

- Aamodt, L. R. and Kuriyagawa, M.**, (1983), Measurement of Instantaneous Shut-In Pressure in Crystalline Rock. In: *Proc. Hydraulic Fracturing Stress Measurements*, Monterey, National Academy Press, Washington, pp.139-142.
- Abou-Sayed, A. S., Brechtel, C. E. and Clifton, R. J.**, (1978), *In situ* Stress Determination by Hydrofracturing: A fracture Mechanics Approach. *Journal of Geophysical research*, Vol. 83, No. B6, pp. 2851-2862.
- Amadei, B. and Stephansson, O.**, (1997). *Rock stresses and its measurements*. Chapman & Hall, Cambridge.
- Australian Mining Consultants Pty Ltd**, (1998), *General Appendix- In situ Virgin Stress Measurement*, AMC, Level 19, 114 William Street, Melbourne, Victoria 3000, Australia.
- Baumgärtner, J. and Rummel, F.**, (1989), Experience with "Fracture Pressurisation tests" as a Stress Measuring Technique in a jointed Rock Mass., *Int. J. of Rock Mech. Min. Sci. & Geomech. Abstr.*, Vol. 26, No. 6, pp. 661-671.
- Bjarnason, B. and Torikka, A.**, (1989), *Field instrumentation for hydrofracturing stress measurements. Documentation of the 1000 m hydrofracturing unit at Luleå University of Technology*. SKB Technical Report 89-17.
- Bjarnason, B.**, (1986), *Hydrofracturing rock stress measurements in the Baltic shield*. Licentiate thesis 1986:12L. Luleå University of Technology, Luleå, Sweden.
- Bjarnason, B., Klasson, H., Leijon, B., Strindell, L. and Öhman, T.**, (1989). *Rock Stress Measurements in Boreholes KAS02, KAS03 and KAS05 on Åspö*. SKB Progress Report 25-89-17.
- Bjarnason, B., Ljunggren, C. and Stephansson, O.**, (1989), New Developments in Hydrofracturing Stress Measurements at Luleå University of Technology. *Int. J. Rock Mech. Min. Sci. & Geomech Abstr.*, **26**, pp. 579-86.
- Cornet, F. H.**, (1981), Interpretation of Hydraulic Injection Test for In-Situ Stress Determination. In: *Proc. Hydraulic Fracturing Stress Measurements, 2-5 Dec. 1981*, National Academy Press, Washington, D.C.
- Christiansson, R.**, (2000), Personal communication, SKB Stockholm
- Delin, P., Olsson, P. and Stille, H.**, (1993a), *Field and laboratory testing of rocks, 700-1475 m*, SKB Progress Report 25-93-02.
- Delin, P., Olsson, P. and Stille, H.**, (1993b), *Rock stress measurements and laboratory testing of rock*, SKB Progress Report 25-94-02.
- Doe, T.W., Hustrulid, W.A., Leijon, B., Invald, K. and Strindell, L.**, (1983), Determination of the State of Stress at the Stripa Mine, Sweden. In: *Proc. Hydraulic Fracturing Stress Measurements*, Monterey, National Academy Press, Washington, pp.119-29.

Duncan Fama, M. E. and Pender, M. J., (1980). Analysis of the Hollow Inclusion Technique for Measuring *In situ* Rock Stress. *Int. J. Rock Mech. Min. Sci. & Geomech. Abstr.* 17, pp. 137-146.

Enever, J. And Chopra, P.N, (1986), Experience with hydraulic fracture stress measurements in granite, In: *Proc. Int. Symp. Rock Stress and Rock Stress Measurements*, Stockholm, Centek Publ., Luleå, pp. 411-20.

Enever, J. R., Cornet, F. and Roegiers, J. C., (1992). Commission on Interpretation of Hydraulic Fracture Records. *Int. J. Rock Mech. Min. Sci. & Geomech. Abstr.* 29 No. 1, pp. 69-72.

Gronseth, J. M, (1982), Determination of the instantaneous shut in pressure from hydraulic fracturing data and its reliability as a measure of the minimum principal stress, In: *Proc. 23rd US Symp. Rock Mech.*, Berkeley, SME/AIME, New York, pp.183-189.

Haimson, B. C., (1978). The Hydrofracturing Stress Measuring Method and Recent Field Results. *Int. J. Rock Mech. Min. Sci. & Geomech. Abstr.* 15, pp. 167-178.

Hallbjörn, L., (1986), Rock stress measurements performed by Swedish State Power Board. In: *Proc. of the International Symp. On Rock Stress and Rock Stress Measurements, Stockholm, 1-3 Sept. 1986.* (Ed. O. Stephansson), Centek Publishers, Luleå.

Hallbjörn, L., Ingevald, K., Martna, J. And Strindell, L., (1989), A new automatic probe for the measurement of triaxial rock stresses in deep boreholes. In: *Proc. of the Rock Mechanics Meeting, Stockholm, 26 Jan. 1989*, Befo, Stockholm.

Hayash, K. and Sakurai, I. (1989), Interpretation of Hydraulic Fracturing Shut-in Curves for Tectonic Stress Measurements. *Int. J. Rock Mech. Min. Sci. & Geomech. Abstr.*, 26, pp. 477-482.

Hiltscher, R., Martna, F. L. and Strindell, L., (1979), The measurement of triaxial rock stresses in deep boreholes and the use of rock stress measurements in the design and construction of rock openings. In: *Proc. 4th International Congress of Rock Mechanics, Montreaux*, Vol. 2, pp. 227-234.

Hoek, E. and Brown, E. T., (1981). *Underground Excavations in Rock*. The Institution of Mining and Metallurgy, London

Hubbert, M.K and Willis, D.G., (1957), Mechanics of Hydraulic Fracturing, *J. of Petroleum Technology* 9, 6, pp. 153-168.

Jaeger, J.C. and Cook, N.G.W., (1979), *Fundamentals of rock mechanics*, Chapman and Hall, London.

Johansson, Maria, C., (1999), Bildanalys av borrhålsbilder för bestämning av bergsprickors orientering och apertur, In: *Proc. of the Rock Mechanics Meeting, Stockholm, 10 March, 1999*, pp. 43-57. Stockholm: SveBeFo (in Swedish).

- Klasson, H.**, (1989), *Bergspänningsmätning hydraulisk spräckning - En tidstudie av tryck-tidssambandet vid testning*, Master thesis 1989:100 E, Luleå University of Technology (in Swedish).
- Lee, M. Hewitt, T. and Stillborg, B.** (1994). *Äspö Virgin Stress Measurement Results - Measurements in Boreholes KA1899A, KA2198A and KA2510A*. SKB Technical Note 25-94-13V.
- Lee, M., Bridges, M. and Stillborg, B.**, (1993), *Äspö Virgin Stress Measurements Results in Section 1050, 1190 and 1620 m of the Access Ramp*, SKB Progress report 25-93-02.
- Leeman, E. R and Hayes, D. J.**, (1966), A technique for determining the complete state of stress in rock using a single borehole. In: *Proc. 1st Cong. of the Int. Soc. Rock Mechanics, Lisbon 25 Sept. – 1 Oct. 1966*, Vol. 2, pp. 17-24, Laboratório Nacional de Engenharia Civil.
- Litterbach, N., Lee, M., Struthers, M. and Stillborg, B.**, (1994), *Virgin Stress Measurement Results Boreholes KA2870A and KA3068A*, SKB Progress report 25-94-32.
- Ljunggren, C. and Amadei, B.**, (1989), Estimation of virgin rock stresses. *Int. J. Rock Mech. Min. Sci. & Geomech. Abstr.*, **26**, pp. 69-78.
- Ljunggren, C. and Bergsten, K-Å.**, (1998), *Rock stress measurements in KA3579G*, SKB Progress report HRL-98-09.
- Martin, C.D. and Christiansson, R.**, (1991), Overcoring in Highly Stressed Granite-the Influence of Microcracking, *Int. J. Rock Mech. Min. Sci. & Geomech. Abstr.*, **28**, pp. 53-70.
- McLennan, J. D. And Roegiers, J.C.**, (1983), Do Instantaneous Shut-in Pressure Accurately Represent the Minimum Principal Stress? In: *Proc. Hydraulic on Hydraulic Fracturing Stress Measurements, 2-5 Dec. 1981*, National Academic Press, Washington, D.C. pp.68-78.
- Nilsson, G., Litterbach, N., Lee, M. and Stillborg, B.**, (1997), *Virgin Stress Measurement Results Borehole KZ0059B*, Äspö HRL Technical note, TN-97-25g.
- Olsson, O.**, (1998), *PM for Authors of SKB Reports - Directions for formatting*, SKB ÄH 8.5v.1
- Ratigan, J. L.**, (1992), The use of Fracture Reopening Pressure in Hydraulic Fracturing Stress Measurements, *Rock Mech. Rock Engng.*, **25 (4)**, pp 225-236.
- RD&D Programme 92** (1992), *Treatment and final disposal of nuclear waste. Programme for encapsulation, deep geological disposal, and research, development and demonstration*. SKB, Stockholm, September 1992.

RD&D Programme 95 (1995), *Treatment and final disposal of nuclear waste. Programme for encapsulation, deep geological disposal, and research, development and demonstration.* SKB, Stockholm, September 1995.

Rhén, I., Gustavsson, G., Stanfors, R. and Wikberg, P., (1997b). *ÅSPÖ HRL - Geoscientific evaluation 1997/5. Models based on site characterization 1986-1995.* SKB TR 97-06.

Rutqvist J., Stephansson, O. and Tsang C.-F. (1999), Uncertainty in estimate of maximum principal stress from hydraulic fracturing due to the presence of the induced fracture *Int. J. Rock Mech. Min. Sci. & Geomech. Abstr.* Accepted February (1999).

Stacey, T. R., (1981). A simple Extension Strain Criterion for Fracture of Brittle Rock. *Int. J. Rock Mech. Min. Sci. & Geomech. Abstr.* Vol. 18, pp. 469-474.

Stephansson, O., Ljunggren, C. and Jing, L., (1991), Stress measurements and tectonic implications for Fennoscandia. *Tectonophysics, Vol. 189, No. 1/4, pp. 317-322.*

Stillborg, B. and Leijon, B., (1982), *A comparative study of rock stress measurements at Luossavaara Mine,* Report FB 8217. Swedish Mining Research Foundation, Kiruna.

Wikman, H., Kornfält, K-A, Riad, L., Munier, R. and Tullborg, E-L, (1988), *Detailed Investigation of the Drillcores KAS02, KAS03 and KAS04 on Åspö Island and KLX01 at Laxemar,* SKB Progress report 25-88-11.

Worotnicki, G., (1993), CSIRO Triaxial Stress Measurement Cell. In: *Comprehensive Rock Engineering, Vol. 3.* Ed. by J. A. Hudson. Pergamon Press, Oxford. pp. 329-394.

ZEDEX, (1996), Numerical modelling, acoustic emission and velocity studies of the excavation disturbed zone at the hard rock laboratory. SKB Technical note TN-97-02z.

Zoback, M.D. and Haimson, B.C., (1982), Status of the hydraulic Fracturing method for in-situ stress measurements. In: *Proc. 23rd US Symp. Rock Mech.,* Berkeley, SME/AIME, New York, pp. 143-156.

Appendix A

Information about the virgin stress measurements.

Units

Depth	[m]
Young's modulus, E	[GPa]
Stress components, σ	[MPa]
Shear components, τ	[MPa]
Dip	[°]
Dip direction	[°]

Table 1 Borehole KAS02

<i>Number</i>	<i>Depth (m)</i>	P_b	P_{r1}	P_{r2}	P_{r3}	P_{s1}	P_{s2}	P_{s3}	P_{s4}	σ_v	σ_{H1}	σ_{H2}	σ_h	<i>Bearing of σ_H</i>	σ_{H2}/σ_h
1	113	13.9	8.1	8.5	8.3	5.4	5.0	4.7	4.5	2.9	7.5	6.0	4.7	-	1.28
2	159	11.4	7.5	7.2	7.0	6.8	6.3	6.1	5.9	4.1	13.6	10.2	5.9	138	1.73
3	229	10.5	6.6	6.2	5.8	6.8	6.7	5.9	5.5	5.9	13.3	10.3	5.5	151	1.87
4	233	9.9	5.3	4.8	4.5	5.3	5.3	5.2	5.0	6.1	13.0	10.3	5.2	145	1.98
5	243	10.5	6.9	6.7	6.6	6.4	5.7	5.4	4.9	6.3	13.0	9.5	5.4	160	1.76
6	250	11.0	7.0	6.8	6.6	6.8	6.2	5.1	5.9	6.5	14.0	10.9	5.9	149	1.85
7	280	13.5	6.8	6.5	6.4	6.3	5.2	4.7	4.6	7.3	9.8	9.1	5.2	168	1.75
8	339	14.8	7.1	6.9	6.8	5.9	5.7	5.1	5.0	8.8	9.6	10.2	5.7	150	1.79
9	364	11.9	9.9	9.1	9.1	7.8	7.3	6.9	6.6	9.5	17.6	10.7	6.6	157	1.62
10	381	11.7	8.2	8.1	7.7	7.2	6.8	6.8	6.7	9.9	16.0	12.3	6.8	160	1.81
11	390	10.5	8.8	8.4	8.2	7.2	6.9	7.1	7.0	10.1	17.8	12.8	7.0	121	1.83
12	426	12.3	.5	9.2	9.0	9.1	8.9	8.8	8.6	11.1	21.4	17.2	8.8	138	1.95
13	495	22.3	18.5	18.2	18.0	16.2	14.8	13.7	13.4	12.9	26.1	22.9	13.7	143	1.67
14	504	23.9	20.3	20.2	19.5	16.0	17.3	17.6	18.8	13.1	31.4	27.8	16.0	144	1.74

15	515	18.0	14.5	14.3	14.3	15.3	12.6	12.6	13.0	13.4	27.1	23.5	12.6	-	1.87
16	547	26.2	22.2	21.9	21.6	19.4	19.1	19.0	19.0	14.2	38.5	35.1	19.0	124	1.85
17	585	32.9	27.8	27.8	28.5	25.0	24.2	23.9	23.9	15.2	46.1	43.9	23.9	-	1.84
18	625	31.8	28.3	27.6	27.0	26.9	24.5	24.2	23.0	16.2	44.5	41.4	23.0	138	1.8
19	661	31.5	27.9	27.3	27.2	23.5	23.1	22.4	21.7	17.2	45.4	39.9	22.4	147	1.78
20	718	33.9	30.9	30.7	30.0	27.0	26.7	24.9	24.4	18.7	46.6	42.5	24.4	112	1.74
21	737	27.8	23.0	22.5	21.9	22.1	21.0	21.0	20.7	19.2	42.9	40.5	21.0	-	1.93

Table 2 Boreholes KAS03

<i>Number</i>	<i>Depth (m)</i>	P_b	P_{r1}	P_{r2}	P_{r3}	P_{s1}	P_{s2}	P_{s3}	P_{s4}	σ_v	$\sigma_{H I}$	$\sigma_{H II}$	σ_h	<i>Bearing of σ_H</i>	$\sigma_{H II} / \sigma_h$
1	131.5	10.8	5.8	5.8	5.7	4.1	3.7	3.6	3.6	3.4	5.7	5.0	3.6	145	1.39
2	153.8	14.9	6.7	6.7	6.7	5.1	5.1	4.5	4.2	4.0	4.3	6.8	4.5	164	1.51
3	347.4	15.6	8.8	8.4	8.3	6.4	5.7	5.5	5.5	-	-	-	-	Horizontal fracture	
4	481.4	18.0	12.6	12.6	12.6	10.4	10.4	10.7	10.9	12.5	19.8	19.5	10.7	160	1.82
5	494.8	16.0	12.0	11.4	10.2	10.4	10.4	10.9	10.9	12.9	22.4	20.7	10.9	126	1.90
6	515.1	20.3	16.0	15.9	15.7	12.9	12.9	11.8	11.6	13.4	20.8	19.4	11.8	136	1.64
7	534.0	14.4	10.3	9.7	9.5	11.3	11.3	11.8	11.8	13.9	26.7	25.1	11.8	144	2.13

8	536.0	17.3	12.8	11.9	11.5	12.3	12.3	12.4	12.	13.9	25.6	24.4	12.4	152	1.97
9	545.9	16.0	11.9	11.5	10.7	10.9	10.9	10.7	79.8	14.2	21.8	20.2	10.7	124	1.89
10	547.9	15.2	1.7	11.3	10.8	11.2	11.2	9.8	9.8	14.2	1.9	17.7	9.8	129	1.81
11	550.9	15.8	11.4	11.3	11.0	10.9	10.9	10.7	9.8	14.2	19.3	18.0	9.8	130	1.84
12	625.3	15.8	11.7	11.3	11.0	12.0	12.0	10.0	9.9	16.3	19.9	18.3	10.0	-	1.83
13	664.0	15.5	10.4	9.9	9.8	9.1	9.1	8.4	8.5	17.3	18.3	15.1	8.5	142	1.78
14	666.0	14.6	10.0	9.7	9.5	9.3	9.3	9.6	9.8	17.3	22.5	18.8	9.6	144	1.96
15	739.4	16.6	15.0	13.4	13.1	13.3	13.3	13.7	13.8	19.2	33.8	26.1	13.7	160	1.91
16	819.8	31.9	29.9	30.6	29.2	25.5	25.5	22.6	22.8	21.3	44.2	37.9	22.6	-	1.68
17	822.3	31.3	25.3	23.3	22.9	23.4	23.4	23.0	23.2	21.4	43.4	43.7	23.0	-	1.9
18	877.4	29.7	24.5	24.1	23.9	21.0	21.0	21.0	21.3	22.8	40.7	38.5	21.0	-	1.83
19	880.4	31.5	24.7	24.1	23.9	22.1	22.1	24.1	21.6	22.9	40.1	39.5	21.4	118	1.85
20	885.4	30.6	24.8	23.8	23.9	23.1	23.1	22.6	22.6	23.0	45.7	43.0	22.6	157	1.9
21	893.3	34.2	26.6	26.1	25.8	25.7	25.7	24.4	24.2	23.2	47.2	46.3	24.3	-	1.91
22	962.8	33.4	26.2	25.8	25.0	24.8	24.8	24.9	24.3	25.0	48.0	48.5	24.9	115	1.95

Table 3 Borehole KAS05

<i>Number</i>	<i>Depth</i>	<i>E</i>	<i>v</i>	σ_x	σ_y	σ_z	τ_{xz}	τ_{yz}	τ_{zx}	σ_1	<i>Dip dir.</i>	<i>Dip</i>	σ_2	<i>Dip dir.</i>	<i>Dip</i>	σ_3	<i>Dip dir.</i>	<i>Dip</i>	σ_H	σ_h	<i>Bearing of σ_H</i>	σ_H/σ_h
1	195.31	58	0.20	-	-	-	-	-	-	10.3	268.0	13.9	2.4	0.4	9.4	1.5	123.4	73.2	9.8	2.4	87.7	4.08
2	196.61	63	0.25	-	-	-	-	-	-	10.2	234.1	23.8	7.9	137.9	13.8	3.9	20.3	62.0	9.3	7.6	68.1	1.22
3	197.41	64	0.13	-	-	-	-	-	-	13.4	273.1	17.4	8.4	64.3	70.3	4.9	180.3	8.9	12.9	5.0	91.9	2.58
4	355.01	74	0.22	-	-	-	-	-	-	20.2	261.6	43.4	14.4	123.6	38.1	-0.7	14.7	22.5	17.0	1.9	100.5	8.95
5	355.91	68	0.19	-	-	-	-	-	-	16.2	86.8	76.2	10.1	305.0	10.9	-3.0	213.4	8.3	10.3	-2.6	122.7	-
6	356.81	62	0.16	-	-	-	-	-	-	10.8	281.4	10.9	5.4	135.1	77.0	-0.7	12.8	7.0	10.6	-0.6	102.2	-
7	357.74	68	0.19	-	-	-	-	-	-	17.7	102.9	2.7	4.9	201.3	71.9	2.1	12.0	17.8	17.7	2.3	102.8	7.70

Table 4 Borehole KA1054A

<i>Number</i>	<i>Depth</i>	<i>E</i>	<i>v</i>	σ_x	σ_y	σ_z	τ_{xz}	τ_{yz}	τ_{zx}	σ_1	<i>Dip dir.</i>	<i>Dip</i>	σ_2	<i>Dip dir.</i>	<i>Dip</i>	σ_3	<i>Dip dir.</i>	<i>Dip</i>	σ_H	σ_h	<i>Bearing of σ_H</i>	σ_H/σ_h
1	143.7	70.1	0.25	8.4	13.3	5.7	-3.7	3.6	0.3	16.2	115	17	7.6	14	31	3.5	230	54	-	-	-	-
2	143.7	72.7	0.27	5.5	10.9	1.9	-2.0	-1.1	-3.4	11.5	109	00	7.2	199	34	-0.4	18	56	-	-	-	-
3	143.7	74.7	0.28	9.5	12.9	4.3	-2.9	1.3	1.6	14.5	119	02	8.8	28	25	3.3	214	65	-	-	-	-

Table 5 Borehole KA1623A

<i>Number</i>	<i>Depth</i>	<i>E</i>	<i>v</i>	σ_x	σ_y	σ_z	τ_{xz}	τ_{yz}	τ_{zx}	σ_1	<i>Dip dir.</i>	<i>Dip</i>	σ_2	<i>Dip dir.</i>	<i>Dip</i>	σ_3	<i>Dip dir.</i>	<i>Dip</i>	σ_H	σ_h	<i>Bearing of σ_H</i>	σ_H/σ_h
1	223	63.8	0.40	14.8	18.9	12.6	-1.3	-1.2	-4.7	19.3	111	05	18.5	205	39	8.6	15	50	19.3	14.4	106	1.34
2	223	53.3	0.40	11.0	14.9	7.0	-1.6	0.7	-1.1	15.6	111	07	10.6	202	12	6.7	353	76	15.5	10.4	110	1.49
3	223	61.9	0.44	9.6	14.2	6.8	-1.9	0.7	-0.8	15.0	110	07	9.0	212	12	6.6	353	76	14.8	8.9	110	1.66

Table 6 Borehole KA1625A

<i>Number</i>	<i>Depth</i>	<i>E</i>	<i>v</i>	σ_x	σ_y	σ_z	τ_{xz}	τ_{yz}	τ_{zx}	σ_1	<i>Dip dir.</i>	<i>Dip</i>	σ_2	<i>Dip dir.</i>	<i>Dip</i>	σ_3	<i>Dip dir.</i>	<i>Dip</i>	σ_H	σ_h	<i>Bearing of σ_H</i>	σ_H/σ_h
1	223	71.7	0.38	12.7	10.9	11.1	-5.1	-1.0	3.8	18.7	324	26	10.1	097	54	6.0	222	23	16.9	6.7	140	2.52
2	223	58.7	0.35	8.6	7.9	6.8	-3.1	-0.9	1.1	11.8	318	16	6.4	123	74	5.1	227	04	11.4	5.1	138	2.24
3	223	59.5	0.33	8.9	9.1	7.3	-3.5	-1.3	0.9	12.9	315	15	7.0	166	72	5.5	046	09	12.5	5.5	134	2.27

Table 7 Borehole KA1626A

<i>Number</i>	<i>Depth</i>	<i>E</i>	<i>v</i>	σ_x	σ_y	σ_z	τ_{xz}	τ_{yz}	τ_{zx}	σ_1	<i>Dip dir.</i>	<i>Dip</i>	σ_2	<i>Dip dir.</i>	<i>Dip</i>	σ_3	<i>Dip dir.</i>	<i>Dip</i>	σ_H	σ_h	<i>Bearing of σ_H</i>	σ_H/σ_h
1	223	58.8	0.43	9.5	11.9	7.7	-1.1	-0.1	-0.3	12.3	111	01	9.1	201	11	7.6	017	79	12.3	9.0	111	1.37
2	223	66.0	0.32	8.2	8.7	5.6	-2.4	0.4	0.7	10.8	313	02	6.6	044	38	5.0	220	52	10.8	6.0	132	1.8
3	223	58.6	0.36	3.7	7.6	3.9	-2.2	-0.1	-0.9	8.6	115	03	4.4	210	61	2.3	023	29	8.6	2.8	114	3.07

Table 8 Borehole KA1899A

<i>Number</i>	<i>Depth</i>	<i>E</i>	<i>v</i>	σ_x	σ_y	σ_z	τ_{xz}	τ_{yz}	τ_{zx}	σ_1	<i>Dip dir.</i>	<i>Dip</i>	σ_2	<i>Dip dir.</i>	<i>Dip</i>	σ_3	<i>Dip dir.</i>	<i>Dip</i>	σ_H	σ_h	<i>Bearing of σ_H</i>	σ_H/σ_h
1	256	63.8	0.41	16.4	12.8	6.6	-6.4	0.5	-0.6	21.3	143	03	7.9	053	01	6.6	305	87	21.2	7.9	143	2.68
2	256	65.0	0.38	14.8	10.6	6.1	-5.4	0.7	-1.3	18.7	146	07	6.9	237	12	5.9	027	76	18.5	6.8	146	2.72
3	256	62.0	0.42	18.5	14.3	8.5	-6.9	1.6	-1.4	23.9	143	08	9.4	050	21	8.1	252	68	23.6	9.2	143	2.57
4	256	59.7	0.40	16.3	11.0	7.5	-4.8	0.8	-0.4	19.2	149	04	8.4	058	25	7.2	247	65	19.1	8.1	150	2.36
5	256	64.3	0.40	19.2	13.0	8.1	-6.5	1.3	0.3	23.3	148	02	9.8	056	36	7.2	240	54	23.3	8.9	148	2.62

Table 9 Borehole KA2198A

<i>Number</i>	<i>Depth</i>	<i>E</i>	<i>v</i>	σ_x	σ_y	σ_z	τ_{xz}	τ_{yz}	τ_{zx}	σ_1	<i>Dip dir.</i>	<i>Dip</i>	σ_2	<i>Dip dir.</i>	<i>Dip</i>	σ_3	<i>Dip dir.</i>	<i>Dip</i>	σ_H	σ_h	<i>Bearing of σ_H</i>	σ_H/σ_h
1	294	56.5	0.30	15.5	16.7	7.4	-8.8	3.4	-1.9	25.8	133	12	7.9	034	35	6.0	238	53	25.0	7.2	134	3.47
2	294	36.5	0.29	9.2	8.7	4.1	-5.2	0.0	-0.6	14.2	137	03	4.4	230	56	3.5	045	34	14.2	3.7	136	3.84
3	294	51.7	0.42	13.3	17.5	10.6	-5.9	1.1	-1.3	21.9	126	08	10.5	241	71	9.0	033	17	21.6	9.1	125	2.37
4	294	53.1	0.33	15.7	17.1	7.8	-7.9	2.9	-2.3	25.1	132	12	8.5	041	08	7.0	278	75	24.3	8.4	133	2.89

Table 10 Borehole KA2510A

<i>Number</i>	<i>Depth</i>	<i>E</i>	<i>v</i>	σ_x	σ_y	σ_z	τ_{xz}	τ_{yz}	τ_{zx}	σ_1	<i>Dip direction</i>	<i>Dip</i>	σ_2	<i>Dip direction</i>	<i>Dip</i>	σ_3	<i>Dip direction</i>	<i>Dip</i>	σ_H	σ_h	<i>Bearing of σ_H</i>	σ_H/σ_h
1	335	71.8	0.39	24.0	30.6	17.7	-6.3	-0.2	2.9	34.6	302	06	21.6	036	30	16.1	203	59	34.4	20.2	121	1.70
2	335	66.7	0.40	19.9	20.6	11.2	-7.4	1.5	1.5	27.7	134	00	14.3	044	34	9.8	224	56	27.7	12.8	134	2.16
3	335	66.1	0.30	17.6	15.2	12.3	-7.5	2.6	2.4	24.0	320	00	14.5	051	58	6.6	229	32	24.0	8.8	140	2.73
4	335	72.1	0.27	17.1	16.8	11.7	-8.3	1.7	1.3	25.3	136	01	12.8	043	63	7.6	226	27	25.3	8.6	136	2.94
5	335	68.8	0.30	16.4	18.1	8.3	-6.8	3.8	0.3	24.5	130	10	12.1	034	32	6.1	234	57	24.1	10.4	132	2.32
6	335	68.9	0.34	17.6	12.2	7.7	-6.3	1.0	2.5	21.9	328	06	10.0	063	41	5.6	231	48	21.8	8.0	147	2.73

Table 11 Borehole KA2870A

<i>Number</i>	<i>Depth</i>	<i>E</i>	<i>v</i>	σ_x	σ_y	σ_z	τ_{xz}	τ_{yz}	τ_{zx}	σ_1	<i>Dip dir.</i>	<i>Dip</i>	σ_2	<i>Dip dir.</i>	<i>Dip</i>	σ_3	<i>Dip dir.</i>	<i>Dip</i>	σ_H	σ_h	<i>Bearing of σ_H</i>	σ_H/σ_h
1	379	64.7	0.33	23.3	31.7	20.8	-10.8	1.4	-9.7	41.4	130	19	24.2	241	46	10.2	024	38	39.1	15.9	124	2.46
2	379	68.2	0.30	20.2	33.1	22.8	-10.3	-1.8	-8.9	39.3	123	11	27.8	230	55	9.0	026	32	38.8	14.5	119	2.68
3	379	63.9	0.27	11.9	23.9	12.9	-7.7	-2.4	-4.0	27.6	296	02	15.8	203	59	5.3	027	31	27.6	8.1	116	3.41
4	379	62.5	0.21	15.0	29.7	12.8	-11.8	-2.2	-3.5	36.3	299	01	15.3	208	59	6.0	029	31	36.3	8.5	119	4.27
5	379	64.8	0.28	21.2	24.2	13.1	-13.4	-3.9	-1.3	36.3	311	05	15.1	213	59	7.0	044	31	36.1	9.2	132	3.92

Table 12 Borehole KA3086A

<i>Borehole</i>	<i>Depth</i>	<i>E</i>	<i>v</i>	σ_x	σ_y	σ_z	τ_{xz}	τ_{yz}	τ_{zx}	σ_1	<i>Dip dir.</i>	<i>Dip</i>	σ_2	<i>Dip dir.</i>	<i>Dip</i>	σ_3	<i>Dip dir.</i>	<i>Dip</i>	σ_H	σ_h	<i>Bearing of σ_H</i>	σ_H/σ_h
1	408	63.9	0.37	15.6	18.6	7.8	-7.9	-2.6	0.6	25.4	309	08	9.7	215	27	6.9	054	62	25.2	9.1	130	2.77
2	408	72.1	0.34	20.0	31.2	10.8	-4.4	-3.4	3.5	33.6	291	11	19.0	024	13	9.5	161	73	32.7	18.5	109	1.77
3	408	71.6	0.31	16.0	34.1	10.4	-2.0	-7.1	-2.4	36.1	274	15	16.9	178	19	7.4	040	65	34.3	15.8	096	2.17
4	408	70.6	0.34	13.4	22.9	9.7	-1.3	-4.7	-1.7	24.4	274	17	14.0	178	19	7.5	043	64	23.1	13.2	098	1.75

Table 13 Borehole KA3579G

<i>Number</i>	<i>Depth</i>	<i>E</i>	<i>v</i>	σ_x	σ_y	σ_z	τ_{xz}	τ_{yz}	τ_{zx}	σ_1	<i>Strike</i>	<i>Dip</i>	σ_2	<i>Strike</i>	<i>Dip</i>	σ_3	<i>Strike</i>	<i>Dip</i>	σ_H	σ_h	<i>Bearing of σ_H</i>	σ_H/σ_h
1	468	73	0.3	-	-	-	-	-	-	34.5	191	36	17.6	284	4	11.4	18	53	26.4	17.5	9	1.51
2	469	73	0.3	-	-	-	-	-	-	29.0	192	48	15.1	79	20	11.0	334	36	20.0	13.8	24	1.45
3	470	73	0.26	-	-	-	-	-	-	43.7	189	33	20.5	95	6	15.8	355	57	35.6	20.4	10	1.75
4	470	65	0.3	-	-	-	-	-	-	30.4	179	42	18.2	88	2	12.7	356	48	22.6	18.2	0	1.24

Appendix B

Information about the secondary stress measurements.

Units

Depth	[m]
Young's modulus, E	[GPa]
Stress components, σ	[MPa]
Shear components, τ	[MPa]
Dip	[°]
Dip direction	[°]

Table 14 Borehole KA1045A

<i>Number</i>	<i>Depth</i>	<i>E</i>	<i>v</i>	σ_x	σ_y	σ_z	τ_{xz}	τ_{yz}	τ_{zx}	σ_1	<i>Dip dir.</i>	<i>Dip</i>	σ_2	<i>Dip dir.</i>	<i>Dip</i>	σ_3	<i>Dip dir.</i>	<i>Dip</i>	σ_H	σ_h	<i>Bearing of σ_H</i>	σ_H / σ_h
1	143	72.3	0.32	23.0	16.7	7.8	4.0	2.3	1.7	25.3	027	08	15.0	118	10	7.2	257	77	-	-	-	-
2	143	65.8	0.44	6.7	6.2	2.9	-1.0	1.0	-0.6	7.7	140	12	5.4	049	08	2.6	287	76	-	-	-	-
3	143	69.5	0.38	7.1	7.4	2.8	-1.5	0.6	-0.1	8.8	132	05	5.8	041	06	2.7	263	82	-	-	-	-

Table 15 Borehole KA1192A

<i>Number</i>	<i>Depth</i>	<i>E</i>	<i>v</i>	σ_x	σ_y	σ_z	τ_{xz}	τ_{yz}	τ_{zx}	σ_1	<i>Dip dir.</i>	<i>Dip</i>	σ_2	<i>Dip dir.</i>	<i>Dip</i>	σ_3	<i>Dip dir.</i>	<i>Dip</i>	σ_H	σ_h	<i>Bearing of σ_H</i>	σ_H / σ_h
1	164	75.3	0.30	8.6	11.0	4.5	1.3	-0.1	0.4	11.5	067	00	8.0	337	07	4.4	159	83	-	-	-	-
2	164	72.3	0.38	12.9	13.9	9.3	1.6	-2.3	1.0	15.4	243	14	12.8	339	16	7.9	126	60	-	-	-	-
3	164	74.8	0.27	6.2	12.3	8.7	-0.9	-3.2	0.1	14.3	277	30	7.0	128	56	6.0	015	15	-	-	-	-

Table 16 Borehole KZ0059B

<i>Number</i>	<i>Depth</i>	<i>E</i>	<i>v</i>	σ_x	σ_y	σ_z	τ_{xz}	τ_{yz}	τ_{zx}	σ_1	<i>Dip dir.</i>	<i>Dip</i>	σ_2	<i>Dip dir.</i>	<i>Dip</i>	σ_3	<i>Dip dir.</i>	<i>Dip</i>	σ_H	σ_h	<i>Bearing of σ_H</i>	σ_H / σ_h
1	416	64.2	0.43	18.2	12.2	13.2	-7.1	1.1	-3.3	23.9	148	18	12.3	295	70	7.4	054	10	22.9	7.5	147	3.05

2	416	65.3	0.49	27.7	13.3	17.7	-5.9	-0.2	-0.1	29.8	160	00	17.7	253	88	11.1	070	02	29.8	11.1	160	2.68
3	416	67.4	0.32	14.8	8.5	12.1	-5.7	-1.0	0.5	18.3	329	08	12.1	181	81	5.1	060	05	18.2	5.1	150	3.57
4	416	62.1	0.43	18.4	9.2	13.4	-6.8	1.3	1.2	22.0	332	03	13.8	075	78	5.3	242	12	22.0	5.6	152	3.93
5	416	61.3	0.48	25.7	13.9	17.3	-7.1	1.5	0.6	29.0	155	01	17.6	062	77	10.1	245	13	29.0	10.5	155	2.76
6	416	64.9	0.44	25.4	14.3	17.0	-7.5	-0.8	0.3	29.3	333	03	17.1	216	84	10.5	063	05	29.2	10.5	153	2.78

Table 17 Borehole KA3597G

<i>Number</i>	<i>Depth</i>	<i>E</i>	<i>v</i>	σ_x	σ_y	σ_z	τ_{xz}	τ_{yz}	τ_{zx}	σ_1	<i>Strike</i>	<i>Dip</i>	σ_2	<i>Strike</i>	<i>Dip</i>	σ_3	<i>Strike</i>	<i>Dip</i>	σ_H	σ_h	<i>Bearing of σ_H</i>	σ_H / σ_h
1	450	104	0.3	-	-	-	-	-	-	21.9	194	39	7.5	77	29	1.1	322	38	15.0	4.6	25	3.26
2	451	99	0.3	-	-	-	-	-	-	18.9	196	43	5.3	91	16	-4.2	346	42	9.6	3.1	38	3.10
3	452	63	0.24	-	-	-	-	-	-	26.1	221	49	5.3	91	30	2.5	345	26	13.7	3.7	47	3.70
4	453	88	0.3	-	-	-	-	-	-	26.7	222	35	6.8	94	41	2.4	335	30	19.8	3.9	46	5.08
5	454	55	0.23	-	-	-	-	-	-	26.1	221	38	10.6	98	36	8.1	341	33	20.0	9.2	45	2.17
6	456	66	0.27	-	-	-	-	-	-	26.7	216	43	14.8	326	21	13.1	75	40	20.7	14.3	32	1.45